CENTRAL RESEARCH LIBRARY
DOCUMENT COLLECTION

[redacted]

MARTIN MARIETTA ENERGY SYSTEMS LIBRARIES
3 4456 0349652 6

ORNL 1714
Special

43A

DECLASSIFIED
CLASSIFICATION CHANGED TO: aec
BY AUTHORITY OF: 5, 7, 70
BY: 12, 2, 70

AEC RESEARCH AND DEVELOPMENT REPORT

GAMMA RADIATION IN A DIVIDED AIRCRAFT SHIELD

F. C. Maienschein
F. T. Bly
T. A. Love

CENTRAL RESEARCH LIBRARY
DOCUMENT COLLECTION
LIBRARY LOAN COPY
DO NOT TRANSFER TO ANOTHER PERSON
If you wish someone else to see this document, send in name with document and the library will arrange a loan.

OAK RIDGE NATIONAL LABORATORY
OPERATED BY
CARBIDE AND CARBON CHEMICALS COMPANY
A DIVISION OF UNION CARBIDE AND CARBON CORPORATION
UCC
POST OFFICE BOX P
OAK RIDGE, TENNESSEE

[redacted]

[redacted]

[redacted]

ORNL-1714

This document consists of 143 pages.
Copy 43 of 141, Series A

Contract No W-7405-Eng-6

Shielding Section
Physics Division

GAMMA RADIATION IN A DIVIDED AIRCRAFT SHIELD

Part I F C Maienschein and T A Love
Part II F C Maienschein and F T Bly*

[redacted]

Date Issued

AUG 20 1954

OAK RIDGE NATIONAL LABORATORY
Operated by
CARBIDE AND CARBON CHEMICALS COMPANY
A Division of Union Carbide and Carbon Corporation
Post Office Box P
Oak Ridge, Tennessee

[redacted]

*Convair

3 4456 0349652 6

[redacted]

INTERNAL DISTRIBUTION

1 H Bethe (consultant)
2 E P Blizard
3 C E Center
4 R A Charpie
5 C E Clifford
6 G T Chapman
7 R G Cochran
8 Sylvan Cromer
9 J B Dee
10 L B Emlet (K-25)
11 W K Ergen
12 A P Fraas
13 H E Hungerford
14 W H Jordan
15 J A Lane
16 C E Larson
17 T A Love
18 F. C Maienschein
19 J L Meem
20 K Z Morgan
21 F H Murray
22 R H Ritchie
23 A Simon
24 A H Snell
25 H E Stern
26 C L Storrs
27 A M Weinberg
28 T A Welton
29 H P Yockey
30 Biology Library
31 Health Physics Library
32-37 ANP Library
38 Metallurgy Library
39 Reactor Experimental Engineering Library
40-44 Central Research Library
45 Laboratory Records, ORNL R C
46-51 Laboratory Records Department

EXTERNAL DISTRIBUTION

52 Air Force Engineering Office, Oak Ridge
53-54 Air Force Plant Representative, Burbank (1 copy to F A Cleveland, Lockheed)
55-56 Air Force Plant Representative, Seattle (1 copy to C J Leisy, Boeing)
57-59 Air Force Plant Representative, Wood-Ridge (1 copy each to K Campbell and H Reese)
60-63 ANP Project Office, Fort Worth (1 copy each to [illegible] C Flack and F Bly)
64-66 Argonne National Laboratory (Kermit Anderson, J W Butler, and J R Dietrich)
67 Armed Forces Special Weapons Project (Sandia)
68 Armed Forces Special Weapons Project, Washington (E C LaVier)
69-77 Atomic Energy Commission, Washington ([illegible] copy each to Col M J Nielsen, Col T A Redfield, C [illegible] Horner, and [illegible] F Thompson)
78 Battelle Memorial Institute
79 Brookhaven National Laboratory (M Fox)
80 Bureau of Aeronautics (R Zirkind)
81 Bureau of Ships (T Rockwell)
82 Carbide and Carbon Chemicals Company (Y-12 Plant)
83 Chief of Naval Research
84 Commonwealth Edison Company
85 Convair, San Diego (C H Helms)
86 Department of the Navy - OP-362
87 Detroit Edison Company
88 duPont Company, Augusta
89 duPont Company, Wilmington
90 Foster Wheeler Corporation

[redacted]

[redacted]

91	General Dynamics Corp , Electric Boat Division
92-94	General Electric Company, ANPD (1 copy to G Thornton)
95	General Electric Company, Richland
96	Glen L Martin Company (T. F Nagey)
97-98	Knolls Atomic Power Laboratory (H E Stone and L H Weinberg)
99	Lockland Area Office
100	Los Alamos Scientific Laboratory
101	Materials Laboratory (WADC) (Col L Hill)
102	Monsanto Chemical Company
103	National Advisory Committee for Aeronautics, Cleveland (A Silverstein)
104	National Advisory Committee for Aeronautics, Washington
105	Naval Research Laboratory (W Faust)
106	North American Aviation, Inc
107-110	Nuclear Development Associates Inc (1 copy each to H Goldstein and R Aronson)
111-115	Nuclear Powered Aircraft Branch, Weapon Systems Division (WADC) (1 copy to Col C D Gasser)
116	Oak Ridge Operations (K Wasschau)
117	Patent Branch, Washington
118	Phillips Petroleum Company
119-122	Powerplant Laboratory (WADC) (1 copy each to A M Nelson and F. M Westfall)
123-124	Pratt and Whitney Aircraft Division (Fox Project) (1 copy to C F deGanahl)
125	Rand Corporation
126	San Francisco Operations Office
127	USAF Headquarters
128	U S Naval Radiological Defense Laboratory
129	University of California Radiation Laboratory, Berkeley
130	University of California Radiation Laboratory, Livermore
131	Walter Kidde Nuclear Laboratories, Inc
132-133	Westinghouse Electric Corporation (1 copy to J. J. Taylor)
134-141	Technical Information Service, Oak Ridge

[redacted]

[redacted]

Table of Contents

		Page No
	ABSTRACT	x
	INTRODUCTION	1
I	EXPERIMENTAL REACTOR SHIELD MEASUREMENTS	3
	Apparatus	4
	Divided Shield Mockup	4
	Reactor Loading and Power Calibration	4
	Spectrometer	8
	Method of operation	8
	Component changes	9
	Energy and sensitivity calibrations	11
	Collimator	13
	Positioning in BSF	16
	Results	16
	Reactor Spectrum	19
	Aircraft Shield Spectra	19
	Source angles	21
	Azimuthal angles	33
	Other Shield Spectra	33
	Discussion	33
	Sources of Gamma Radiation	33
	Angular Distributions	34
	Attenuations	41
	Water	41
	Lead	41
	Boron	44
	Dose	44
II	AIR SCATTERING CALCULATIONS	50
	General Air Scattering Calculations	51
	Partitions	56
	Radial Emission of Photons	57
	Skew Emission Calculation	60
	Unscattered Radiation Calculations	61
	Results and Discussion	62

[redacted]

[redacted]

Table of Contents Cont

			Page No
App	A	DETERMINATION OF EXPRESSIONS FOR THE SCATTERING ANGLE AND THE POSTSCATTERING LENGTH	77
App	B.	TEST OF RADIAL EMISSION ASSUMPTION	79
App	C	TRANSFORMATION OF VARIABLE	82
App	D	GEOMETRY OF SKEW EMISSION CALCULATION	84
App	E	PARTITIONS USED IN CALCULATIONS	96
App	F	POSTSCATTER ENERGY, FLUX, AND DOSE FOR INDIVIDUAL CELLS	100
		Radial Emission	100
		Skew Emission	126
		Direct Beam	132

[redacted]

[redacted]

List of Figures

Fig No		Page No
1	Divided Shield Mockup	5
2	Section of Divided Shield Mockup Showing Spectrometer and Bismuth Shield	6
3	Block Diagram of Gamma-Ray Spectrometer	10
4	Sensitivity of Multiple-Crystal Gamma-Ray Spectrometer	12
5	Solid Angle of Gamma-Ray Spectrometer Collimator	15
6	Experimental Arrangement for Measurement of Bulk Shielding Reactor Gamma-Ray Spectrum	20
7	Gamma-Ray Spectrum of the Bulk Shielding Reactor	22
8	Gamma Isodose Curve around Reactor Shield without Shadow Disks and Dose along Isodose Curve with Shadow Disks in Position	23
9	Gamma-Ray Flux 97 cm from the Bulk Shielding Reactor (OW and DSM)	24
10	Gamma-Ray Flux 147 cm from the Bulk Shielding Reactor (OW)	25
11	Gamma-Ray Flux 147 cm from the Bulk Shielding Reactor (DSMB)	26
12	Gamma-Ray Flux 147 cm from the Bulk Shielding Reactor (OW and DSM)	27
13	Gamma-Ray Flux behind Lead Disks ($\alpha = 0$, DSML)	28
14	Gamma-Ray Flux behind Lead Disks ($\alpha = 50^{\circ}$, DSML)	29
15	Gamma-Ray Flux at Edge of Lead Disks as a Function of θ	30

[redacted]

[redacted]

List of Figures Cont

Fig No		Page No
16	Gamma-Ray Flux at Edge of Lead Disks as a Function of ϕ^*	31
17	Gamma-Ray Flux as a Function of Energy and Distance from the Bulk Shielding Reactor (OW and DSM)	32
18	Gamma-Ray Flux as a Function of θ for Various Energies (DSM) (Linear Plot)	36
19	Gamma-Ray Flux as a Function of θ for Various Energies (DSM) (Log Plot)	37
20	Gamma-Ray Flux as a Function of θ for Various Energies (DSML, $\alpha = 0^\circ$)	38
21	Gamma-Ray Flux as a Function of θ for Various Energies (DSML, $\alpha = 50^\circ$)	39
22	Gamma-Ray Flux as a Function of θ for Various Energies (DSML, $\alpha = 60^\circ$)	40
23	Gamma-Ray Attenuation in Water as a Function of Energy	42
24	Reduction of Gamma-Ray Flux Due to Presence of Lead Disks	43
25	Gamma-Ray Dose 147 cm from the Bulk Shielding Reactor (DSM)	46
26	Gamma-Ray Dose 147 cm from the Bulk Shielding Reactor (DSML)	47
27	Gamma-Ray Dose 147 cm from the Bulk Shielding Reactor as a Function of $\cos\theta$ (DSM)	48
28	Gamma-Ray Dose 147 cm from the Bulk Shielding Reactor as a Function of $\cos\theta$ (DSML)	49
29	Geometry of the Divided Shield	52
30	Divided Shield Geometry Showing Vectors Used in Calculations	53

[redacted]

[redacted]

[redacted]

List of Figures Cont

Fig No		Page No
31	Gamma-Ray Flux at Crew Shield Due to Air Scattering from Individual Cells -- Radial Emission	65
32	Gamma-Ray Dose inside Crew Shield Due to Air Scattering from Individual Cells -- Radial and Skew Emission	66
33	Gamma-Ray Flux at Crew Shield Due to Air Scattering	69
34	Gamma-Ray Dose inside Crew Shield Due to Air Scattering	70
35	Scattered Gamma-Ray Dose as a Function of Prescatter Energy	71
36	Scattered Gamma-Ray Dose as a Function of Postscatter Energy	72
37	Scattered Gamma-Ray Dose as a Function of Source Angle	73
38	Scattered Gamma-Ray Dose as a Function of Receiver Angle	74
39	Direct Gamma-Ray Dose as a Function of Source Energy	75
40	Direct Gamma-Ray Dose as a Function of Source Angle	76
41	Typical Variation of Emerging Gamma-Ray Flux with Shield Thickness	81
42	Geometry for Skew Emission Calculation	86
43	Typical Angular Distribution of Skew Emission Radiation ($\alpha = 60^{\circ}$)	90
44	Angular Distribution of Fig 43 Plotted against ϕ	91
45	Typical Angular Distribution of Skew Emission Radiation ($\alpha = 50^{\circ}$)	92
46	Geometry for Average Values of θ and ϕ for Skew Emission	94

[redacted]

Acknowledgements

The authors wish to thank Dr J L Meem for many valuable discussions and Mrs Grace McCammon Estabrook for preparation of many of the graphs The computations were largely performed by Mrs Susie Ezzell Atta of the ORNL Mathematics Panel

[redacted]

ABSTRACT

The first section of this report describes measurements made with the multiple-crystal scintillation gamma-ray spectrometer and the reactor portion of a divided shield mockup The mockup was a simplified model of the reactor aircraft shield described by the 1950 ANP Shielding Board, and gamma-ray spectra and angular distributions were determined at several positions along the shield boundary The second section of this report describes a calculation of the gamma-ray air scattering and subsequent crew shield penetration Dose values inside the crew shield are determined as a function of pre- and postscatter energies and source and receiver angles

[redacted]

INTRODUCTION

The introduction and gradual acceptance of a divided shield for nuclear-powered aircraft has increased the difficulty of determining the radiation dose received by the aircraft crew It is important to note, however, that the added complication of determining the radiation scattered by air into the crew compartment is present for any shield which utilizes the shadow principle, regardless of the degree of shield division

The most direct method of determining the attenuation of air-scattered radiation of a particular aircraft shield is to mock up the shield around a reactor supported in air The Tower Shielding Facility, now being put into operation at ORNL, will of course be used for this purpose Before this facility was available it was possible to attack the over-all attenuation problem by using experimental results obtainable from the ORNL Bulk Shielding Facility together with data from the unclassified literature The results of such a procedure are presented in this report

It is presumed that this information will be of value in attempting to optimize parameters before construction of the necessarily expensive engineering mockups to be tested with the Tower Shielding Facility The usefulness of the conclusions drawn from this report are

limited somewhat owing to the fact that a specific mockup of a particular shield, the ANP-53 shield,[1] was utilized for the spectrometer measurements described in Part I A simpler configuration, more amenable to analysis, would have been more valuable However, the use of the mockup of the ANP-53 shield does permit comparisons of the crew gamma-ray dose both with the values calculated in the report of the Shielding Board[1] and with experimental results available from the Skyshine experiments[2] at the Bulk Shielding Facility These comparisons are made in Part II

---

1 "Report of the Shielding Board for the Aircraft Nuclear Propulsion Program," ANP-53 (Oct 16, 1950)

2 H E Hungerford, "The Skyshine Experiments at the Bulk Shielding Facility," ORNL-1611

I EXPERIMENTAL REACTOR SHIELD MEASUREMENTS[1]

The characteristics of the radiation penetrating the reactor shield that are needed for air-scattering calculations are (1) the intensity over the shield surface, (2) the energy, and (3) the directional distribution For the gamma radiation leaving a reactor shield this information was obtained by the use of a multiple-crystal scintillation spectrometer, a rather complicated instrument chosen because of its relatively unique gamma-ray energy response Angular distributions were measured by means of a lead shield which acted as a gamma-ray collimator for the spectrometer Measurements were made at relatively few positions on the reactor shield surface because of the long time required to complete the differential-type spectral measurements This paucity of data rather severely limits the accuracy of the calculations in Part II of this report, but it appears obvious that a limited amount of information is better than none at all

For these experiments the source of radiations was the Bulk Shielding Reactor and the shield used was a mockup of the reactor shield portion of the divided shield described in the report[2] of the 1950 ANP Shield Board This shield design is commonly referred to as the ANP-53 shield

---

1 Many of these measurements have been reported previously in a series of memoranda F C Maienschein, "Gamma-Ray Spectral Measurements with the Divided Shield Mockup," Part I, ORNL-CF-52-3-1 (Mar 3, 1952), Part II, ORNL-CF-52-7-71 (July 8, 1952), Part III, ORNL-CF-52-8-38 (Aug 8, 1952), and T A Love, Part IV, ORNL-CF-52-11-124 (Nov 17, 1952)

2 "Report of the Shielding Board for the Aircraft Nuclear Propulsion Program," ANP-53 (Oct 16, 1950)

Apparatus

Divided Shield Mockup*

The divided shield mockup was furnished by GE-ANP It consisted of a cylindrical steel tank with one ellipsoidal end and the other end slotted to allow the Bulk Shielding Reactor to be rolled into it The BSR was loaded so as to fill the tank slot as nearly as possible Air voids on the sides of the tank simulated a 4-ft right cylindrical reactor Figure 1 shows a photograph of the mockup and reactor and Fig 2 shows the end and side sections

The mockup tank was constructed of steel sheet, the inner walls being 3/8 in thick and the outer walls 1/4 in thick The tank could be filled with either borated or unborated water The extent of the boration, when used, was 0 4% boron by weight

Two lead disks were used to mock up the shadow shield of ANP-53 The complex shapes used are shown in Fig 2 The disks had a total lead thickness of 4 5 in and were encased in steel liners with a total thickness 1.5 in

Reactor Loading and Power Calibration

The presence of the divided shield mockup (DSM) modified the flux distribution in the Bulk Shielding Reactor (BSR) so that a loading of fuel elements different from that used in open water (OW) was necessary When the

---

* Throughout this report the mockup of the reactor shield portion of the ANP-53 shield is referred to as the divided shield mockup

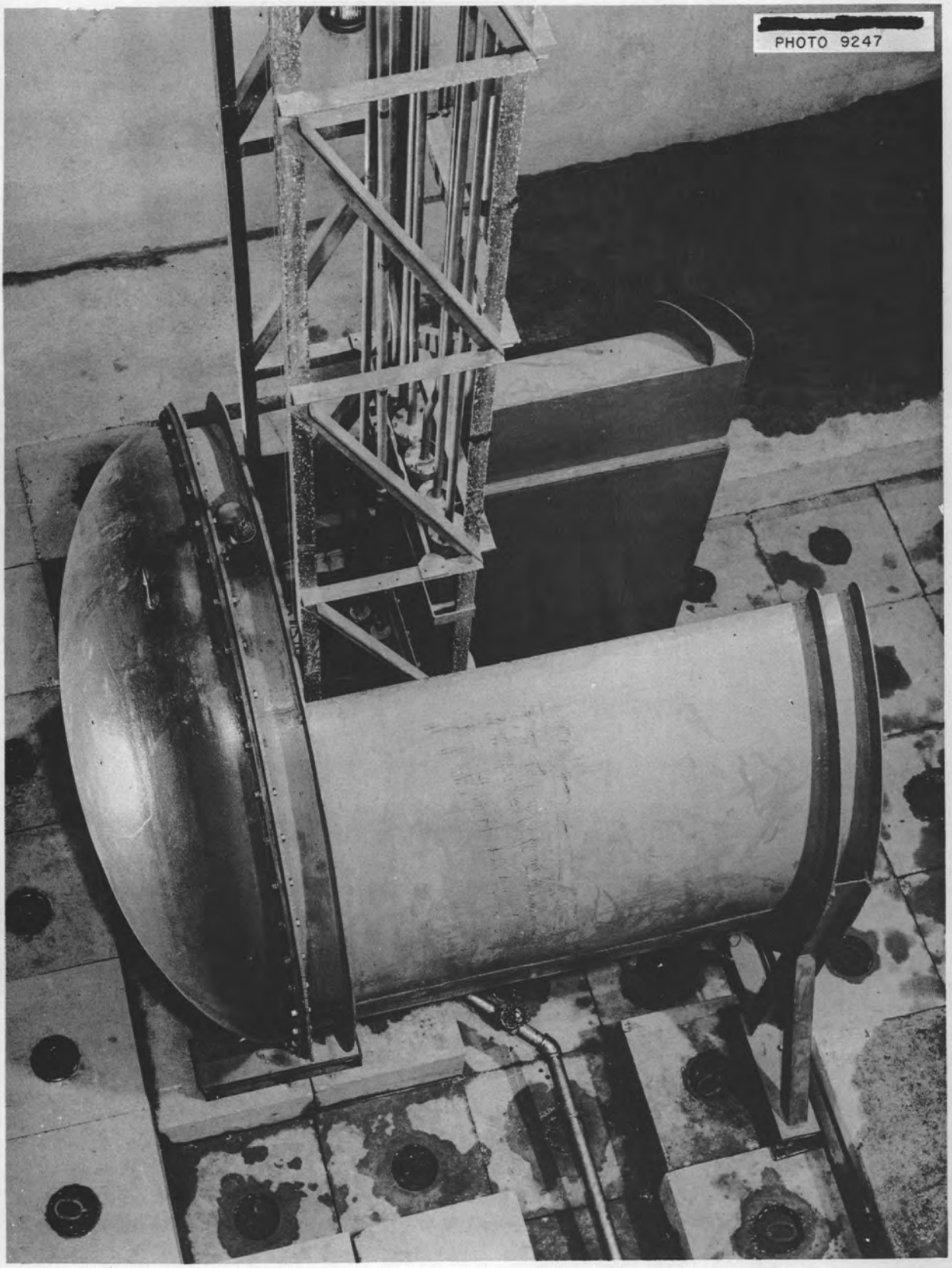

Fig. 1. Mockup of Reactor Shield Portion of ANP-53 Divided Aircraft Shield.

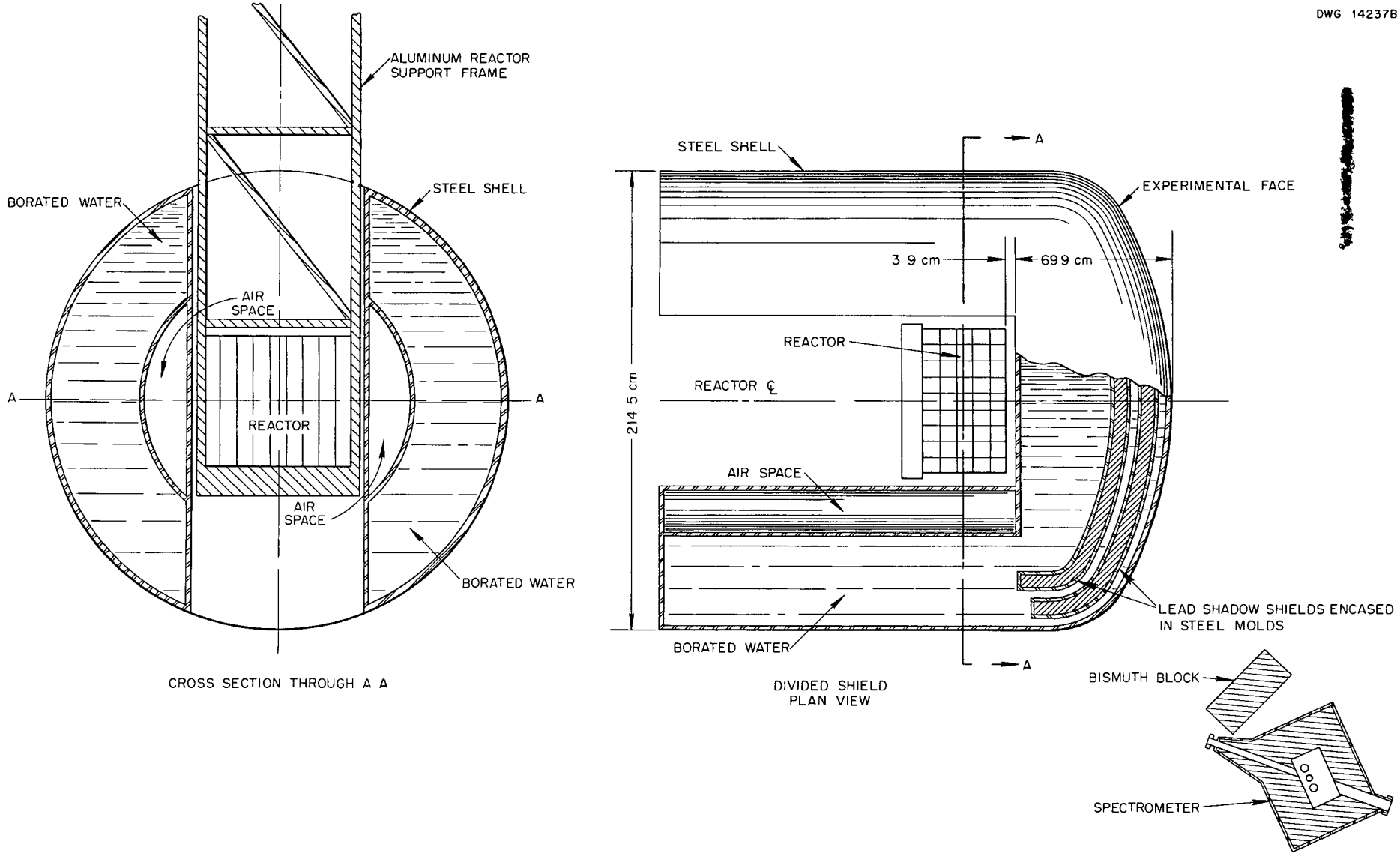

Fig 2 Sect o of D ded Sh eld Mock p Show g Spect omete and B sm th Sh eld

mockup was filled with borated water (DSMB) the flux distribution was changed further Therefore a power calibration was needed for each set of conditions The usual method was used, to wit, integration over a thermal-neutron flux distribution obtained by gold foil activation

The results of the power calibrations, described in detail in a separate report,[3] are summarized in Table 1 One particular loading in which the mockup was filled with unborated water was not calibrated, but only two spectral measurements were made with this arrangement The reactor power shown in Table 1 for this loading was assumed to be intermediate between the powers for open water and the borated mockup measurements

Table 1 Reactor Power Calibrations

Reactor Arrangement	Symbol	Loading No	Calibration (watts/nominal watt[a])
No shield, Be reflector, hot[b] fuel elements	OW	8	0 99
No shield, water reflector, cold[c] fuel elements	OW	22F	1 18
Divided shield mockup, borated	DSMB	9	0 85
Divided shield mockup, unborated	DSM	11	0 92 (assumed)

a As indicated on the reactor control instruments

b Reactor fuel elements which can be operated up to 100 kw

c Reactor fuel elements not previously operated above 1 watt

3 E B Johnson and J L Meem, "Determination of the Power of the Bulk Shielding Reactor," Part II, ORNL-1438 (April 21, 1953)

Spectrometer

The scintillation spectrometer used for the measurements described in this report has been discussed previously,[4] therefore only a brief review of the methods of operation and calibration is included here

Method of Operation The scintillation spectrometer utilizes either (1) the Compton effect or (2) pair production in order to give a unique energy response over the energy interval studied (0 2 to 10 Mev) For the method using the Compton effect, two crystals are required, one measuring the energy of the Compton-recoil electron, E_e, and the other detecting the scattered gamma ray[5] Since the angle θ between the incident and scattered gamma rays is known, the incident gamma-ray energy, E_γ, can be determined by the equation

$$E_\gamma = E_e/2 \left\{1 + \left[1 + 4/E_e(1 - \cos\theta)\right]\right\}^{1/2}$$

The lead collimator which defined the direction of the incident gamma ray is shown in Fig 2

For the method utilizing pair production, three crystals are used as shown in Fig 2 The center crystal measures the energy of the electron-positron pair, while the side crystals detect the two annihilation quanta[6] The energy of the incident gamma ray then was simply

$$E_\gamma = E_e + 2\, m_o c^2$$

---

4 F C Maienschein, "Multiple Crystal Gamma-ray Spectrometer," ORNL-1142 (July 3, 1952)

5 R Hofstadter and J A McIntyre, "Measurements of Gamma-Ray Energies with Two Crystals in Coincidence," Phys Rev 78, 619 (1950)

6 Sven A E Johansson, "A Scintillation Spectrometer for High-Energy Gamma-Rays," Nature (London), 166, 794 (1950), J K Bair and F C Maienschein, "Three-Crystal Scintillation Spectrometer," Rev Sci Instr 22, 343 (1951)

For both methods the pulses from the side crystals were analyzed with single-channel analyzers[7] after suitable amplification and only those pulses corresponding to an energy of 0 1 to 0 6 Mev were fed into the gate circuit Energies above these limits were surely not attributable to primary interactions in the center crystal The lower limit was determined by consideration of amplifier noise and analyzer stability The signals from the recoil-electron detecting center crystal were fed to a 20-channel analyzer after this instrument became available and to a single-channel analyzer for earlier runs These signals, of course, passed through the gate operated by the pulses from the side crystals to insure that only coincidences were recorded A block diagram of the electronic equipment is shown in Fig 3

Component Changes Changes and modifications made in the electronic equipment since the report[3] describing the spectrometer was published are to be described in detail in a separate memorandum[8] The major changes include (1) a new preamp designed to permit driving longer cables at higher counting rates, (2) a new coincidence circuit which utilizes the relatively fast PHS output of the A-1 linear amplifiers and thus permits a shorter resolving time (~ 4 μsec), and (3) the use of multichannel analyzers for analysis of the signal from the initial crystal This last change, of course, permits data to be accumulated much more rapidly

---

7 J E Francis, Jr , P R Bell and J C Gundlach, "Single-Channel Analyzer," Rev Sci Instr 22, 133 (1951)

8 T A Love and F C Maienschein (to be written)

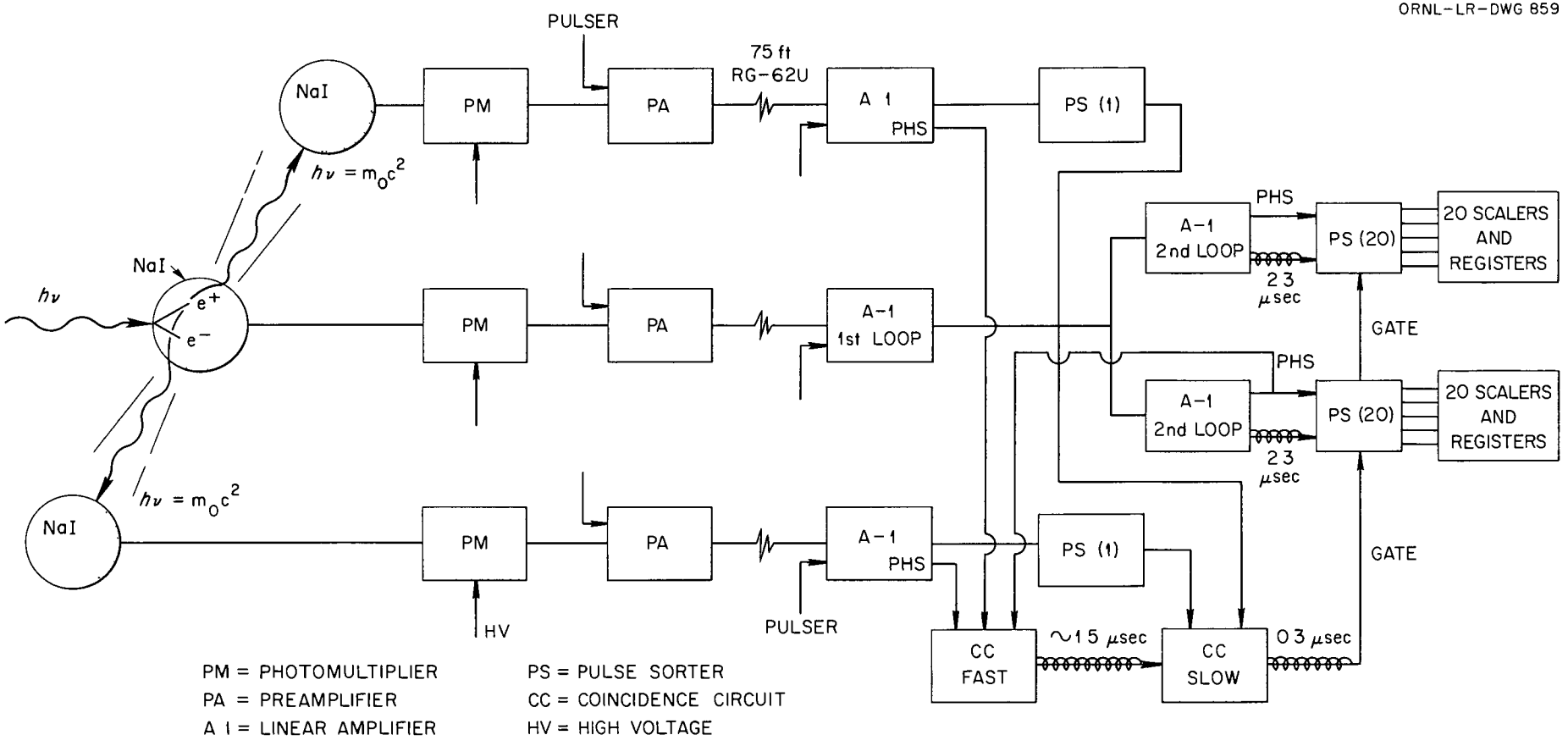

Fig 3 Block Diagram of Gamma-Ray Spectrometer (Arrangement Shown Is for Pair Spectrometer)

In addition to these changes, NaI(Tl) crystals already canned in a light-reflecting container have become available from Harshaw Chemical Co Some of these crystals have maintained good resolution ($\sim 8\%$ with Cs^{137}) for over a year DuMont photomultiplier tubes were substituted for the RCA-type because of the consistently better resolution obtainable

Energy and Sensitivity Calibrations Energy calibration of the spectrometer was carried out with sources of Cs^{137} (0 66 Mev), Co^{60} (1 17 + 1 33 Mev), ThC" (0 59 + 2 62 Mev), and Po-Be (0 80 + 4 43 Mev)

Sensitivity calibrations were made with large sources at sufficient distances from the spectrometer collimator so that the incident gamma rays were essentially parallel Then, after the source disintegration rates had been determined with an ionization chamber, taking into account the internal conversion coefficients and absorption of the gamma radiation in air, the incident flux at the spectrometer collimator could be determined The resulting sensitivities, expressed in coincidence counts per unit flux, are shown in Fig 4 For the Compton spectrometer, five sources were used For the pair spectrometer, only Na^{24} was available for a direct measurement However, a ThC" point was obtained by using the Compton sensitivity found above and a Po-Be point was obtained from the known neutron production rate and an estimate [9] of the fraction of the neutrons leading to the excited state of C^{12}

The solid lines of Fig 4 are theoretical curves calculated from the known cross section[10] of sodium iodide and the known solid angles of the

---

9 J Terrell, "Gamma-Rays from Be^9 (α,n)," Phys Rev 80, 1076 (1950)

10 Gladys R White, "X Ray Attenuation Coefficients from 10 Kev to 100 Mev," NBS-1003 (May 13, 1952)

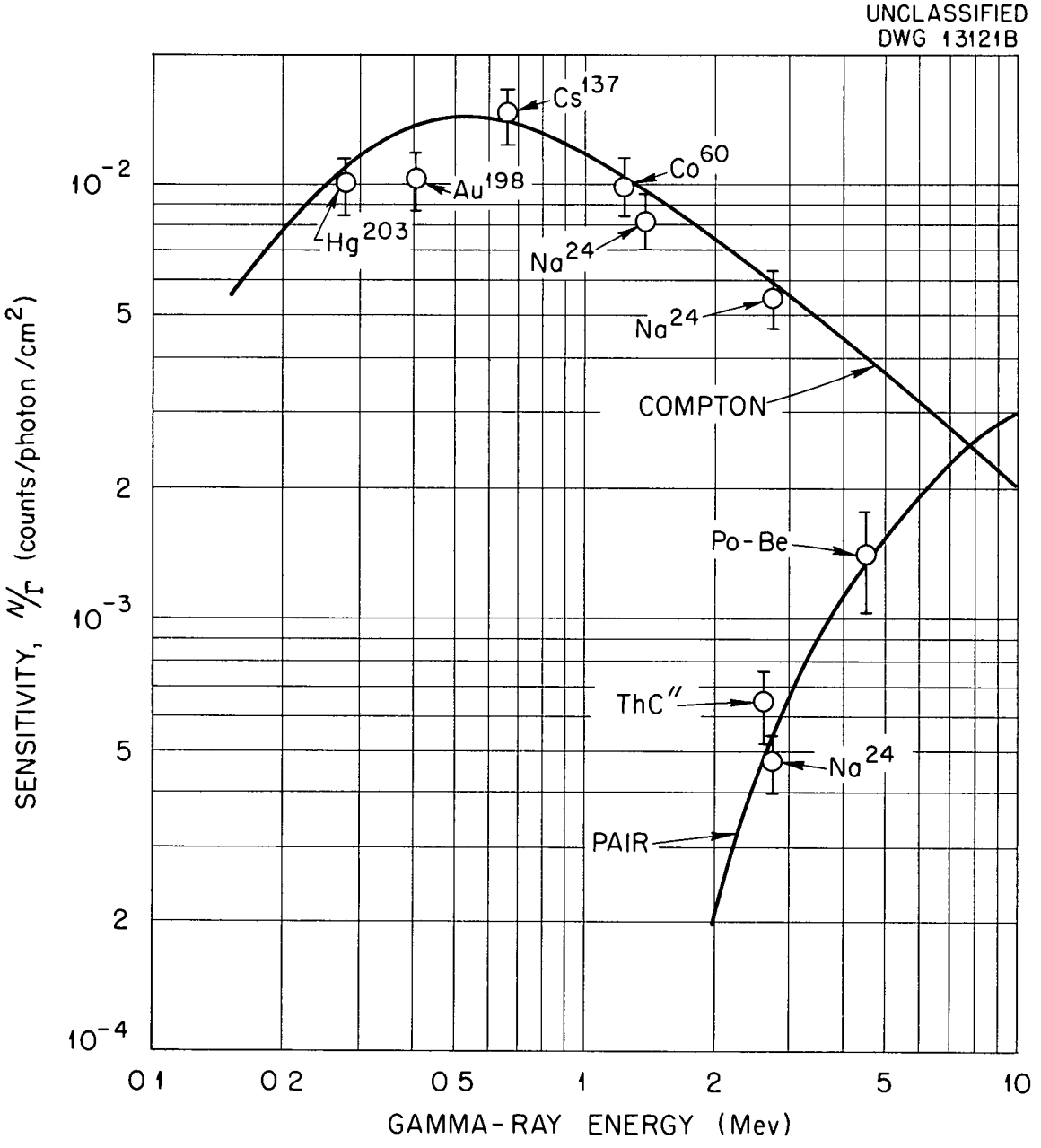

Fig 4 Sensitivity of Multiple-Crystal Gamma-Ray Spectrometer

spectrometer. Since the possible errors for this calculation were about ±15%, the good agreement with the experimental results must be somewhat fortuitous

The calibrations shown in the earlier report[3] indicate the extent to which the spectrometer response is not unique The pulses observed with a monoenergetic gamma ray which correspond to energies other than those of the recoil electrons are due to loss of electrons from the center crystal and to secondary processes occurring in the crystals The loss of electrons from the center crystal is small for reasons which differ with the detection arrangement In the Compton spectrometer, the scattered gamma rays which arise near the front edge of the crystal have the greatest probability of escaping to produce a count in the side crystal, and the recoil electrons produced in this part of the crystal have less chance to escape from the crystal For pair production the positron is required to stop in the center crystal in order for annihilation quanta to strike the two side crystals It appears probable therefore that most of the low-energy background pulses are due to secondary processes such as multiple scattering and loss of electron energy by bremsstrahlung radiation

Owing to the nature of the spectra measured (decreasing intensity with increasing energy) it was not considered necessary to correct for the background of pulses at the "wrong" energy in converting the raw data into gamma-ray spectral data

Collimator The shield around the spectrometer, as shown in Fig 2, consisted of a liner of 1/4 in of "boral"* and 6 in of lead with additional

---

* B_4C-impregnated aluminum sheet

lead in the forward direction The collimating hole in the forward direction consisted of a 7/8 in diameter unlined hole through the lead The first 6 in of lead surrounding the hole (2-in O D) could be removed and replaced with a solid lead plug for background measurements The solid angle subtended by the collimator was calculated as 1 81 x 10^{-3} steradian The angular definition was investigated with radioactive sources of various energies with results as shown in Fig 5 The counting rate is plotted as a function of angular displacement for Cs^{137} (0 66 Mev) and ThC" (2 62 Mev) sources The detector was biased rather low ($\sim$0 1 Mev) in both cases so that it would detect scattered radiation The solid line in Fig 5 presents the calculated expected behavior

The 6-in lead shield described above was quite adequate for gamma-ray shielding when the collimator was pointing toward the reactor For measurements with the collimator pointing away from the reactor, as shown in Fig 2, it was necessary to provide additional shielding between the reactor and the spectrometer crystals The extra shield used to stop this direct radiation was a bismuth block 8 in thick and 15 in wide By using this extra shield, the background radiation penetrating the spectrometer walls was in general kept small compared with the radiation accepted through the collimator At certain angles, however, it was difficult to block the direct radiation without also affecting the scattered radiation being measured At one particular angular position, indicated in Table 2, it was physically impossible to place the bismuth between the spectrometer and reactor For all angular measurements, the rear hole of the spectrometer was closed with a lead plug

UNCLASSIFIED
DWG 16835

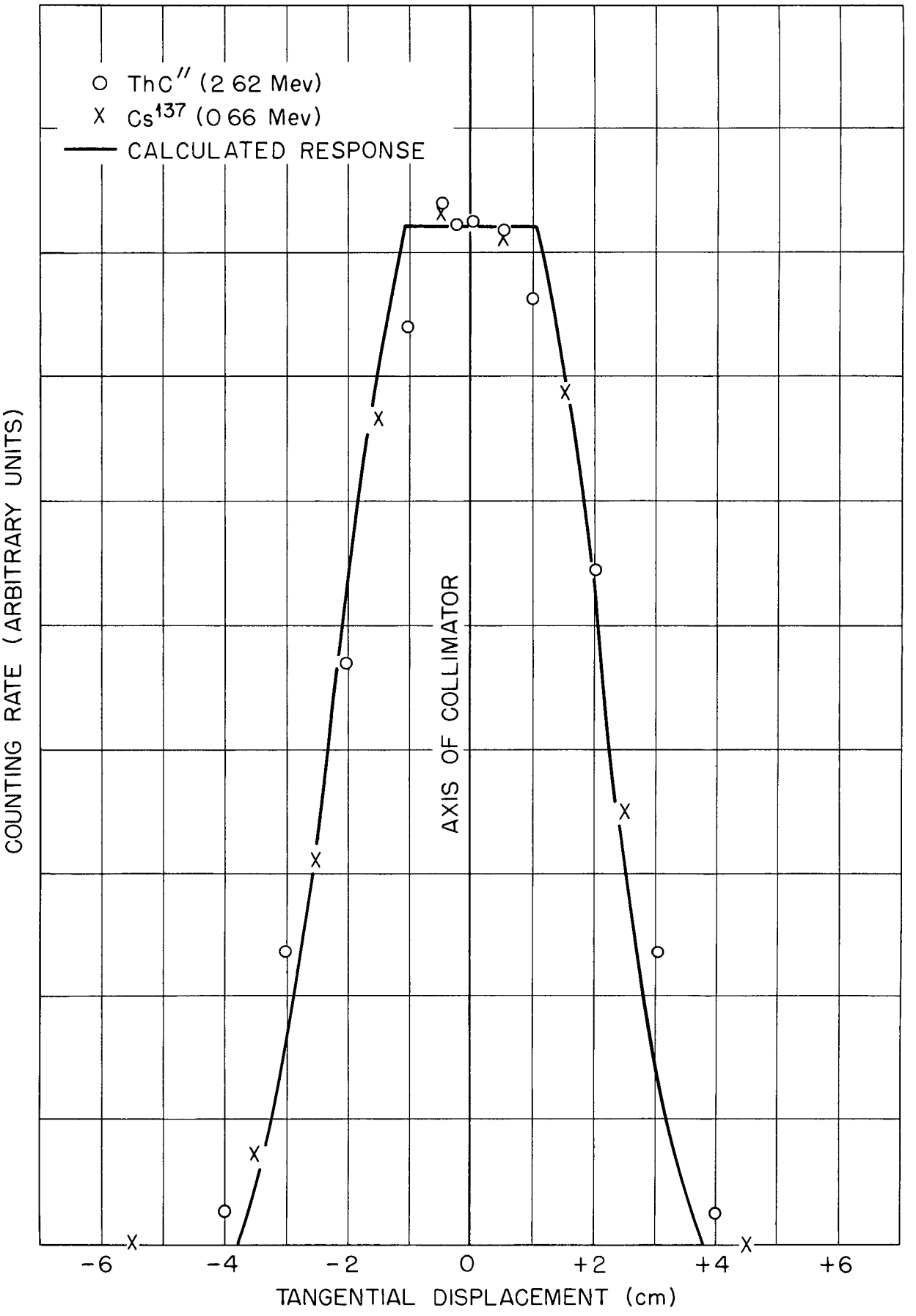

Fig 5 Solid Angle of Gamma-Ray Spectrometer Collimator

The 1/4-in boral neutron shield, together with the water of the reactor shield, reduced the neutron-induced background in the spectrometer to a negligible level For the measurement of the reactor spectrum itself with no water shield, a special arrangement was used which will be described later

Positioning in BSF The gamma-ray spectrometer was suspended from the instrument bridge of the BSF Its position was desiginated in terms of the following parameters

d = distance from reactor center to end of spectrometer collimator, which corresponds to the point of photon emergence from the reactor shield

d' = distance from the front edge of the reactor core to the end of the spectrometer collimator For $\alpha = 0$, $d = d' + 21$ cm

α = source angle, the angle between the reactor shield centerline and the line along which d is measured

θ = spectrometer elevation angle, the angle between the spectrometer collimator and the line along which d is measured

ϕ^* = spectrometer azimuth angle, the maximum angle between the horizontal plane through the reactor shield center and a line drawn from the end of the spectrometer collimator perpendicular to the aircraft shield axis (see Fig 42)

Results

An over-all summary of the spectral data obtained with the divided shield mockup is presented in Table 2 In addition to the parameters discussed above, Table 2 contains columns showing the shielding material present and the

Table 2 Spectrometer Positions for Gamma-Ray Spectral Measurements

d or d' (cm)[a]	Shield[b] Material	Source Angle, α (deg)[a]	Azimuth Angle, ϕ^* (deg)[a]	Elevation Angle, θ (deg)[a]	Fig No[c]
0	None	0	0	0	7
97	OW	0	0	0	9
				20	9
				40	9
	DSMB	0	0	0	9
				20[d]	9
	DSM	0	0	0	9
147	OW	0	0	0	10,12
				14	12
				20	12
				40	12
	DSMB	0	0	0	11,12
				10	11,12
				14	11,12
				20	11,12
				25	11
				30	11
				40	11,12
				60	11
	DSM	0	0	0	12
	DSML	0	0	0	13
				10	13
				20	13
				30	13
				40	13
				50	13
168	DSML	50	0	-20[e]	14
				-10	14
				0	14
				10	14
				20	14
				30	14

Table 2 Cont

d or d' (cm)[a]	Shield[b] Material	Source Angle, α (deg)[a]	Azimuth Angle, ϕ (deg)[a]	Elevation Angle, θ (deg)[a]	Fig No[c]
168	DSML	50	0	40	14
				50	14
				60	14
				70	14
	DSML	60	0	-30	15
				-20	15
				-10	15
				0	15
				10	15
				20	15
				30	15
				40	15
				50	15
				60	15
				70	15
				80	15
			5	f	16
			10	f	16
			15	f	16
			20	f	16
			25	f	16
			30	f	16
207	OW	0	0	0	17
	DSMB	0	0	0	17
267	OW	0	0	0	17
	DSMB	0	0	0	17

a See pg 15 for explanation of these symbols For $\alpha = 0$, values of d' are given in column 1 For $\alpha \neq 0$, values of d are given in column 1

b Symbols representing shield materials are
OW = water only,
DSM = divided shield mockup filled with plain water,
DSMB = divided shield mockup filled with borated water,
DSML = divided shield mockup filled with borated water and with lead shadow shield added

c This column presents the figure numbers in which the data described can be found

d The bismuth shield could not be used at this position

e A positive value of the angle θ is shown in Fig 2 Clockwise rotation of the spectrometer produced negative values of θ

f The angle θ for these measurements was determined so that the spectrometer collimator would always look at the edge of the lead disks in the divided shield mockup

figure number in this report where the data is plotted

Reactor Spectrum

Measurements of the gamma-ray spectrum with no shielding material present correspond to the spectrum of the Bulk Shielding Reactor itself The experimental arrangement used for this particular measurement is shown in Fig 6 The spectrometer nose could not be placed directly against the reactor face since the neutron-induced background in the spectrometer was prohibitively large Therefore, the air column, as shown in Fig 6, was used The water shielding surrounding the air column served to reduce the neutron-induced background to a negligible level The background for this part of the experiment was measured with the lead plug inserted in the nose of the spectrometer Use of a cold* set of fuel elements in the reactor reduced the fission product activity to a low level The reactor spectrum was investigated in considerably more detail (better statistics and more points) than the shielding data

Aircraft Shield Spectra

A shield thickness (d') of 147 cm was chosen as being typical of the ANP-53 reactor shield and was used for the bulk of the shield spectral measurements The 147-cm distance was measured from the edge of the reactor core to the end of the spectrometer collimator and included 7 cm of BeO reflector and 140 cm of water As shown in Fig 2, only the first 70 cm of the water could be borated

---

* Elements which have not previously been operated above 1 watt

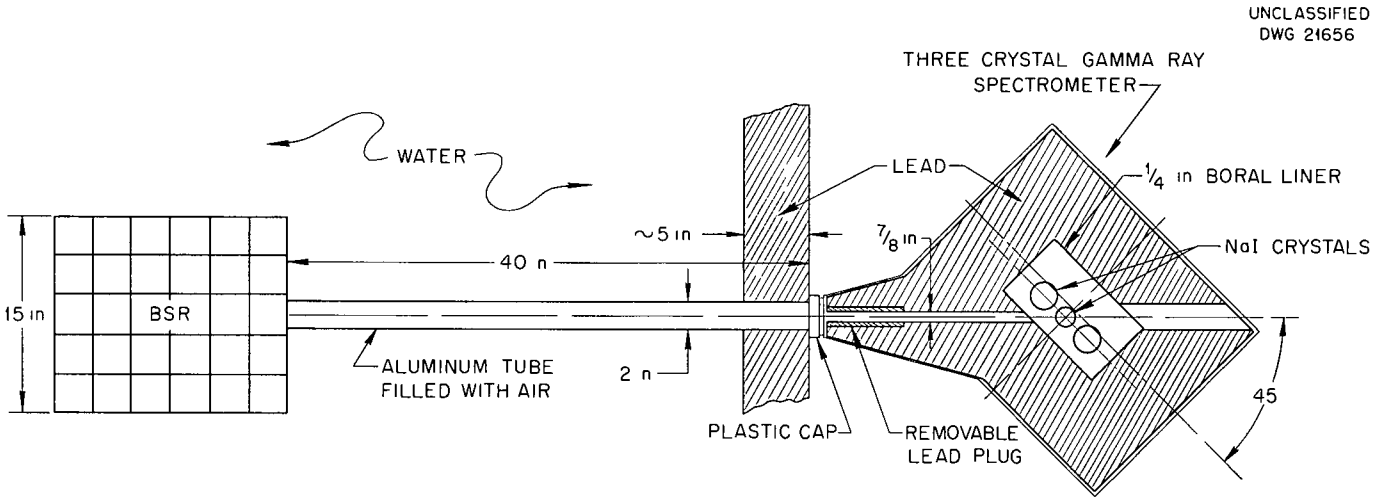

Fig 1

Fig 6 Experimental Arrangement for Measurement of Bulk Shielding Reactor Gamma Ray Spectrum

Source Angles The largest group of measurements were made at a source angle $\alpha = 0$ (i e , on the reactor-shield centerline) with no lead shadow shield The measurements made at this position were presumed to be applicable for all parts of the aircraft shield without lead shadow shielding

After the lead shadow shield was added, measurements were again taken at $\alpha = 0$ The choice of positions for further measurements was based on a gamma-ray isodose curve measured with an ion chamber by H E Hungerford (see Fig 8)[11] It is apparent that an isodose curve drawn through the point at $\alpha = 0$, $d' = 147$ cm is very nearly a segment of a circle with radius of 168 0 cm The center of this circle is referred to as the reactor pseudo center and it is located 21 cm behind the front edge of the reactor core, while the geometrical center of this reactor was about 15 cm behind the front face of the core The angle α has its apex at the reactor pseudo center

Figure 8 also shows the gamma-ray dose behind the lead shadow shield as a function of α Since this curve showed little change out to about $\alpha = 40^{\circ}$, it was presumed that the data for $\alpha = 0$ would be applicable over this entire region The open water data would again become applicable at about $\alpha = 70^{\circ}$ Further measurements were made at $\alpha = 50$ and 60°, which angles are in the transition region where radiation is leaking around the edge of the shadow shield

---

11 Previously published in CF-53-5-239, "Nuclear Dose Measurements on the Divided Shield Mockup at the Bulk Shielding Facility," by H E Hungerford (May 20, 1953)

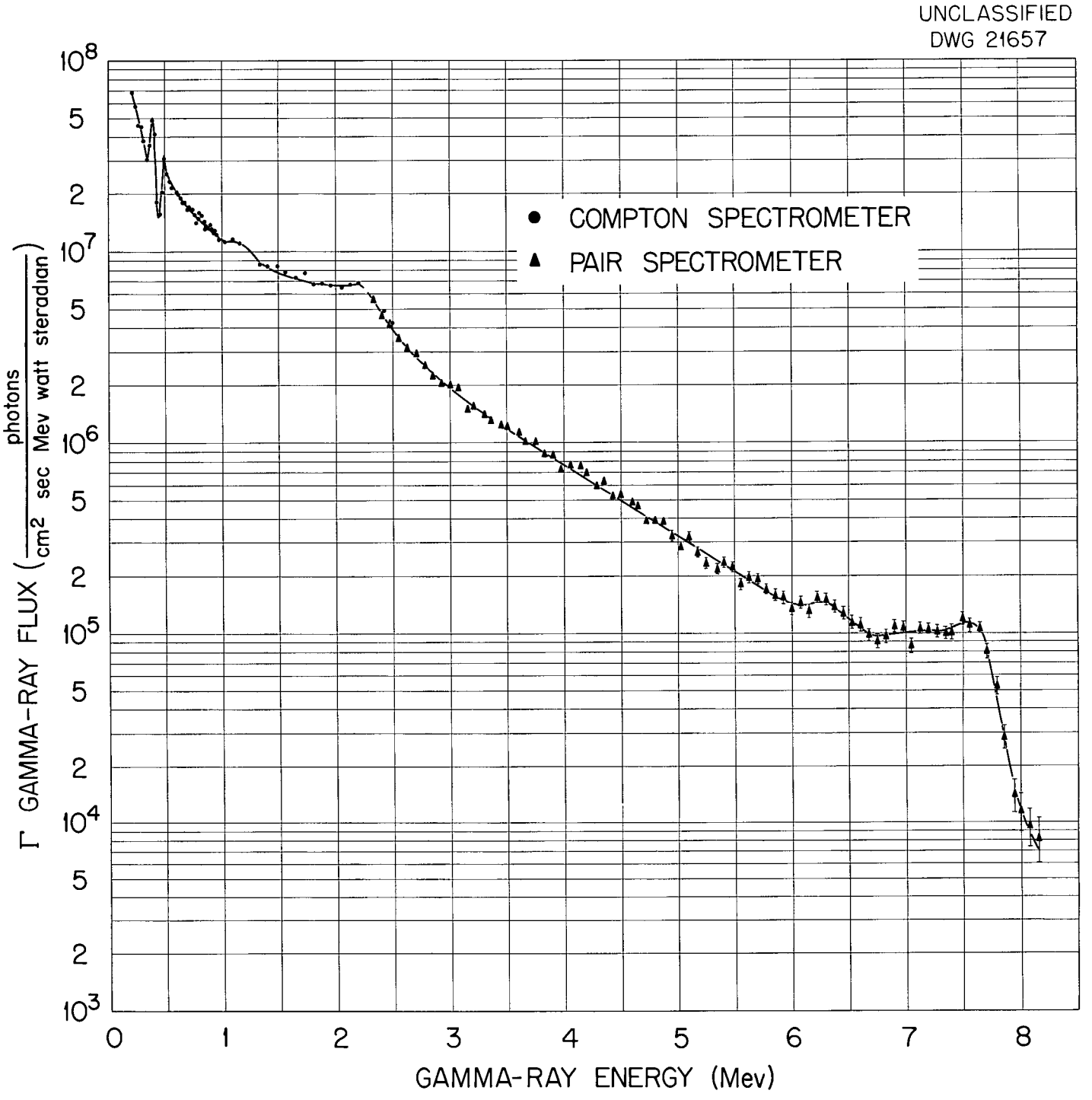

Fig 7 Gamma-Ray Spectrum of the Bulk Shielding Reactor

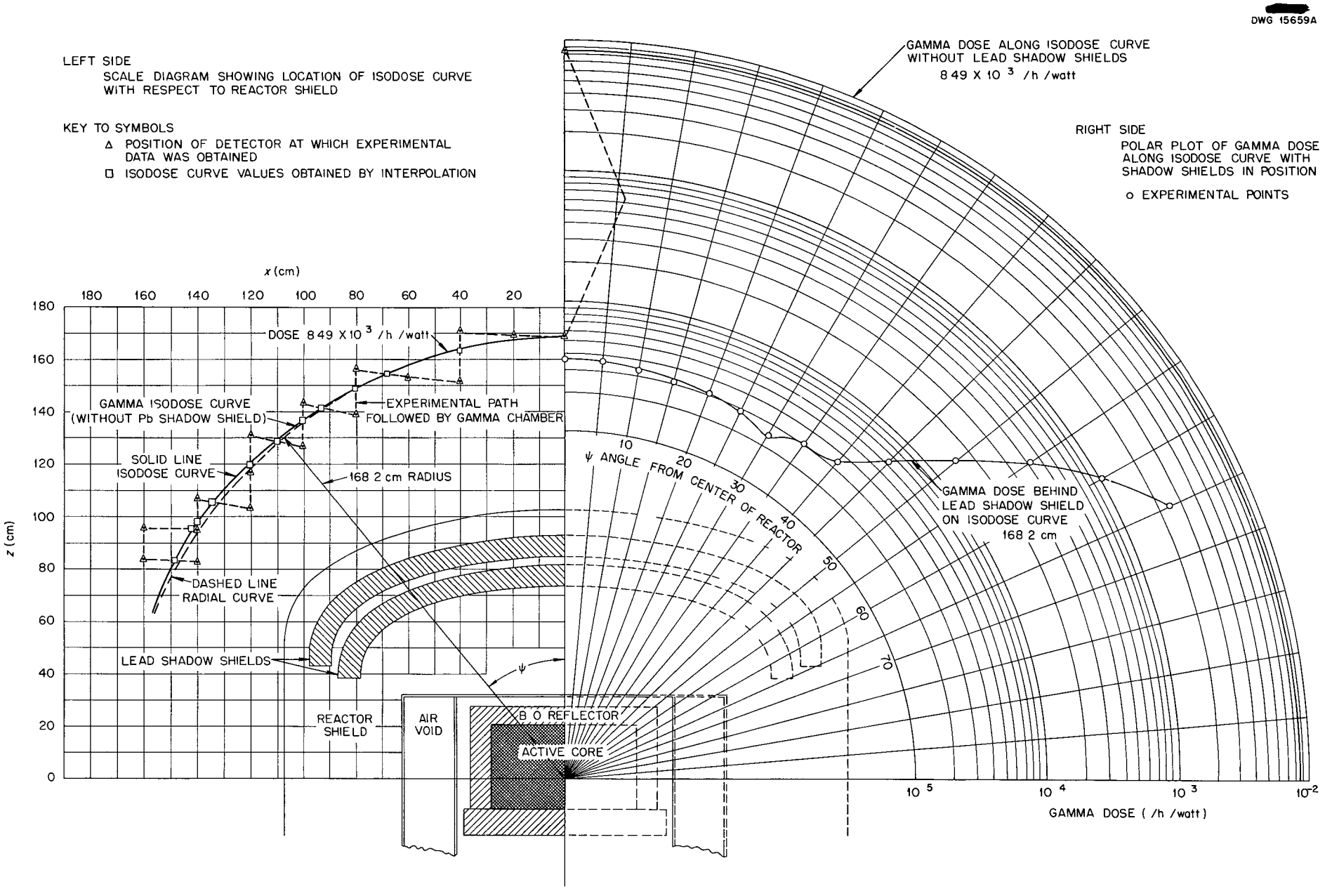

F g 8 Gamma Isodose Curve Around Reacto Shield W thout Shodow D sks and Dose olong Isodose Cu ve w th Shodow D sks in Pos t on

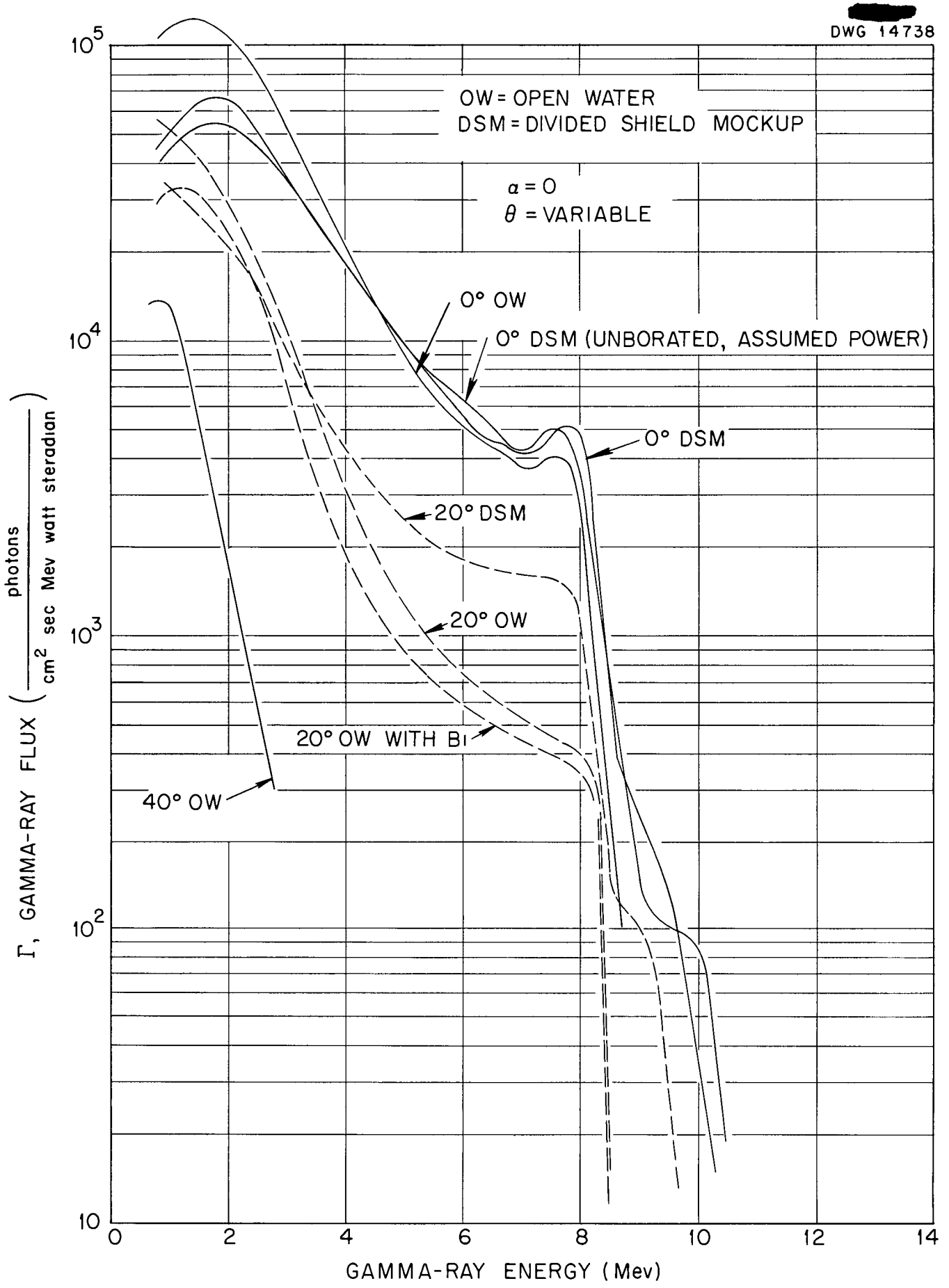

Fig 9 Gamma-Ray Flux 97 cm from the Bulk Shielding Reactor (OW and DSM)

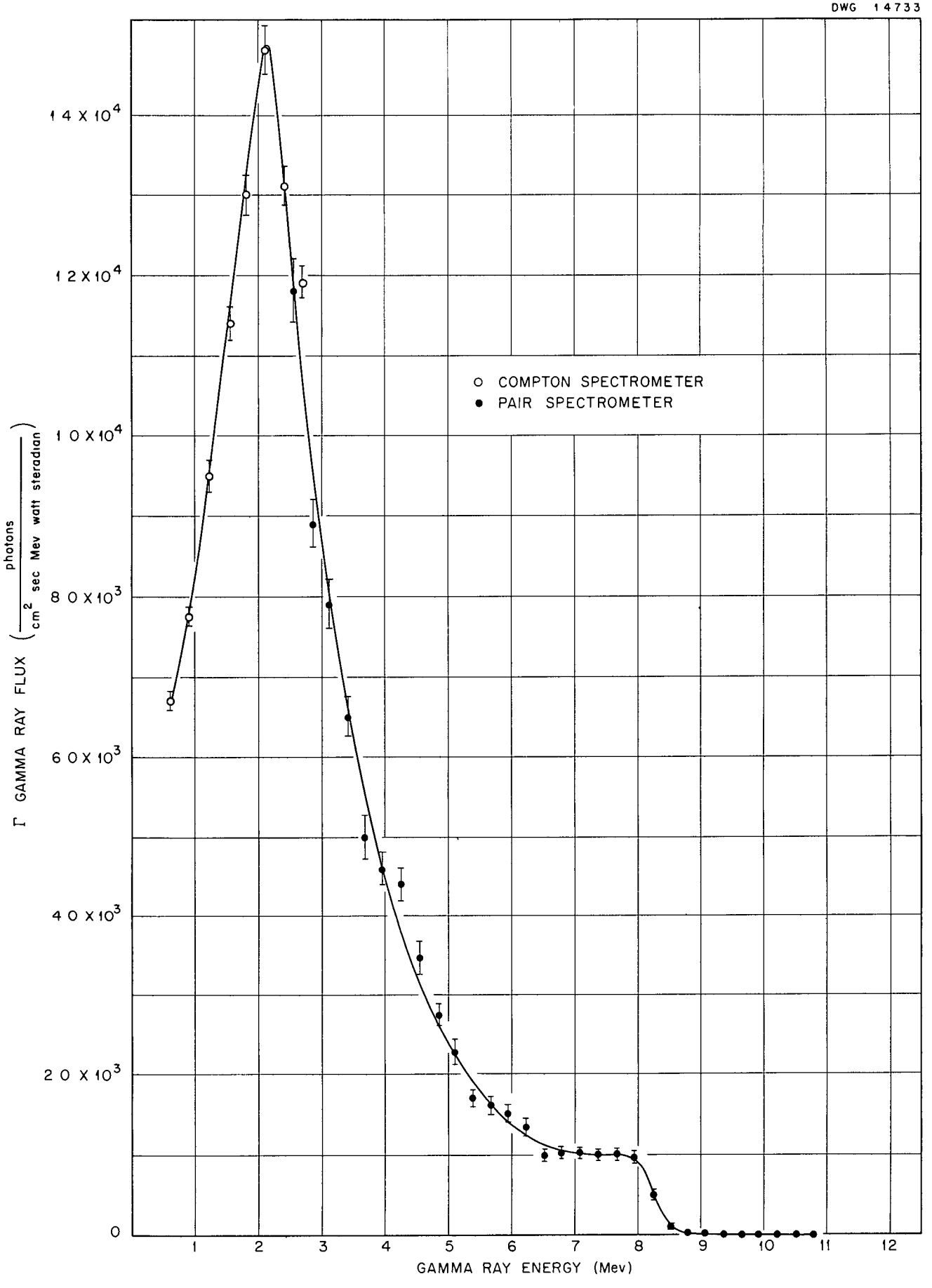

Fig 10 Gamma Ray Flux 147cm from the Bulk Shielding Reactor (OW)

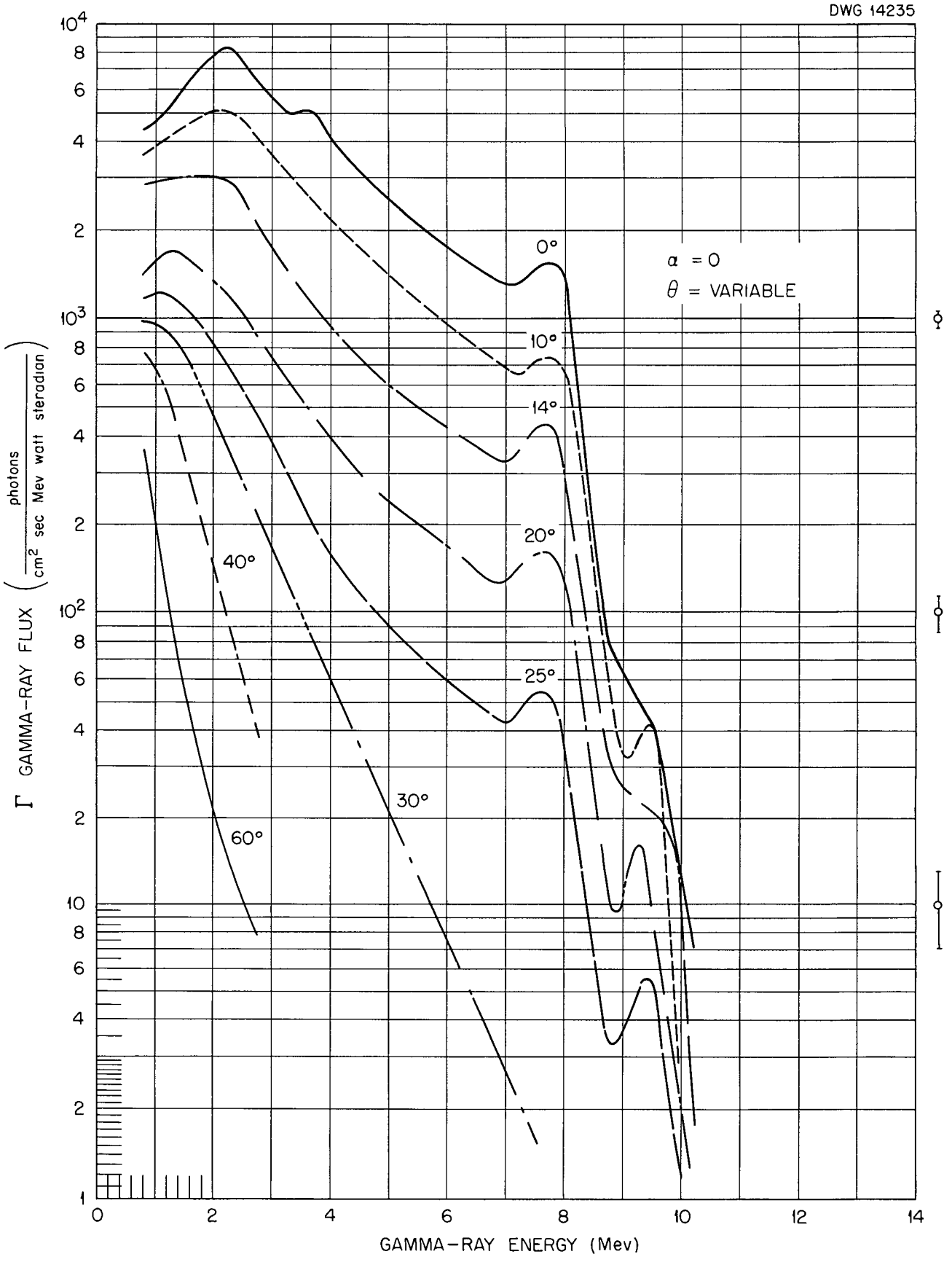

Fig 11 Gamma-Ray Flux 147 cm from the Bulk Shielding Reactor (DSMB)

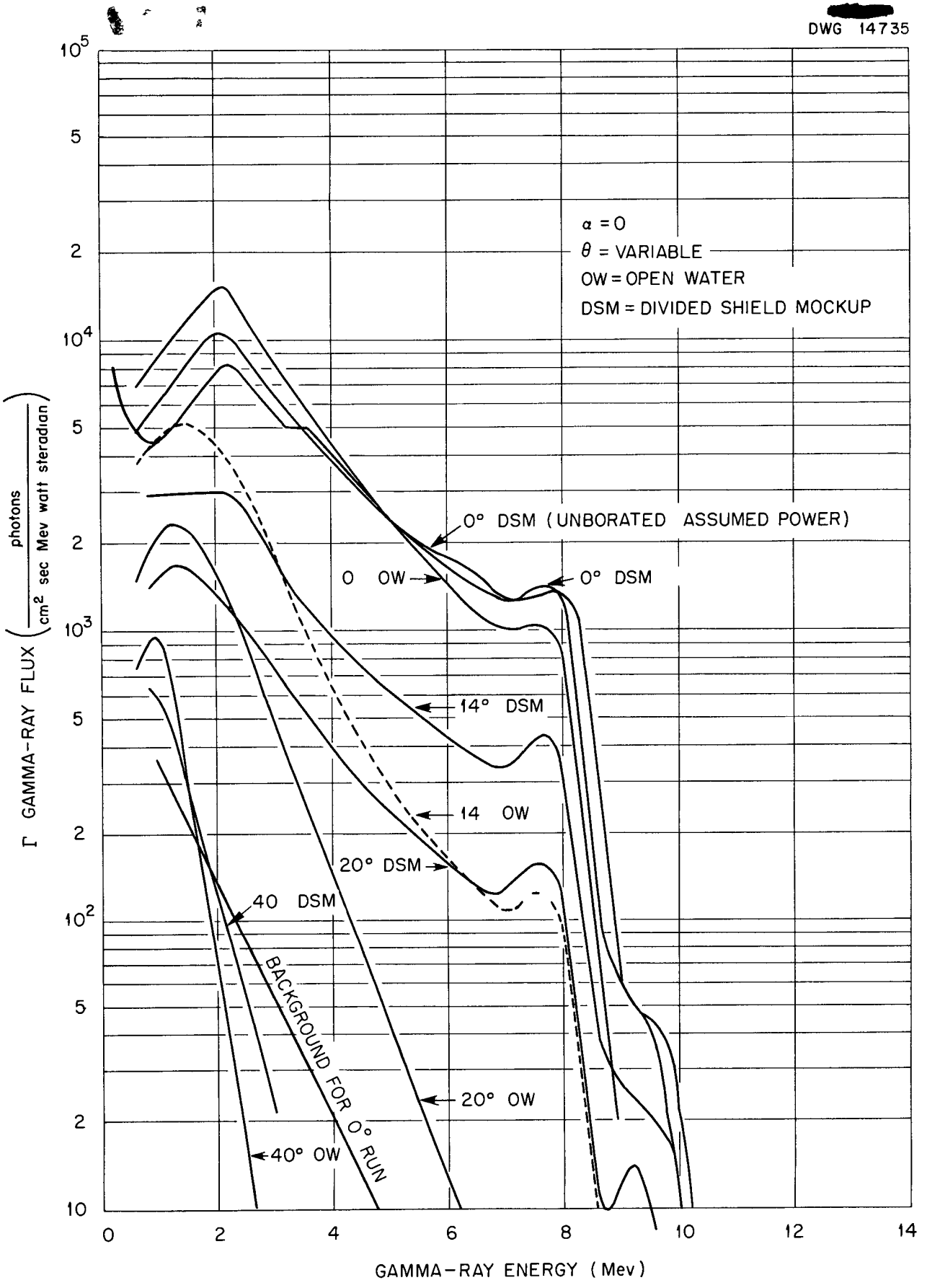

Fig 12 Gamma-Ray Flux 147 cm from the Bulk Shielding Reactor (OW and DSM)

[redacted]

[redacted] DWG 15660

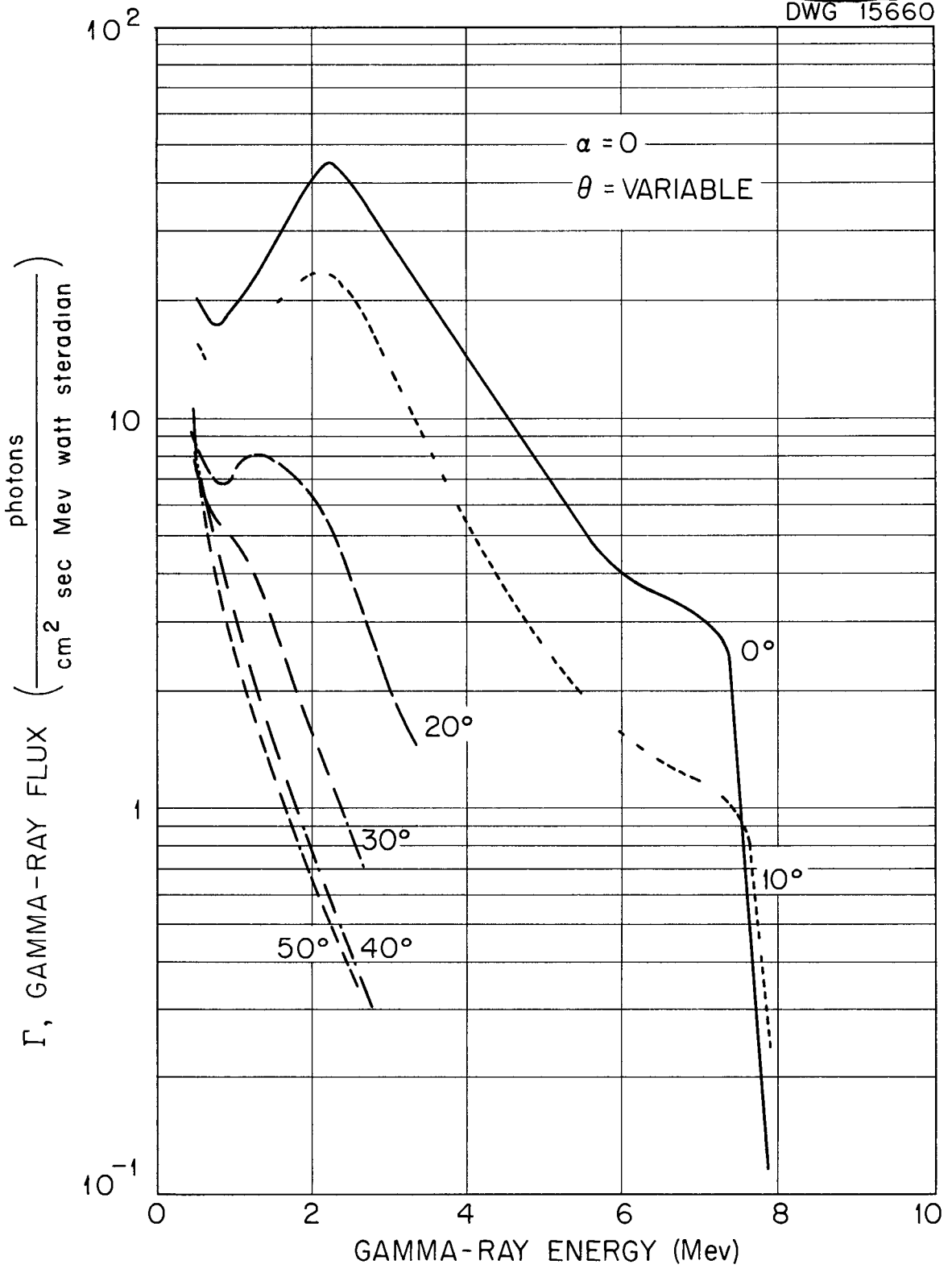

Fig 13 Gamma-Ray Flux Behind Lead Disks ($\alpha = 0$, DSML)

[redacted]

[redacted]

DWG 15661

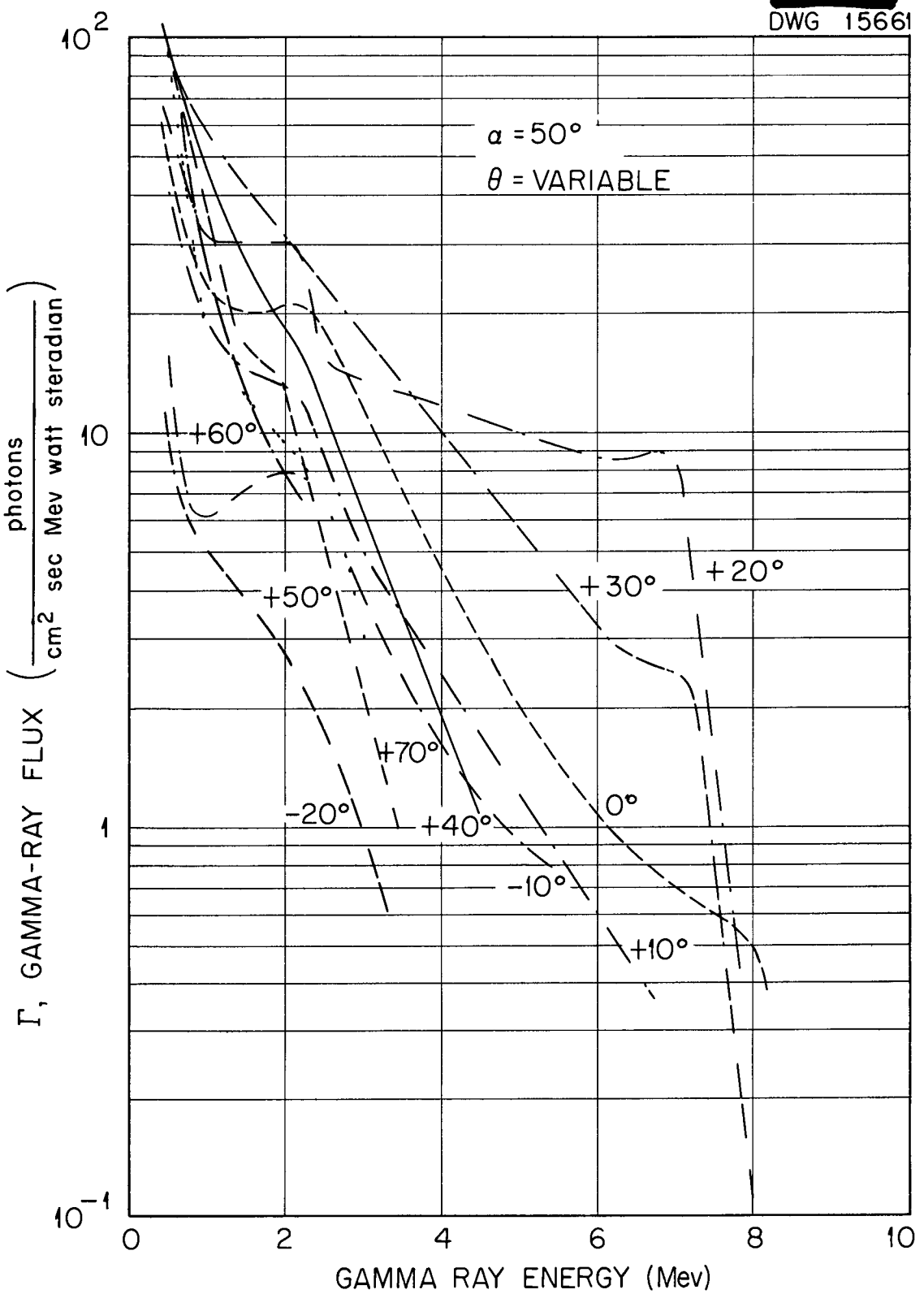

Fig 14 Gamma-Ray Flux Behind Lead Disks (α=50°, DSML)

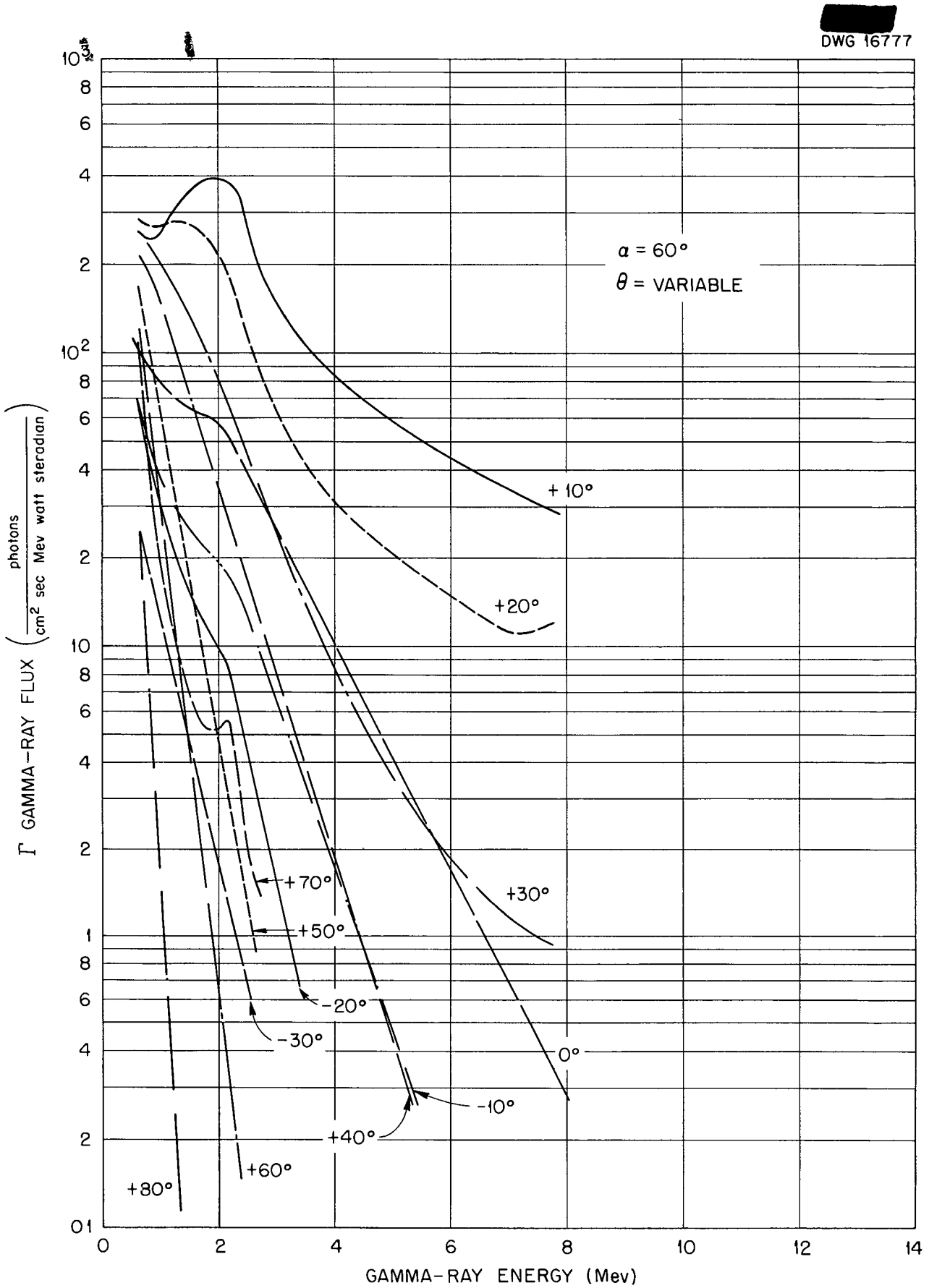

Fig 15 Gamma-Ray Flux at Edge of Lead Disks as a Function of θ

[redacted]

[redacted]

DWG 16776

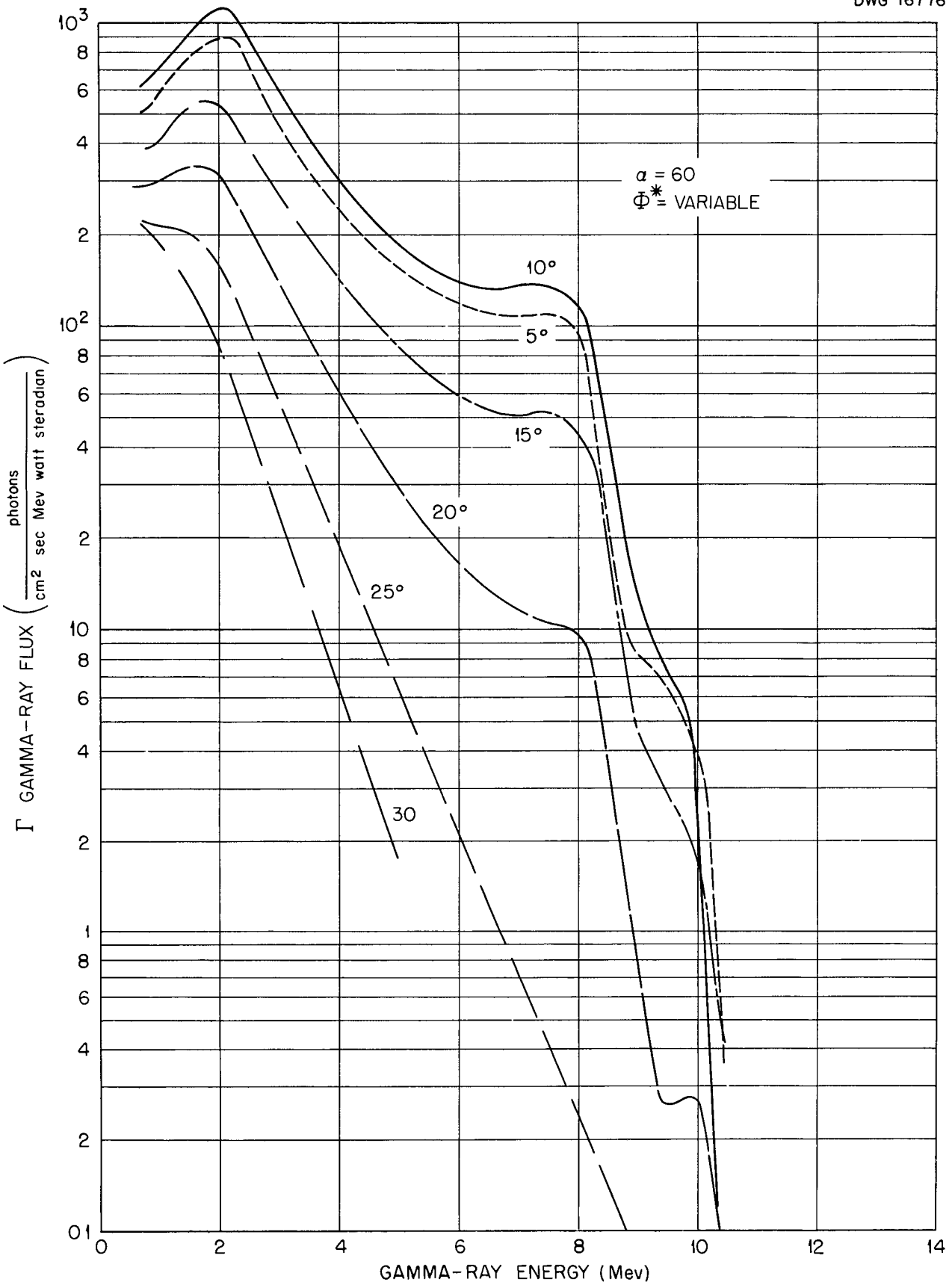

Fig 16 Gamma-Ray Flux at Edge of Lead Disks as a Function of Φ^*

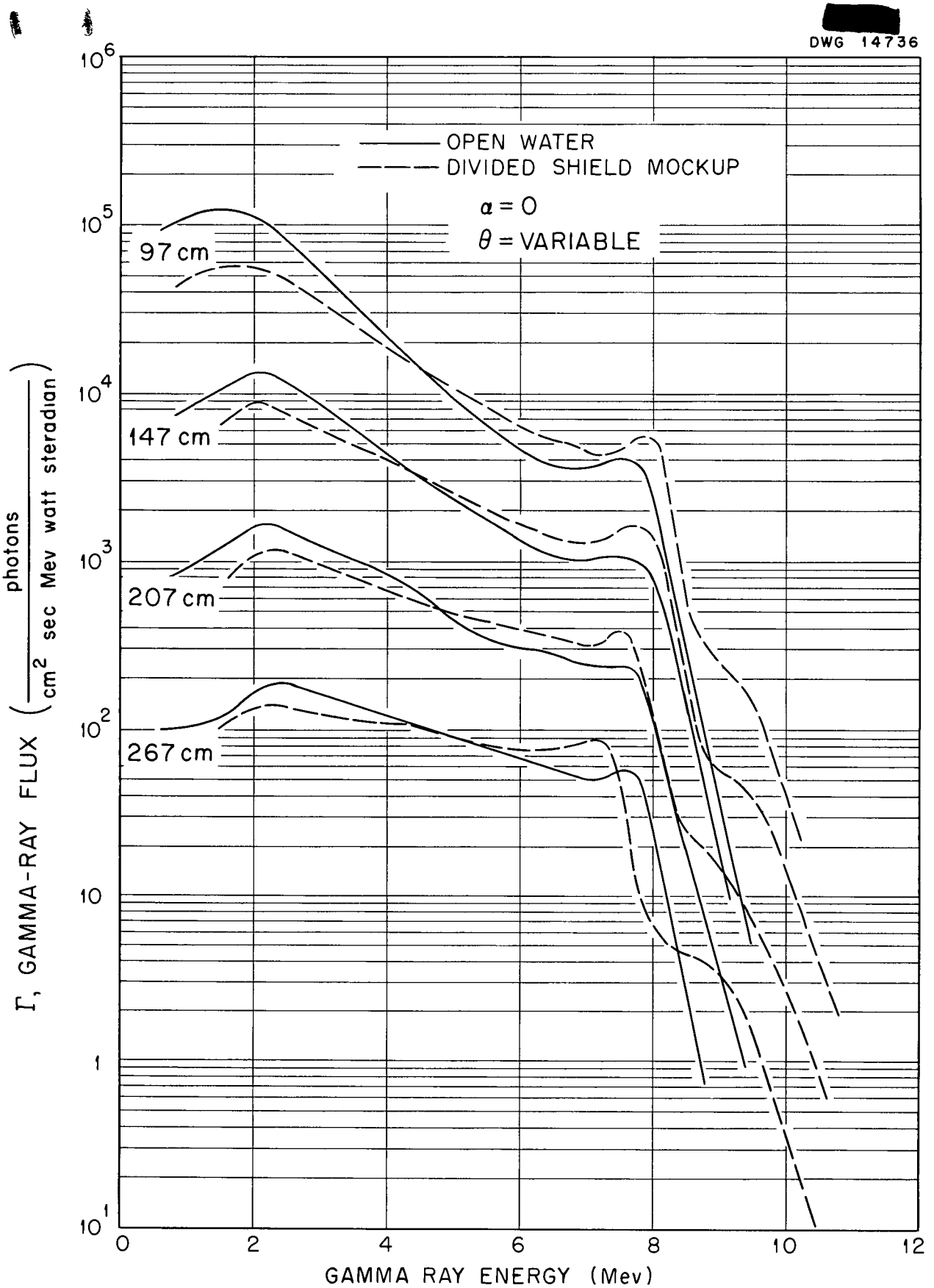

Fig 17 Gamma-Ray Flux as a Function of Energy and Distance from the Bulk Shielding Reactor (OW and DSM)

Azimuthal Angles Further measurements were made in an effort to learn something of the dependence of the angular distribution of the gamma-ray energy spectra upon the azimuthal angle (see Fig 12), that is, the angle out of the horizontal plane through the reactor center Unfortunately, the gamma-ray spectrometer was not designed for such measurements, since the collimator could not be moved from the horizontal plane However, information was obtained by vertically displacing the spectrometer out of the center plane (plane No 1 in Fig 42), while the collimator remained horizontal The angle θ was adjusted throughout these measurements so that the collimator always looked at the edge of the shadow shield The rather complicated geometry which resulted is discussed further in Appendix D

Other Shield Spectra

A limited number of measurements were carried out at other shield thicknesses The angular distribution was measured at 97 cm which was near the edge of the steel tank of the divided shield mockup Straight-ahead measurements ($\alpha = 0$) only were made at 207 and 267 cm

Discussion

Sources of Gamma Radiation

The major sources of gamma radiation emitted from the reactor are prompt-fission gamma rays, fission-product gamma rays, and neutron-capture gamma rays Gamma radiation produced in the shield arises from neutron capture and inelastic scattering Little is known about these sources except the neutron-capture gamma rays which have been extensively

investigated above 3 Mev by Kinsey and co-workers at Chalk River [12] Some of the peaks which appear in the spectra are explained by known capture levels (see Table 3)

Table 3 Peaks in Reactor and Shield Spectra

Energy (Mev)	Possible Source of Radiation
0 40	?
0 49	$B^{10}(n,\alpha)Li^{7*}$ (from boron in spectrometer liner) and annihilation radiation
2 2	$H(n,\gamma)$ (from water)
6 2	$Al^{27}(n,\gamma)$ (from aluminum reactor structure) ?
7 6	$Al^{27}(n,\gamma)$ (from aluminum reactor structure)
9 4[a]	$Fe^{54}(n,\gamma)$ (from steel tank in divided shield mockup)

a Figures 9, 11, 12, and 17 show this gamma-ray peak It should be noted that Fe^{54} is only 6% abundant and that Fe^{56} capture gamma rays make a much larger contribution to the spectrum but are not so apparent because of their lower energy

Angular Distributions

For calculations of the air scattering of gamma radiation into the crew shield, it was necessary to have a knowledge of the angular distribution of radiation emerging from the reactor shield Such distributions could be readily derived from the energy spectra as a function of angle, where

12 B B Kinsey and G A Bartholomew, "Neutron Capture γ-Rays from Titanium, Chromium, Iron, Nickel, and Zinc," Phys Rev 89, 375 (1953)

sufficient angles had been measured Figure 18 shows the angular distribution for $\alpha = 0$, $d' = 147$ cm for five values of gamma-ray energy Figure 19 presents the same data on a logarithmic-polar plot and all later angular distributions are also plotted on logarithmic scales The linear plot of Fig 18, however, does clearly show the very marked degree of collimation of the radiation escaping from the reactor shield As expected, the higher energy radiation was more collimated than the lower energy radiation In particular, for energies below that of the water capture gamma ray, the distribution becomes quite broad

The angular distribution behind the lead disks ($\alpha = 0$) is shown in Fig 20 The intensities were such that only relatively few points could be taken for the high energy gamma radiation but the distributions do not look appreciably different from those obtained with no lead in the water shield

The angular distributions obtained near the edge of the shadow shield are shown in Figs 21 and 22 As would be expected the curves are rather more complicated than those at $\alpha = 0$ However, the radiation at $\alpha = 50^{\circ}$ appears to be divided into two components (1) a radial component which corresponds to the radiation seen at $\alpha = 0$, and (2) another component which apparently has its origin at the edge of the shadow shield Since this latter component is strong even at high energy, it would appear likely that it is not scattered around the edge of the shield but is rather due to capture gamma radiation produced in the steel tank at the side of the reactor. At $\alpha = 60^{\circ}$, the two above components merge into one broad peak

[redacted]

DWG 14737A

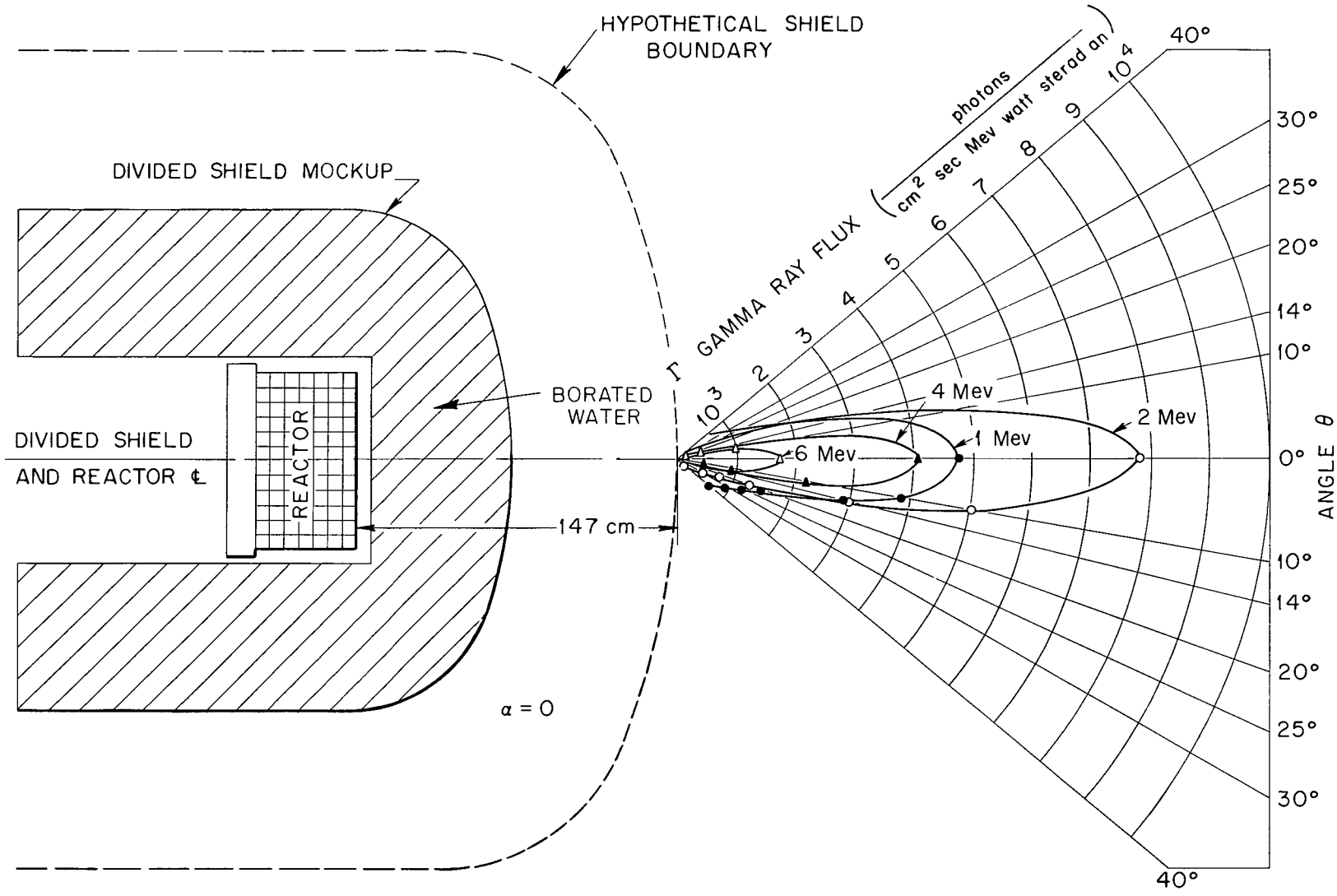

Fig 18 Gamma Ray Flux as a Function of θ for Various Energies (DSM) (Linear Plot)

[redacted]

DWG 14236R1

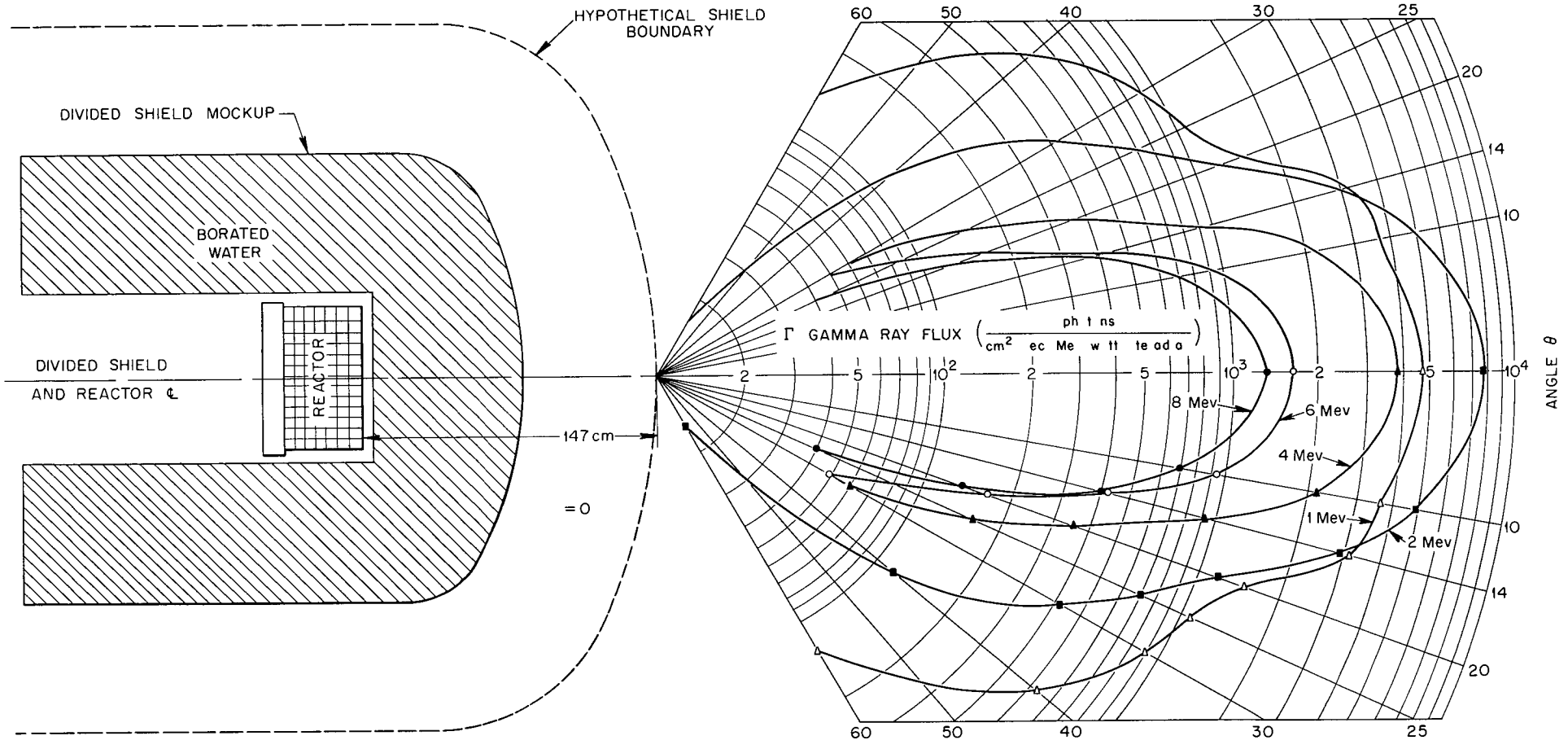

Fig 19 Gamma Ray Flux as a Function of θ for Various Energies (DSM) (Log Plot)

[redacted]

[redacted]

DWG 15757

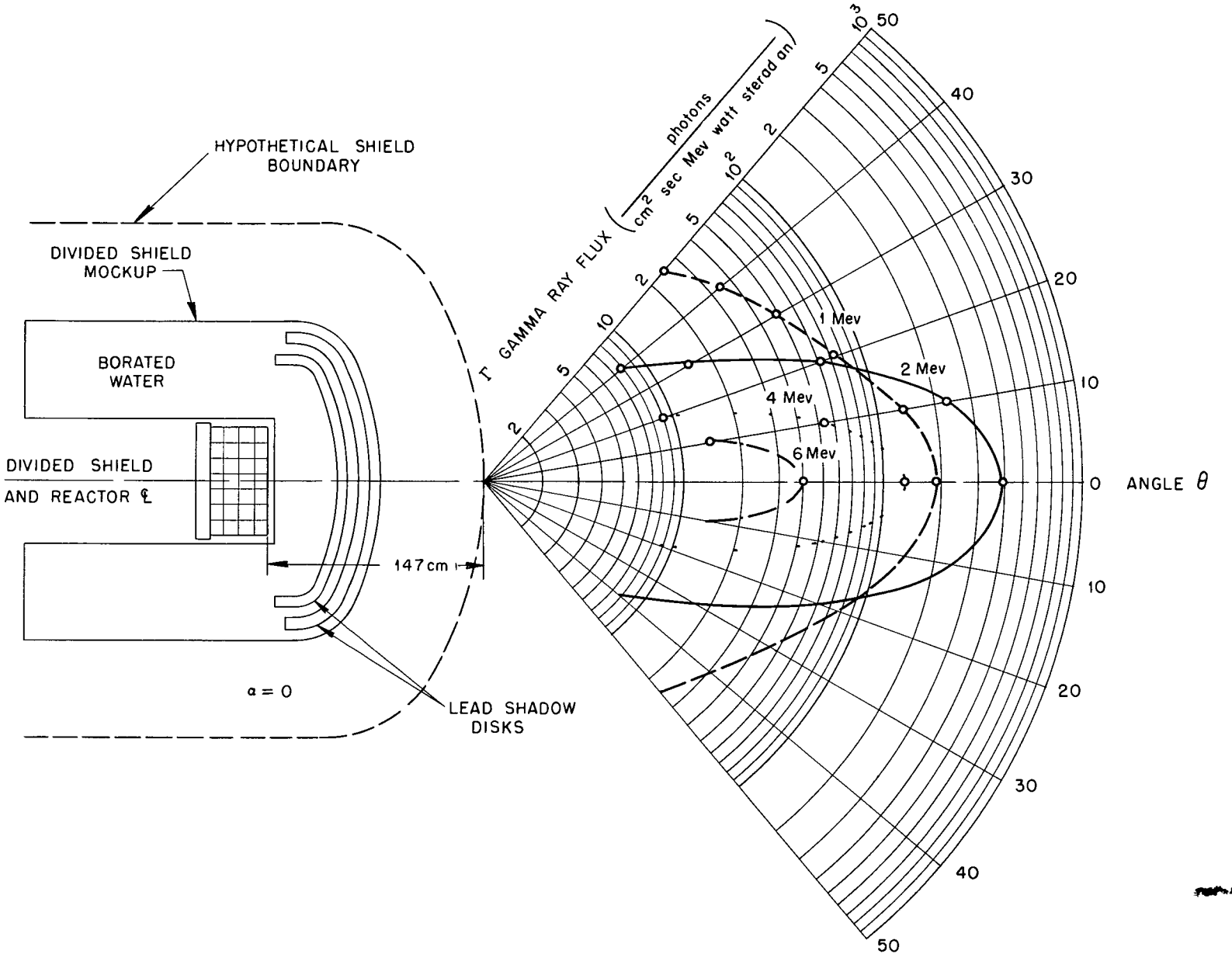

Fig 20 Gamma Ray Flux as a Function of θ for Various Energies (DSML α = 0)

[redacted]

[redacted]

DWG 15758

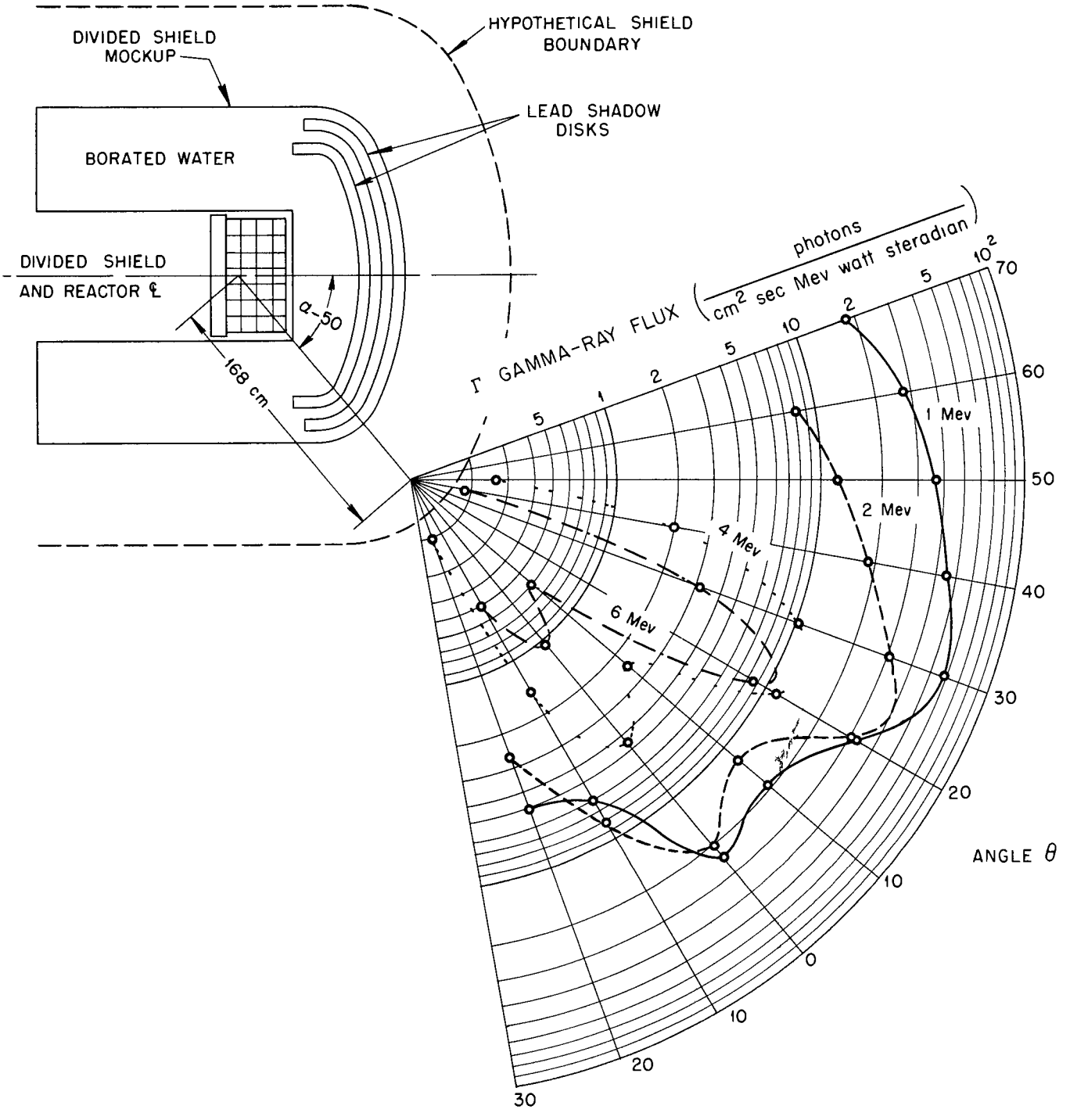

Fig 21 Gamma Ray Flux as a Function of θ for Various Energies (DSML $\alpha = 50$)

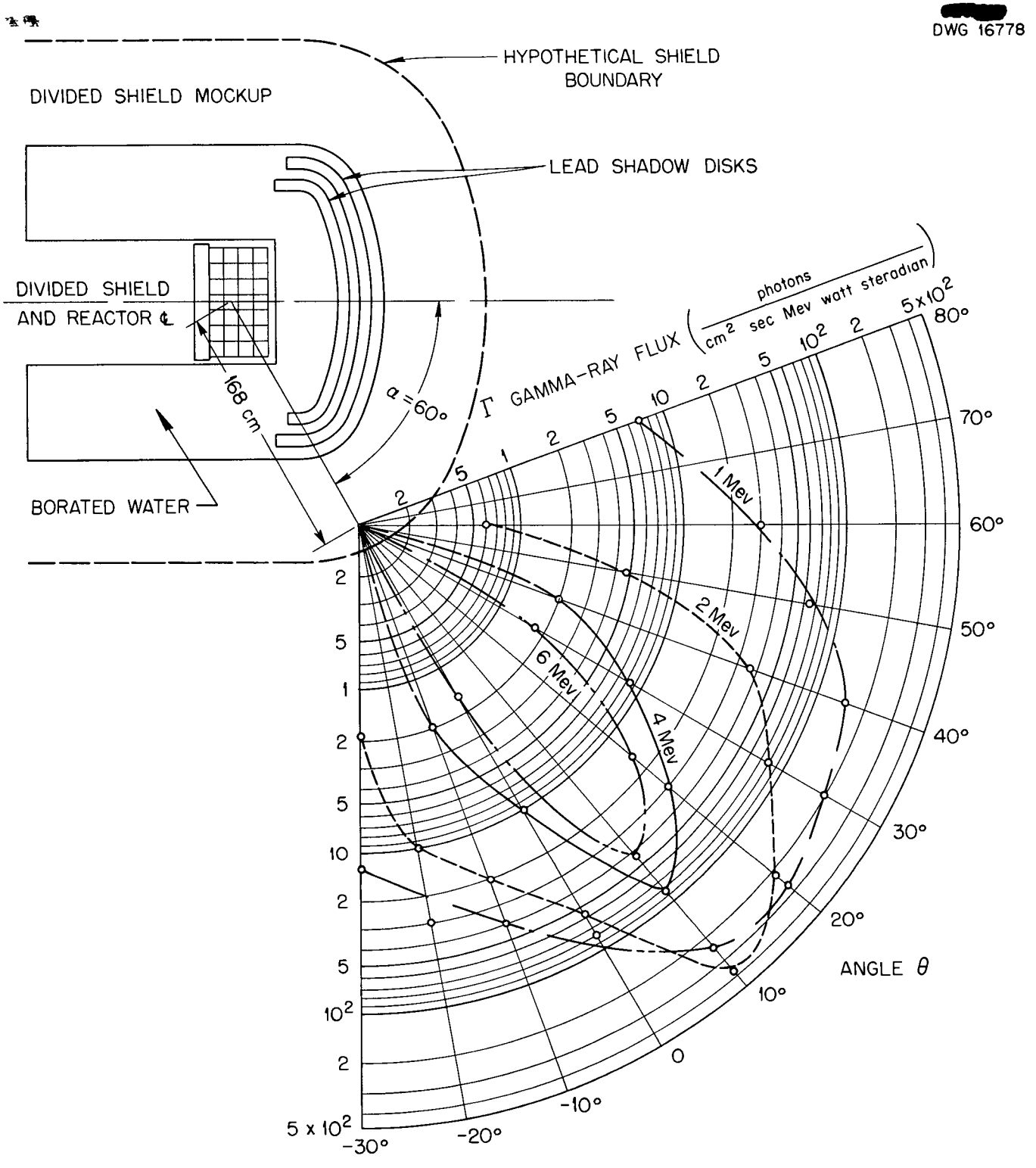

Fig 22 Gamma-Ray Flux as a Function of θ for Various Energies (α = 60°, DSML)

Attenuations

Water Upon examining the gamma-ray spectra as measured through various thicknesses of water (Fig 17) a definite tendency toward increased flatness with increasing shield thickness is observed This "hardening" of the spectrum would be expected because of the decrease in the water cross section with increasing gamma-ray energy Counteracting this effect somewhat, however, is the "buildup" of the lower energy gamma rays due to degradation by Compton scattering of higher energy gamma radiation

When the gamma-ray attenuations as a function of energy are plotted (Fig 23), straight lines (within a few percent) result over most of the region from 97 cm outward. Therefore, apparent attenuation lengths may be determined as a function of energy Table 4 contains the results of such calculations together with a comparison with attenuation lengths calculated from the known gamma-ray cross sections It is seen that good agreement exists for the high energy radiation, while at lower energies, the effect of buildup and neutron capture rapidly increases the experimentally determined relaxation lengths

Lead The attenuation of the gamma-ray flux by the two lead disks is shown in Fig 24 as a function of energy The fraction of radiation transmitted is plotted for different values of the angle θ ($d' = 147$ cm, $\alpha = 0$) For the data at $\theta = 0$, which would be expected to be the least affected by scattered radiation, a peak in the transmission is observed at about 2 5 Mev As θ increases, the peak moves to lower energies until at $\theta = 30^{\circ}$ the transmission decreases smoothly with increasing energy It should be noted that the 4 5-in lead shield was encased in a total of 1 5 in. of steel

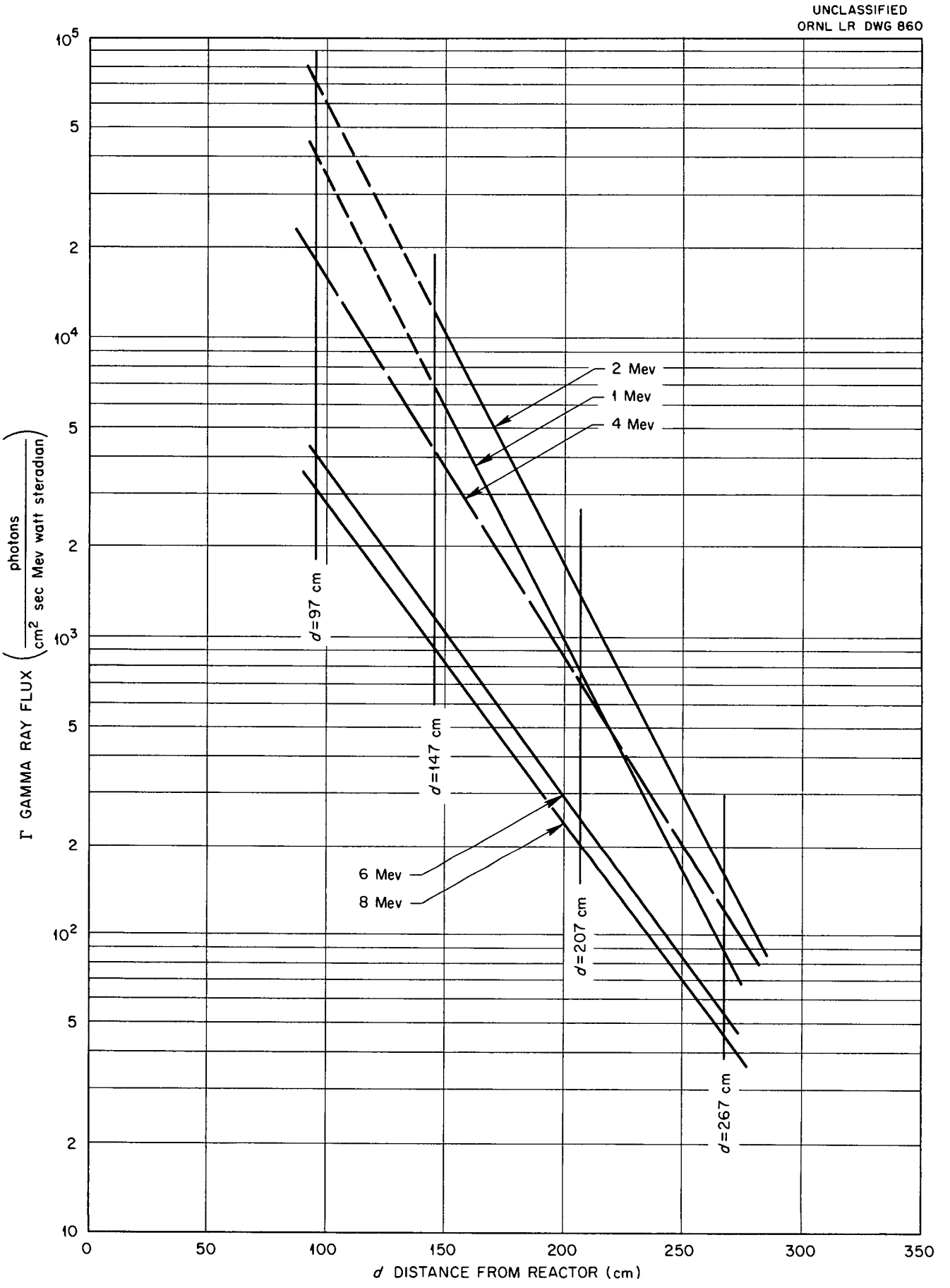

Fig 23 Gamma-Ray Attenuation in Water as a Function of Energy

[redacted]

ORNL-LR-DWG 861

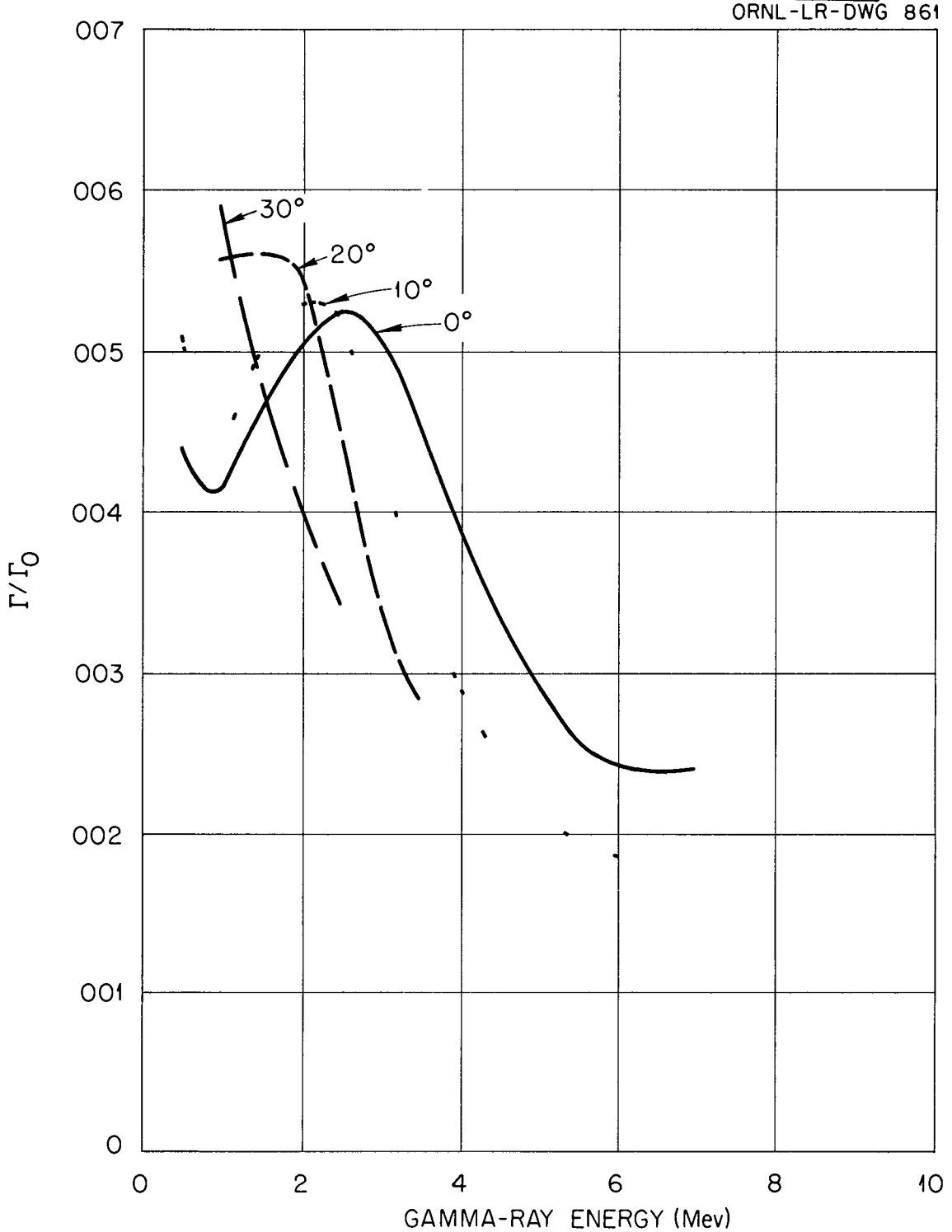

Fig 24 Reduction of Gamma-Ray Flux Due to Presence of Lead Disks

Table 4 Apparent Relaxation Lengths for Various Energy Gamma Rays from the BSR in Water

Gamma-Ray Energy (Mev)	d', Reactor-Spectrometer Distance for Which Straight Line Is Obtained (cm)	Relaxation Length (cm)	
		From This Experiment	From Cross Section
1	147 to 267	28	14
2	147 to 267	29	20
4	97 to 267	34	30
6	97 to 267	40	37
7 6	97 to 267	40	41

Boron Suppression of capture gamma radiation by the boron in the boared water of the divided shield mockup may be seen directly in Figs 9, 12, and 17 The effect is most pronounced at the energy of the water capture gamma ray (2 2 Mev) At 7 5 Mev, the borated water had no appreciable effect at all In fact, the high energy radiation was higher with the borated divided shield mockup than with open water owing to the captures in the steel tank of the mockup

Dose

The angular distribution data for d'= 147 cm and $\alpha = 0^{\circ}$ were sufficiently complete to permit an estimate of the gamma-ray dose at this point The dose is given by [13]

13 R H Ritchie, "Tentative Comparison of Ionization Chamber and Spectrometer Measurements at the BSF," CF-51-10-203 (Oct 31, 1951)

$$D = 2\pi \int_{-1}^{1} d\mu \int_{0}^{E_{max}} \frac{\Gamma(E,\theta)}{\gamma(E)} dE \qquad (\mu = \cos\theta)$$

where D is given in r/hr/watt if $\gamma(E)$ is the dose-to-flux conversion factor in (photons/cm^{2}sec Mev)/(r/hr) and $\Gamma(E,\theta)$ is the gamma-ray flux in photons/cm^2 sec Mev In order to carry out the integration, $\Gamma(E,\theta)$ was taken from Figs 11 and 13 which present data for the divided shield mockup without and with the lead disks, respectively Dividing $\Gamma(E,\theta)$ by $\gamma(E)$ resulted in curves of $D(E,\theta)$ as shown in Figs 25 and 26 An integration over E gave values of $D(\theta)$ vs $\cos\theta$, as shown in Figs 27 and 28 The final integration over the elevation angle θ gave the dose values shown in Table 5, where the corresponding values obtained with an ionization chamber are also shown In both cases the dose as calculated from the spectrometer data is about a factor of 3 larger than the ionization chamber data It appears likely that this discrepancy is partly due to background radiation penetrating the collimator walls at large values of the angle θ The background contribution due to scattering down the spectrometer collimator does not appear to be large from the data shown in Fig 5, but, of course, no studies of the collimator could be carried out with high energy gamma radiation

Table 5 Gamma-Ray Dose behind the Divided Shield Mockup
($d' = 147$ cm, $\alpha = 0$)

Shield	Dose (r/hr watt)	
	Calculated from Gamma-Ray Flux	Measured with Ion Chamber
DSMB	$2\ 3 \times 10^{-2}$	$6\ 26 \times 10^{-3}$
DSML	$8\ 6 \times 10^{-5}$	$2\ 97 \times 10^{-5}$

[redacted]

DWG 14732

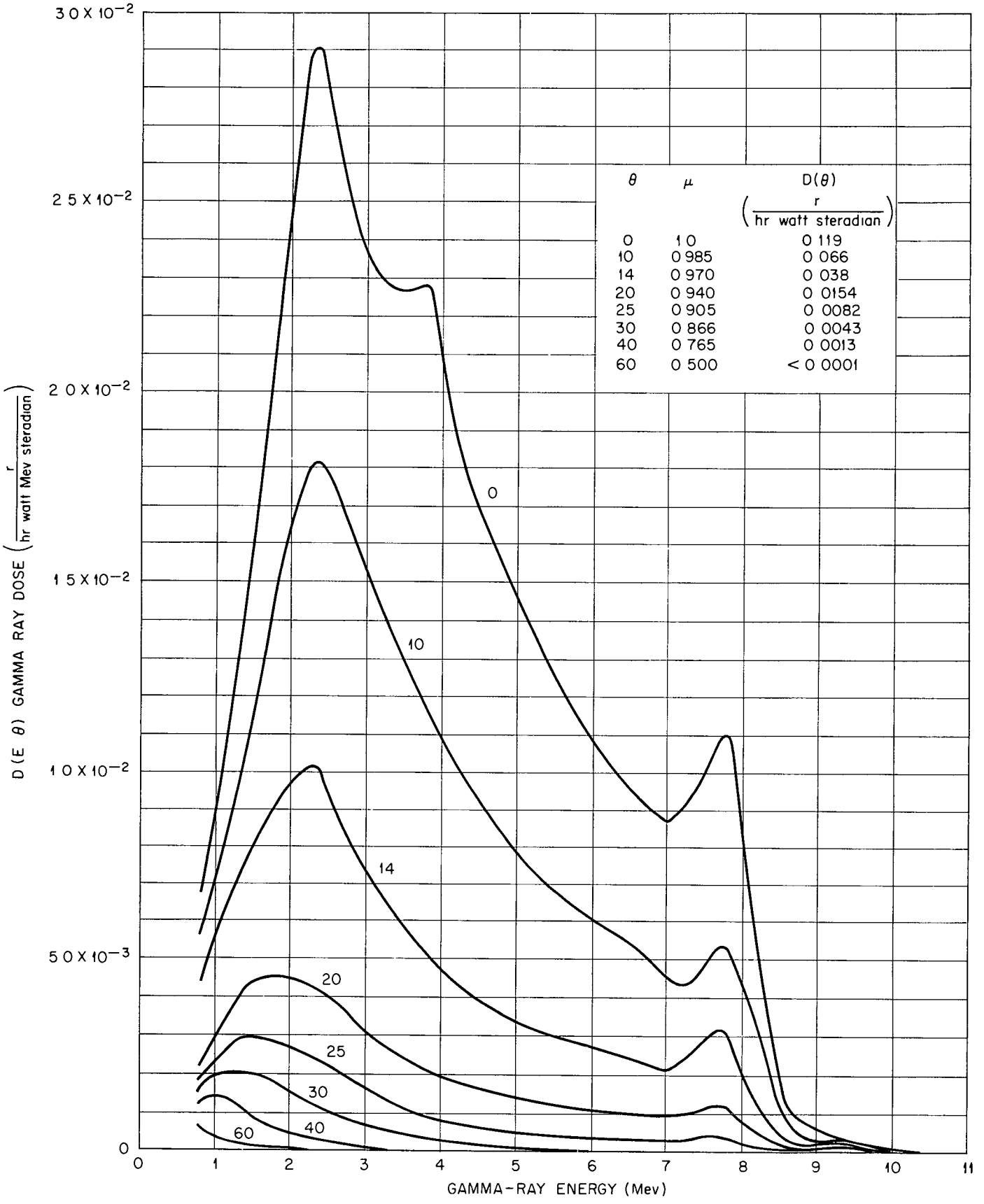

θ	μ	D(θ) (r / hr watt steradian)
0	1 0	0 119
10	0 985	0 066
14	0 970	0 038
20	0 940	0 0154
25	0 905	0 0082
30	0 866	0 0043
40	0 765	0 0013
60	0 500	< 0 0001

Fig 25 Gamma-Ray Dose 147cm from the Bulk Shielding Reactor (DSM)

[redacted]

ORNL LR DWG 862

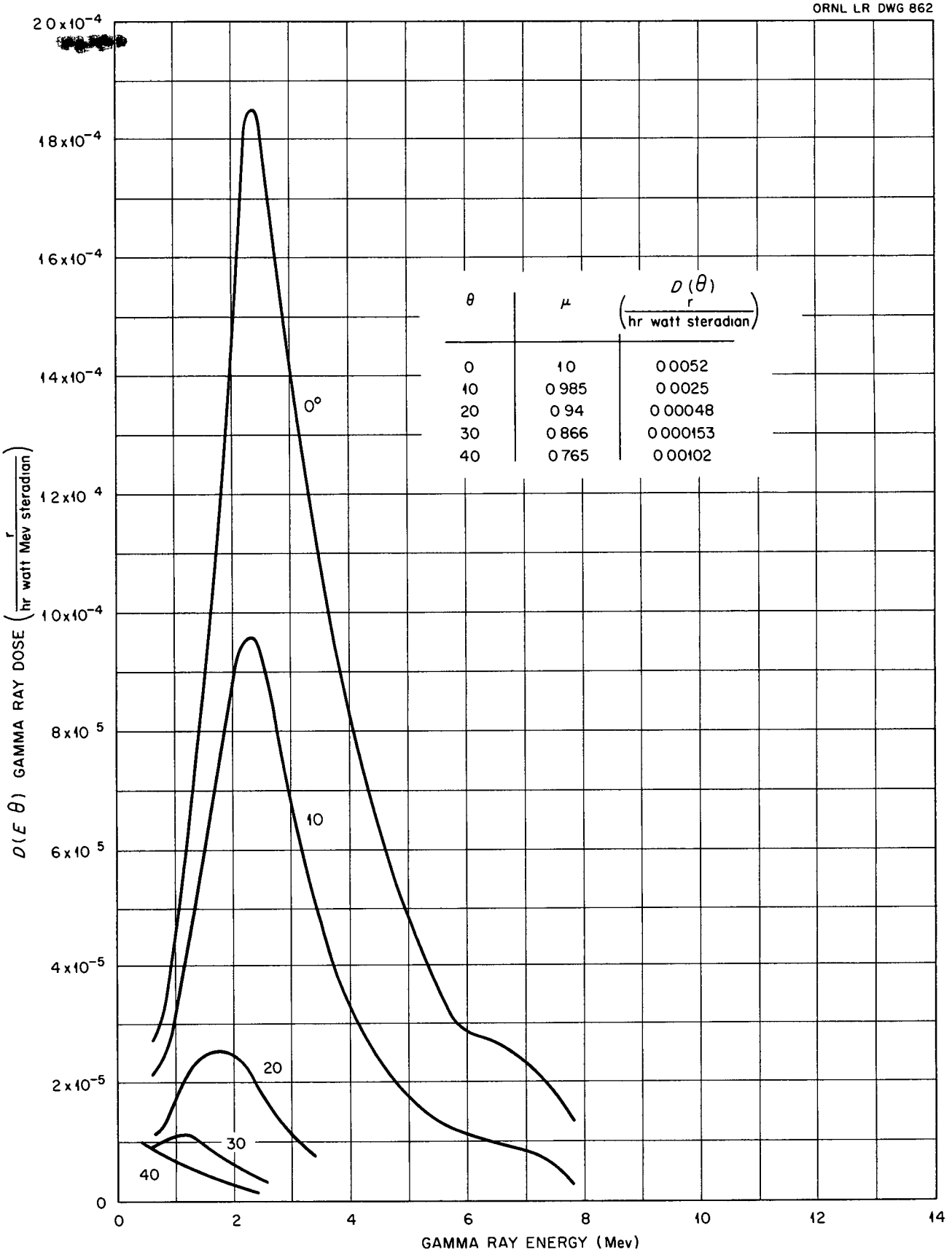

θ	μ	D(θ) (r / hr watt steradian)
0	1.0	0.0052
10	0.985	0.0025
20	0.94	0.00048
30	0.866	0.000153
40	0.765	0.00102

Fig 26 Gamma Ray Dose 147 cm from the Bulk Shielding Reactor (DSML)

[redacted]

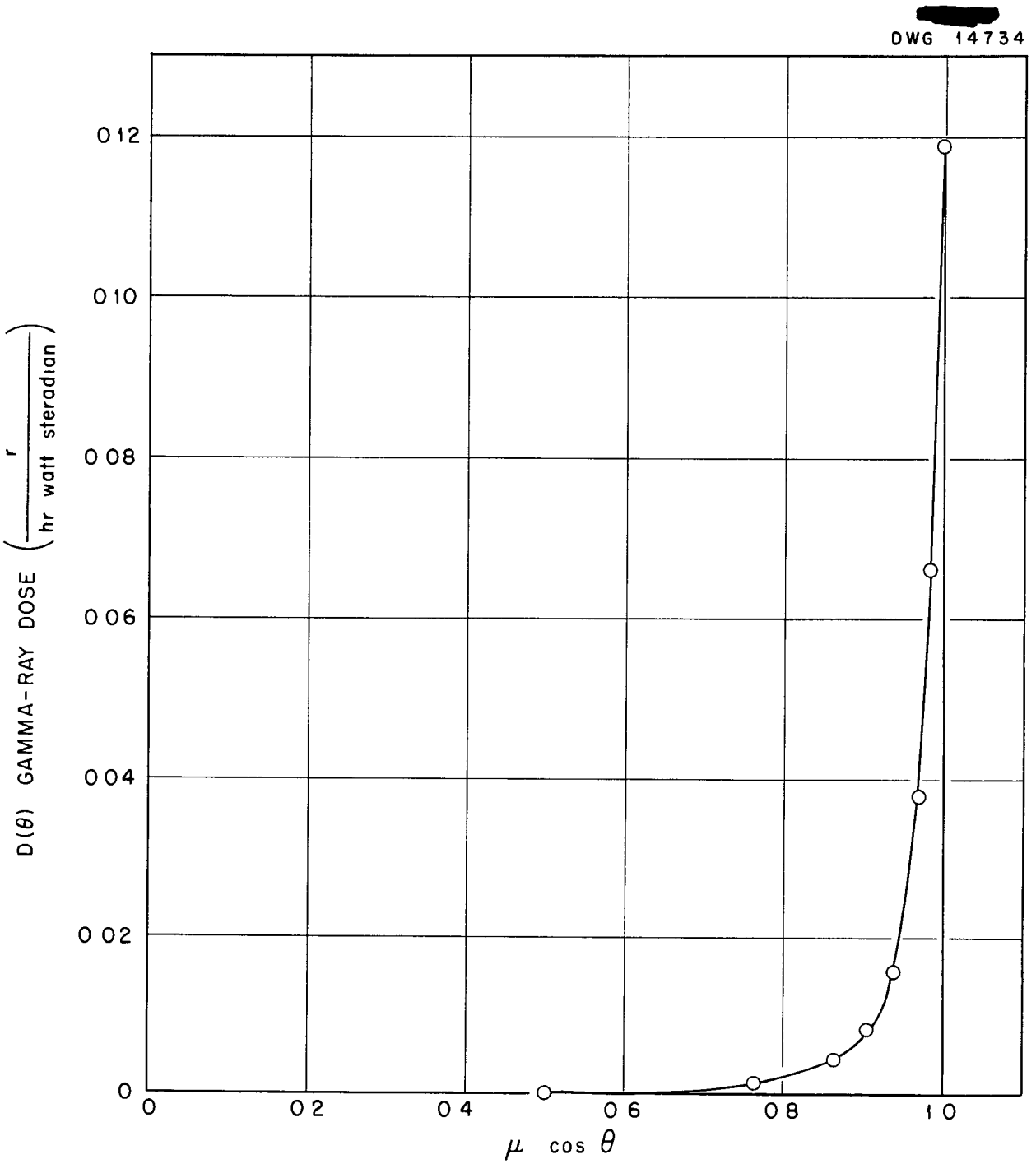

Fig 27 Gamma-Ray Dose 147 cm from the Bulk Shielding Reactor as a Function of cos θ (DSM)

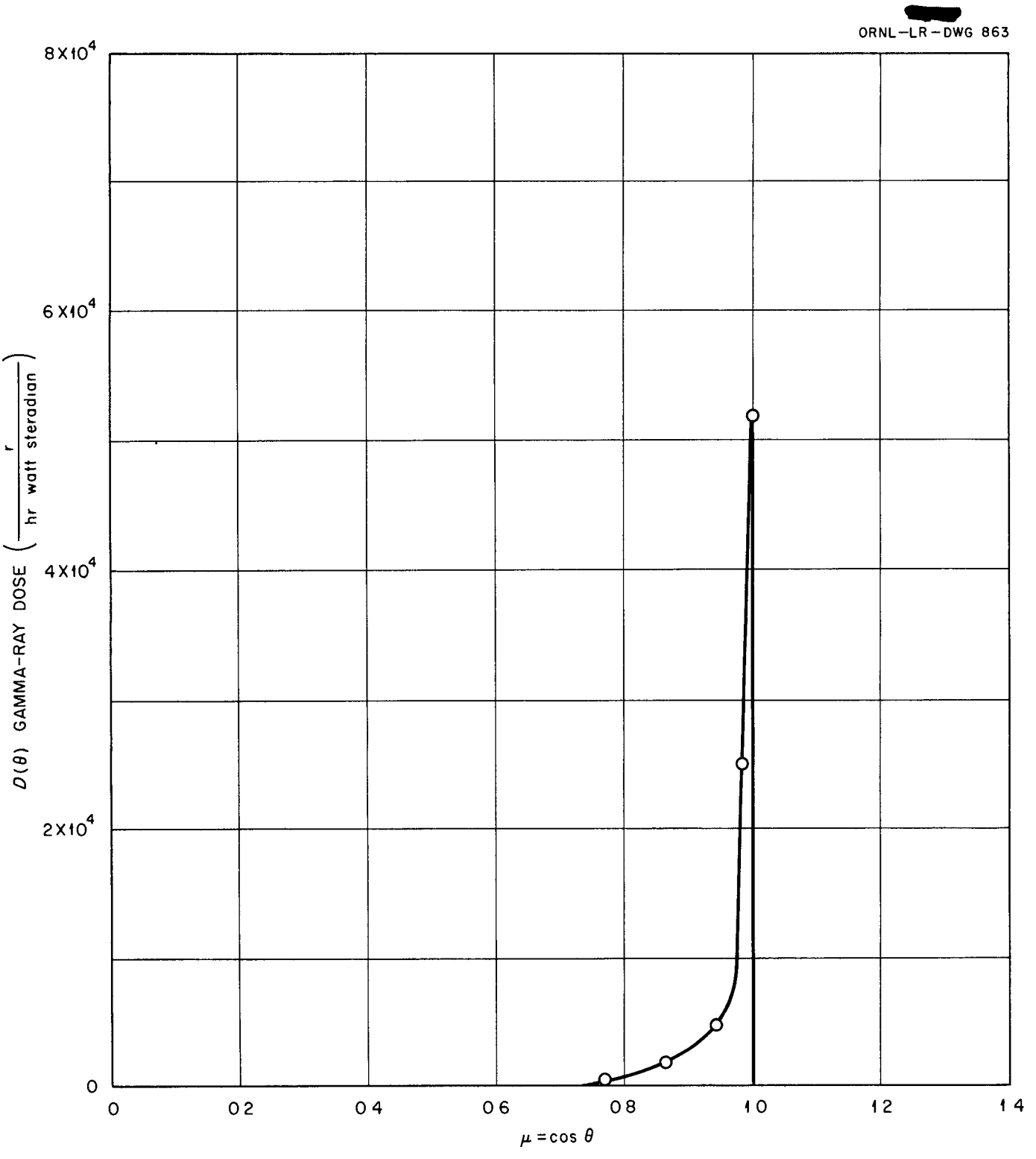

Fig 28 Gamma-Ray Dose 147 cm from the Bulk Shielding Reactor as a Function of cos θ (DSML)

II AIR SCATTERING CALCULATIONS[1]

In this section is presented a method for the calculation of the air scattering of the gamma radiation escaping from the ANP-53 reactor shield The experimental measurements of gamma-ray spectra and angular distribution presented in Part I of this report are used in these calculations and should make them more reliable than earlier calculations[2] of gamma-ray air scattering which used arbitrary energies and angular distributions However, as mentioned earlier, the experimental measurements are still far from complete and the necessary extrapolation of the data could give rise to large errors

The following assumptions were made

(1) The actual scattering geometry used by the 1950 ANP Shielding Board[2] was employed except that the crew compartment was replaced by a simple cylinder of about the same dimensions The reactor shield as a source of radiation was assumed to be cylindrically symmetric about the aircraft axis

(2) Single scattering was assumed

---

1 Earlier calculations of the gamma radiation reaching the outside of the ANP-53 crew compartment were reported by Frank Bly and F C Maienschein, "A Calculation of the Gamma Radiation Reaching the ANP-53 Crew Shield, ORNL-CF-53-5-117 (May 23, 1953)

2 "Report of the Shielding Board for the Aircraft Nuclear Propulsion Program," ANP-53 (Oct 16, 1950)

(3) Air attenuation was neglected

Figure 29 shows the geometry of the divided shield The reactor shield, although represented as spherical, is actually closer to the revolution of a logarithmic spiral Since the thick side is forward, the shield radius, r^*, decreases with an increasing source angle α The receiver is taken to be a sphere of 1-cm^2 cross section located at the center of the crew compartment In addition to the source angle α, the angles β, ϕ, θ and Ψ will be referred to respectively as the receiver, azimuth, elevation, and scattering angles The lengths, r, R, and H are respectively the prescattering, postscattering and direct radiation paths The reactor-crew separation distance is s Figure 30 shows a simplified sketch of the same system and defines the various lengths as vectors

General Air Scattering Calculations

An expression for the number of gammas hitting the receiver can now be derived At $[\gamma E]$, the point of gamma emergence,

$$\frac{\text{photons}}{\text{watt}\cdot\text{Mev cm}^2\text{ sec steradian}} \equiv \Gamma(\alpha, E, \phi, \theta)$$

where E is the photon energy (Mev) before scatter At $[\gamma S]$, the point of gamma scatter,

$$\frac{\text{photons}}{\text{watt Mev cm}^2\text{ sec}} = \int_{-\pi}^{\pi} \int_{0}^{\pi/2} \Gamma \sin\theta \, d\theta \, d\phi$$

$$= 2 \int_{0}^{\pi} \int_{0}^{\pi/2} \Gamma \sin\theta \, d\theta \, d\phi$$

[redacted]

DWG 19856

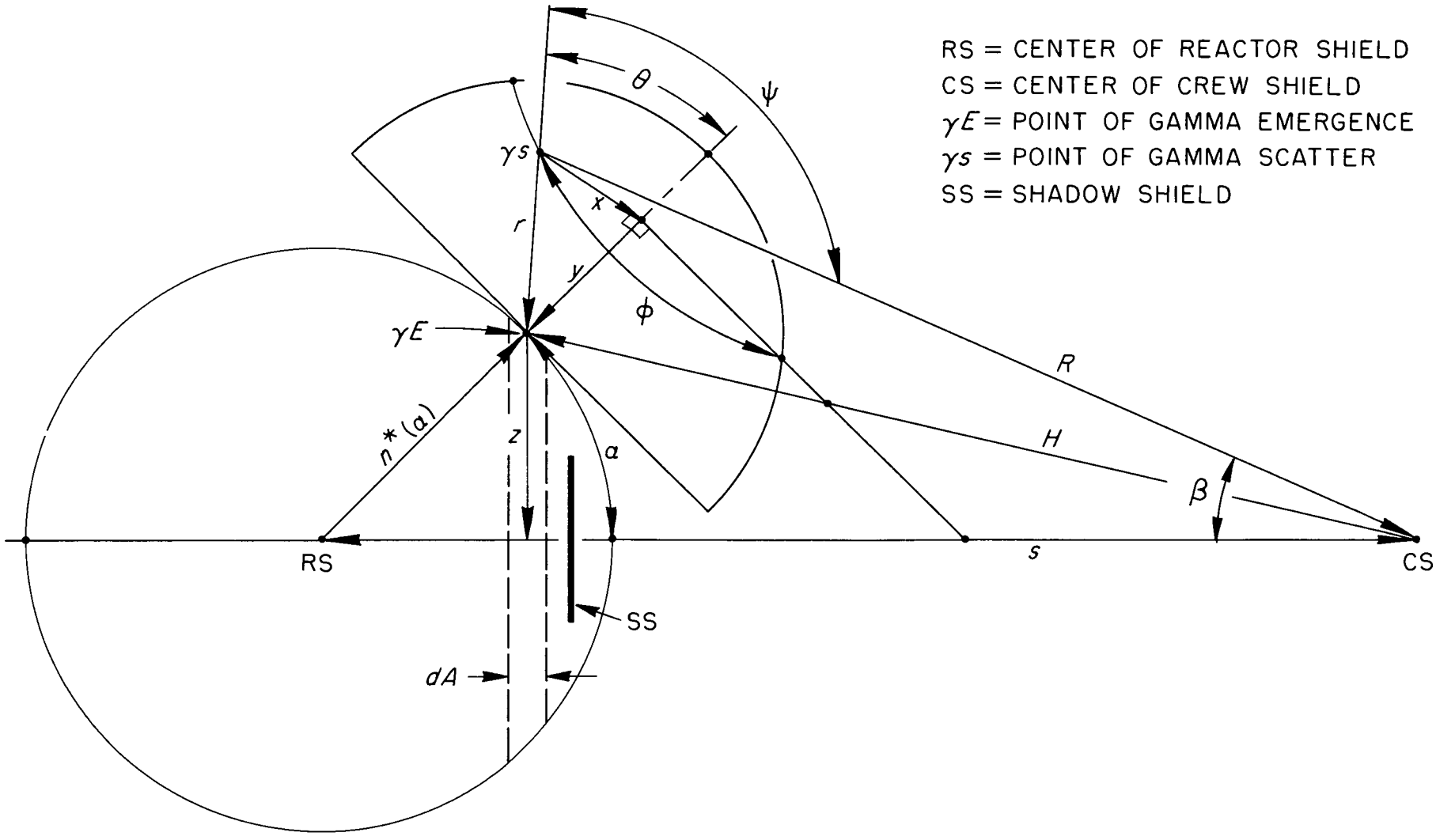

Fig 29 Geometry of the Divided Shield

[redacted]

DWG 19857

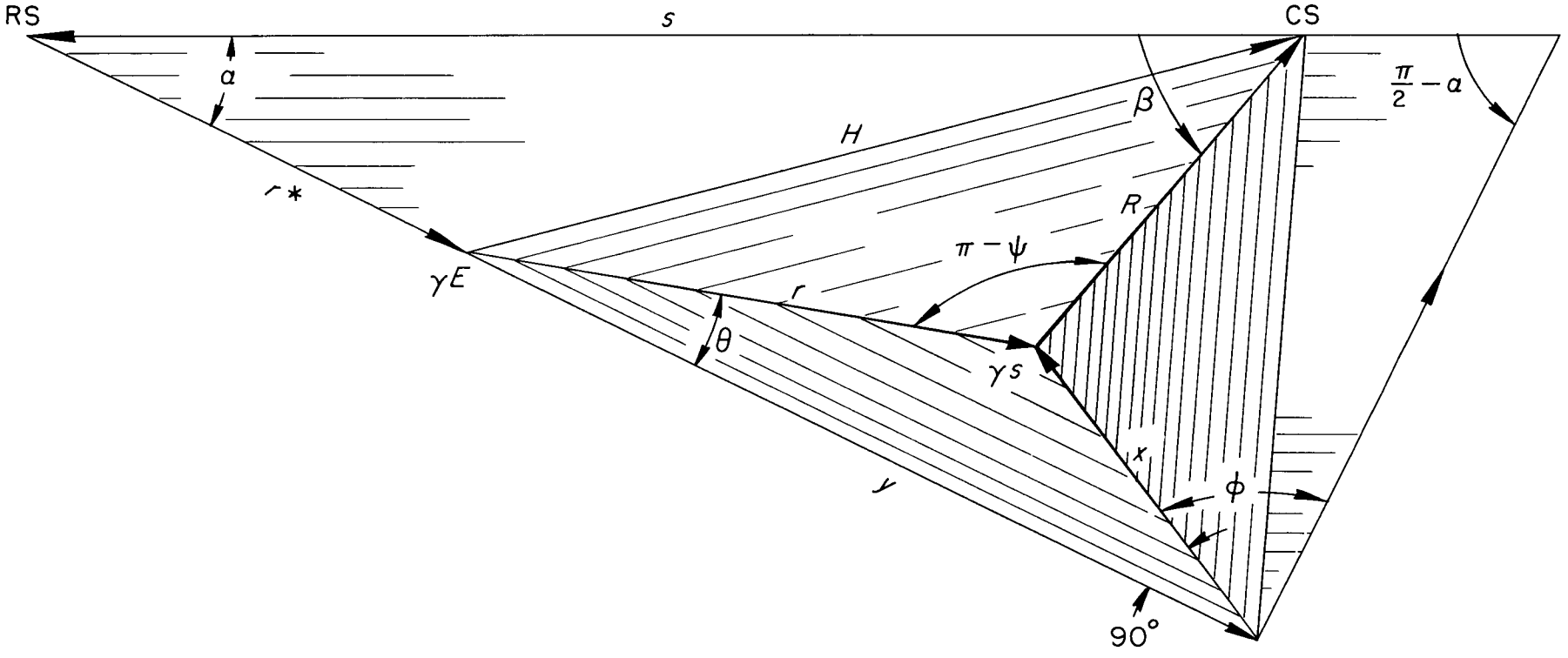

Fig 30 Divided Shield Geometry, Showing Vectors Used in Calculations

since $\Gamma(\phi,\theta)$ is symmetrical about the plane [RS] [γE] [CS], where [RS] is the center of the reactor shield and [CS] is the center of the crew-shield At [CS],

$$\frac{\text{photons toward receiver}}{\text{watt Mev cm}^2\ \text{sec}} \equiv \frac{\Phi}{P}(\alpha,E,\phi,\theta)$$

$$= 2N_e \int_0^{\pi} \int_0^{\pi/2} \int_{r_a}^{r_b} K(\Psi,E)R^{-2}(\alpha,r,\phi,\theta)\ \sin\theta\ dr\ d\theta\ d\phi$$

where

P = reactor power (watts),

N_e = electron density of air = 3 88 x 10^{20} cm^{-3},

$K(\Psi,E)$ = Klein-Nishina cross section (cm^2/electron steradian),

Ψ = scattering angle, which is determined by the other variables,

$R^{-2}(\alpha,r,\phi,\theta)$ = reciprocal square of postscattering path

= solid angle subtended by receiver from point of scatter

If an integration is made over the energy and reactor shield surface,

$$\frac{\Phi}{P} = \frac{\text{photons hitting receiver}}{\text{sec watt}}$$

$$= 2N_e \int^{A} \int_{E_a}^{E_b} \int_0^{\pi} \int_0^{\pi/2} \int_{r_a}^{r_b} KR^{-2}\Gamma \sin\theta\ dr\ d\theta\ d\phi\ dE\ dA$$

$$= 4\pi N_e \int_{\alpha_a}^{\alpha_b} r^{*2}(\alpha)\ \sin\alpha \int_0^{\pi/2} \sin\theta \int_0^{\pi}\int_{r_a}^{r_b} R^{-2} \int_{E_a}^{E_b} \Gamma K\ dE\ dr\ d\phi\ d\alpha \quad (1)$$

In order for Eq (1) to be of use, K and R^{-2} must be found as functions

of the variables of integration One form of the expression for K is [3]

$$K(\Psi,E) = 3\ 971 \times 10^{-26} \left\{ \frac{1}{1 + 1\ 96E(1 - \cos\psi)^2} \left[1 + \cos^2\psi + \frac{(1\ 96E)^2\ (1 - \cos\psi)^2}{1 + 1\ 96E(1 - \cos\Psi)} \right] \right\} \tag{2}$$

where

$$\cos\Psi = \frac{1}{R}\left[s(\cos\alpha\ \cos\theta + \sin\alpha\ \cos\phi\ \sin\theta) - r - r^* \cos\theta \right] \tag{3}$$

as determined in Appendix A An expression for R^{-2} is also determined in Appendix A

$$R^2 = r^2 + 2rr^* \cos\theta - 2rs(\cos\theta\ \cos\alpha + \sin\theta\ \cos\phi\ \sin\alpha) - 2r^* s\ \cos\alpha + r^{*2} + s^2 \tag{4}$$

The energy after scattering, E', can be found from the Compton equation

$$E' = \frac{E}{\left[1 + 1\ 96E(1 - \cos\Psi)\right]} \tag{5}$$

The angle β is found by substituting $R_{\bar{j}} = R\cos\beta$ into the second equation of Eqs (25) in Appendix A and rearranging,

$$\cos\beta = \frac{1}{R}\left[s - r(\cos\theta\ \cos\alpha + \sin\theta\ \cos\phi\ \sin\alpha) - r^* \cos\alpha \right] \tag{6}$$

---

3 C M Davisson and R D Evans, "Gamma-Ray Absorption Coefficients," Rev Mod Phys 24, 79 (1952)

Partitions

In principle, Eqs (1), (2), (3), and (4) give the gamma radiation reaching the crew position For numerical integration, Eq (1) can be approximated as follows Partition α, θ, ϕ, r, E and β at several points each, represented by α_k, θ_i, ϕ_j, r_m, E_n, and β_p, respectively, and let

$$\delta\eta_v = \eta_v - \eta_{v-1}$$

$$\bar{\eta}_v = \frac{\eta_v + \eta_{v-1}}{2}$$

$$f_v = f(\bar{\eta}_v)$$

Then, if sub q = sub kijmn,

$$\Phi_q/P = 4\pi N_e r_k^{*2} \sin\alpha_k \, \delta\alpha_k \sin\theta_i \, \delta\theta_i \, \delta\phi_j \, R_{kijm}^{-2} \, \delta r_m \, \Gamma_{kijm} \, K_{kijmn} \, \delta E_n \tag{7}$$

where

$$\left.\begin{aligned}
R_{kijm}^2 &= \bar{r}_m^2 + 2\bar{r}_m r_k^* \cos\bar{\theta}_i - 2\bar{r}_m s(\cos\bar{\theta}_i \cos\bar{\alpha}_k + \sin\bar{\theta}_i \cos\bar{\phi}_j \sin\bar{\alpha}_k) \\
K_{kijmn} &= 3\ 971 \times 10^{-26} \left\{ \frac{1}{\left[1 + 1\ 96\bar{E}_n(1 - \cos\Psi_{kijm})\right]^2} \left[1 + \cos^2\Psi_{kijm} \right.\right. \\
&\qquad \left.\left. + \frac{(1\ 96\bar{E}_n)^2(1 - \cos\Psi_{kijm})^2}{1 + 1\ 96\bar{E}_n(1 - \cos\Psi_{kijm})} \right] \right\} \\
\cos\Psi_{kijm} &= \frac{1}{R_{kijm}} \left[s(\cos\bar{\alpha}_k \cos\bar{\theta}_i + \sin\bar{\alpha}_k \cos\bar{\phi}_j \sin\bar{\theta}_i) - \bar{r}_m - r_k^* \cos\bar{\theta}_i \right]
\end{aligned}\right\} \tag{8}$$

Furthermore,

$$\left.\begin{aligned} E'_q &= \frac{\bar{E}_n}{\left[1 + 1\ 96\bar{E}_n(1 - \cos\Psi_{kijm})\right.} \\ \cos\beta_q &= \frac{1}{R_{kijm}}\left[s - \bar{r}_m(\cos\bar{\theta}_i \cos\bar{\alpha}_k + \sin\bar{\theta}_i \cos\bar{\phi}_j \sin\bar{\alpha}_k) - r_k^* \cos\bar{\alpha}_k\right] \end{aligned}\right\} \quad (9)$$

From Eqs (7), (8), and (9), then, β_q, E'_q and Φ_q/P can be computed

Further if

$D(\beta,E')$ = dosage rate inside crew shield,

$\gamma(E')$ = proportionality factor between gamma-ray flux and dosage,

$\mu(\beta,E')$ = absorption coefficient of crew shield,

$\epsilon(\beta,E')$ = buildup factor of crew shield,

$t(\beta)$ = oblique thickness of crew shield,

$$\frac{D_q}{P} = \gamma_q \frac{\Phi_q}{P} e^{-\mu_q t_q} (1 - \epsilon_q) \quad (10)$$

and the total dosage rate, D, is given by

$$\frac{D}{P} = \sum_q \frac{D_q}{P} \quad (11)$$

When no crew shield is considered, of course,

$$\frac{D_q}{P} = \gamma_q \frac{\Phi_q}{P} \quad (12)$$

Radial Emission of Photons

It is apparent that for a reasonably fine meah, q takes on 10^4 to 10^5

values Thus it is highly desirable to reduce, if feasible, the number of variables of integration One manner in which this can be done is to assume radial emission of photons This assumption appears logical because of the marked radial character of the gamma radiation as was shown clearly in Fig 18 A calculation for a typical cell was carried out using both the radial assumption and the actual distribution (see Appendix B) Since the results differed by only about 18%, the radial emission assumption was used at all points except at the edge of the shadow shield For calculations around the edge of the shadow shield see the section "Skew Emission Calculations" below For radial emission one may define

$$\frac{\text{photons}}{\text{watt}\cdot\text{Mev cm}^2\ \text{sec}} = \Gamma^*(\alpha,E)$$

$$= 2\int_0^{\pi}\int_0^{\pi/2} \Gamma \sin\theta\, d\theta\, d\phi$$

Since $\theta = 0$, Eqs (7), (8), and (9) now become, respectively,

$$\frac{\Phi_q}{P} = 2\pi N_e r_k^{*2} \sin\bar{\alpha}_k\, \delta\alpha_k\, R_{km}^{-2}\, \delta r_m\, \Gamma^*_{kn}\, K_{kmn}\, \delta E_n \tag{13}$$

$$\left.\begin{aligned}
R_{km}^2 &= (\bar{r}_m + r_k^*)^2 - 2s(\bar{r}_m + r_k^*)\cos\bar{\alpha}_k + s^2 \\
K_{kmn} &= 3\ 971 \times 10^{-26}\left\{\frac{1}{\left[1 + 1\ 96\bar{E}_n(1 - \cos\Psi_{km})^2\right]}\left[1 + \cos^2\Psi_{km} + \frac{(1\ 96\bar{E}_n)^2(1 - \cos\Psi_{km})^2}{1 + 1\ 96\bar{E}_n(1 - \cos\Psi_{km})}\right]\right\} \\
\cos\Psi_{km} &= \frac{1}{R_{km}}\left[s\cos\bar{\alpha}_k - (\bar{r}_m + r_k^*)\right]
\end{aligned}\right\} \tag{14}$$

$$\left.\begin{aligned} E'_q &= \frac{\bar{E}_n}{\left[1 + 1\ 96\bar{E}_n(1 - \cos\psi_{km})\right]} \\ \beta &= \psi - \alpha \end{aligned}\right\} \quad (15)$$

To avoid computational difficulty due to tabulating β_q, it was desirable to take β as a variable of integration in place of r This transformation of variables, shown in Appendix C, converts Eqs (13) and (14) into the following

$$\frac{\Phi_q}{P} = 2\pi N_e r_k^{*2} \sin\bar{\alpha}_k\ \delta\alpha_k\ R_{kp}^{-2}\ F_{kp}\ \delta\beta_p\ \Gamma^*_{kn}\ K_{kmn}\ \delta E_n \quad (16)$$

$$\left.\begin{aligned} R^2 &= s^2\left[(\cos\bar{\alpha}_k + \sin\bar{\alpha}_k \cot\bar{\beta}_p)^{-2} - 2(1 + \tan\bar{\alpha}_k \cot\bar{\beta}_p)^{-1} + 1\right] \\ K_{knp} &= 3\ 971 \times 10^{-26}\left\{\frac{1}{\left[1 + 1\ 96E_n(1 - \cos\psi_{kp})\right]^2}\left[1 + \cos^2\psi_{kp} + \frac{(1\ 96\bar{E}_n)^2(1 - \cos\psi_{kp})^2}{1 + 1\ 96\bar{E}_n(1 - \cos\psi_{kp})}\right]\right\} \\ \psi_{kp} &= \bar{\alpha}_k + \bar{\beta}_p \end{aligned}\right\}^* \quad (17)$$

(In this case, sub q = sub knp and E'_q is found as before)

where

$$F(\alpha,\beta) \equiv \frac{s \sin\alpha}{\sin^2(\alpha + \beta)}$$

Values of the variables in these equations were determined as follows r_k^{*2} was scaled from the report[2] of the 1950 Shielding Board, s was taken as 1716 cm, the distance from the center of the reactor to the midpoint of the crew compartment, values of Γ^*_{kn} were determined as in Appendix B, α and β were partitioned at 10° intervals between 0 and 180°, E was partitioned at

* As shown in Reactor Handbook, Vol 1, Chap 2 9, p 831, Technical Information Service, U S Atomic Energy Commission (June, 1953), R^{-2} and F partially cancel out

1 2- to 2 5-Mev intervals between 0 8 and 10 25 Mev, and Φ_q/P and E'_q were computed on a UNIVAC after programming and coding by the ORNL Mathematics Panel

The dosage reaching the receiver was then computed by Eqs (11) and (12) Values of γ_q were taken from Blizard[4] Values of μ_q were obtained from Gladys White[5], and finally values of ϵ_q were taken from the Reactor Handbook[6]

Skew Emission Calculation

The experimental gamma-ray angular distribution curves showed that at the edge of the shadow shield most of the escaping photons take a prescattering path (r) which is skew with the shield axis From $\alpha = 60^\circ$, $\Gamma(\alpha,\theta,\phi^*, E)$ is shown in Fig 16 Adoption of the angle ϕ^* (see Fig 42) was necessary because the experimental arrangement constrained the spectrometer collimator to a horizontal plane, as mentioned earlier Spectra were determined for five values of θ with $\phi^* \neq 0$ At each position one spectrum was determined at such θ and ϕ^* that the collimator was aimed directly at the edge of the shadow shield while maintaining a constant distance from the reactor center The geometry involved is described in detail in Appendix D

The calculations were carried out as in the radial emission case, using Eqs (7) and (8) by replacing $\bar{\theta}_i$ and $\bar{\phi}_j$ by θ^*_{nk} and ϕ^*_{nk} These

4 E P Blizard, "Introduction to Shield Design," Part I Revised, p 41 (Jan 30, 1952)

5 Gladys R White, "X Ray Attenuation Coefficients from 10 Kev to 100 Mev," NBS-1003 (May 13, 1952)

6 H Goldstein, "Air Scattering of Gamma Rays and Neutrons," Reactor Handbook, Vol 1, p 831, Technical Information Service, U S Atomic Energy Commission (June, 1953)

quantities are defined in Appendix D Values of E' and β_q were computed from Eq (9) The variable r was partitioned at 5' intervals to 100', 50' intervals to 1000', and 500' intervals to 2000' Other partitions were as described in the preceding discussion on radial emission

The calculations were again coded and computed on the UNIVAC computer by the ORNL Mathematics Panel The dose was calculated as for the radial emission case

Unscattered Radiation Calculations

With reference to Fig 29, calculation of the unscattered radiation reaching the crew position is quite straightforward In this case, β becomes the angle between $\bar{s}$ and $\bar{H}$, and θ becomes the angle between $\bar{H}$ and $\bar{y}$, then

$$\Gamma^*(\alpha,E) = H^{-2}(\alpha)\,\Gamma(\alpha,E)$$

and

$$\frac{\Phi}{P} = 2\pi \int_0^{\alpha_b} r^{*2}(\alpha)\, H^{-2}(\alpha)\, \sin\alpha \int_{E_a}^{E_b} \Gamma(\alpha,E)\, dE\, d\alpha$$

The expressions corresponding to Eqs (7), (8), and (9) are

$$\frac{\Phi_q}{P} = 2\pi r_k^{*2} H_k^{-2} \sin\bar{\alpha}_k\, \delta\alpha_k\, \Gamma_{kn} \delta E_n \cos\theta_k \tag{18}$$

$$\left.\begin{aligned} H_k^2 &= s^2 + r_k^{*2} - 2r_k^* s \cos\bar{\alpha}_k \\ \sin\theta_k &= \frac{s}{\bar{H}_k} \sin\bar{\alpha}_k \end{aligned}\right\} \tag{19}$$

$$\left.\begin{aligned} \beta_q &= \theta_k - \bar{\alpha}_k \\ E'_q &= \bar{E}_n \\ &\text{(In this case sub q = sub kn)} \end{aligned}\right\} \qquad (20)$$

Partitions were taken as before and the dose was calculated as before except that different buildup factors were used

$$\frac{D_q}{P} = \gamma_q \frac{\Phi_q}{P} B_q \, e^{-\mu_q t_q} \qquad (21)$$

where the values of B_q were determined from the Reactor Handbook[7]

Results and Discussion

The results of the various calculations of air scattering are presented in several forms Table 6 is an over-all summary of the dose and flux values obtained and further contains a comparison with other results The first two lines of the table show that although the skew beam flux at the outside of the crew shield is very small compared with the radial beam, the dose inside the crew compartment due to this flux is comparable to the total radial beam dose This is expected since the skew beam gamma rays, having scattered through smaller angles on the average than the radial beam gamma rays, are of higher energy and thus penetrate the crew shield more readily

---

7 U Fano, "Gamma-ray Attenuation," Reactor Handbook, Vol 1, p 753, Technical Information Service, U S Atomic Energy Commission (June, 1953)

The total dose inside the crew compartment due to scattered gamma rays calculated by this method is somewhat lower than that calculated by the 1950 Shielding Board[2] (ANP-53 method), however, the agreement is good considering that for the ANP-53 calculations it was assumed that all the gamma rays were of 3-Mev energy and all were radially emitted from the reactor shield The agreement would be less close if the unknown correction for leakage ratios between the two reactors were applied

Table 6 Gamma-Ray Flux and Dose at the Crew Compartment

Method	$\frac{\Phi}{P}$, Flux Outside Crew Compartment (photons/sec watt)	D, Dose Inside Crew Compartment (r/hr watt)
Radial Scattered	4 5	$0\ 36 \times 10^{-9}$
Skew Scattered	0 016	$0\ 19 \times 10^{-9}$
Direct	16 0	130×10^{-9}
ANP-53 Scattered[a]		$1\ 2 \times 10^{-9}$
ANP-53 Direct[a]		$1\ 2 \times 10^{-9}$
Skyshine[b]		$1\ 14 \times 10^{-9}$

a No correction has been made for reactor leakage

b H E Hungerford, "The Skyshine Experiments at the Bulk Shielding Facility," ORNL-1611

The large increase in the dose due to the direct beam calculated by this method over that calculated by the ANP-53 method is caused primarily by the gamma radiation escaping around the edges of the

shadow shield In Figs 21 and 22 it was seen that large numbers of low energy (~ 2 Mev) gamma rays emerge from the reactor shield in a direction such that they may strike the crew shield without scattering Unfortunately, the spectrometer background at such positions was so large that little value can be placed upon the absolute magnitude of the dose In general, for all results from the calculations of this report, the shapes of the curves obtained are considerably more reliable than the absolute magnitudes

Scattered flux and dose contributions of the various regions outside the reactor and crew shields are listed in Appendix F These contributions are also shown in diagrams in Figs 31 and 32 which show their geometrical relation to the aircraft reactor and crew shield Figures 33 and 34 are shaded diagrams of the same data These curves show the effect of the shadow shield and further show that regions far from the aircraft make a large contribution to the flux outside the crew shield However, the contribution to the dose is much smaller since scattering which occurs far from the aircraft axis must be large-angle scattering with consequent energy reduction and poor penetration of the crew shield In all cases, only the penetration through the side wall of the crew shield has been tabulated since the front and rear wall contributions were entirely negligible Complete calculations were carried out for the front wall for both radial and skew emission in order to prove that these contributions were actually small

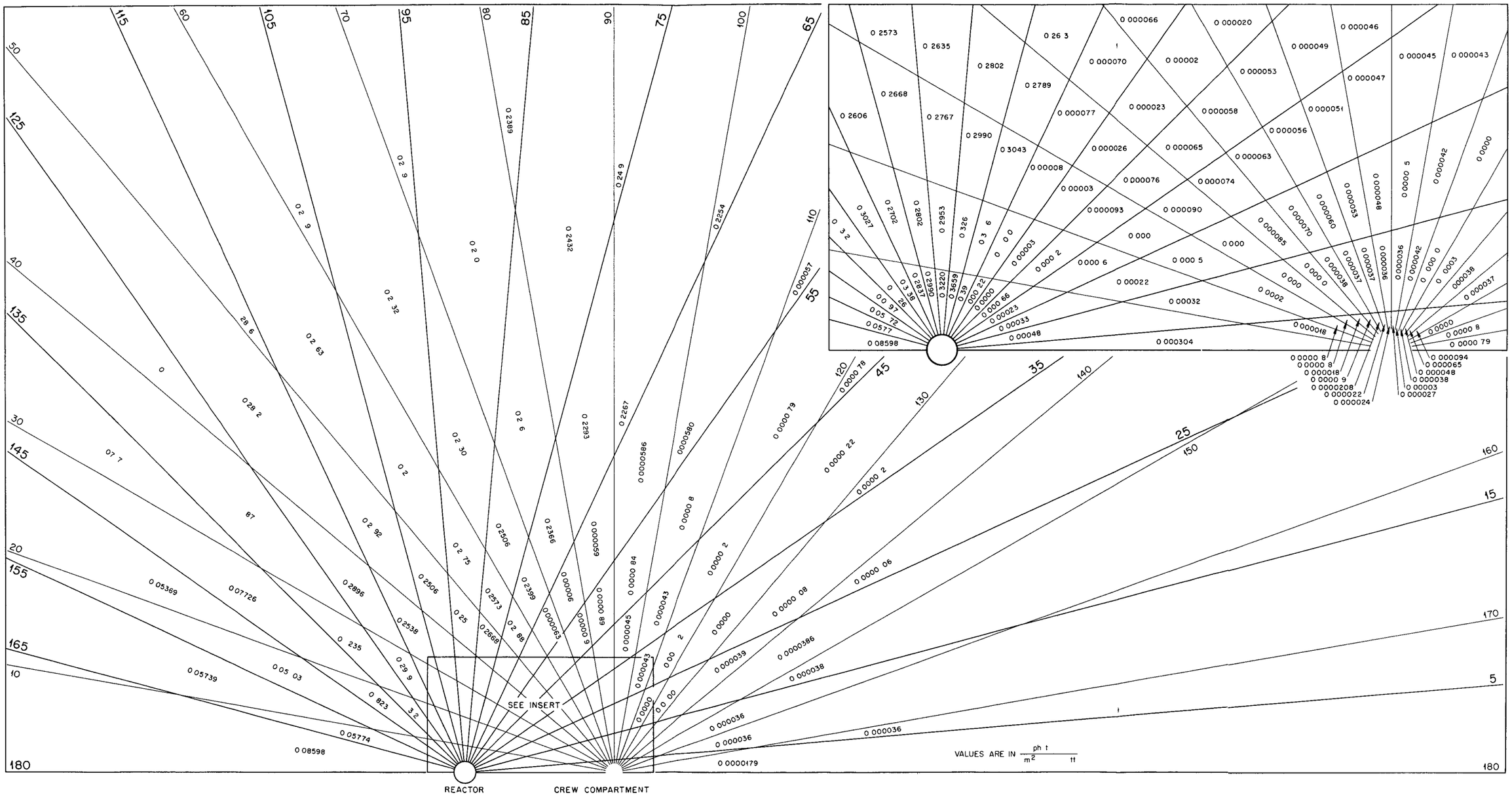

Fig 31 Gamma-Ray Flux at Crew Shield Due to Air Scattering from Individual Cells Radial Emission

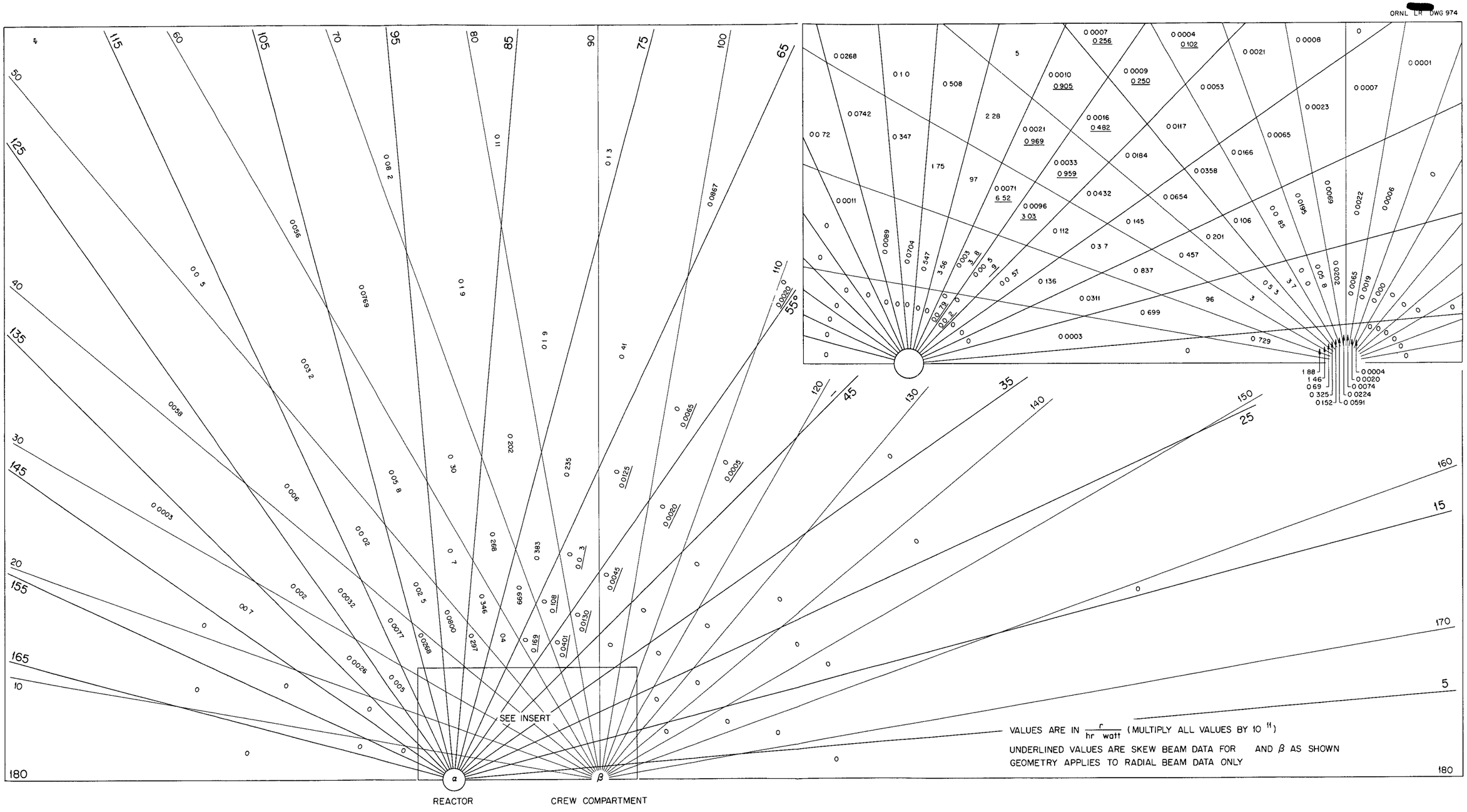

Fig 32 Gamma-Ray Dose Inside Crew Shield Due to Air Scattering from Individual Cells Radial and Skew Emission

Figure 35 shows the dependence of the scattered dose (for all angles) upon the prescatter energy and Fig 36 presents the dependence upon the postscatter energy It is interesting to note that the average energy for the skew emission dose is higher than that for radial emission dose

Figures 37 and 38 present the scattered dose as a function of the source and receiver angles The distribution around the reactor shield (Fig 37) shows clearly the peak in the forward direction which is due to the relatively favorable geometry for radiation starting forward After a drop of a factor of about 300 out to 55°, the dose contribution rises rapidly at the edge of the shadow shield and again falls off owing to geometry It would thus appear obvious that the shadow shield should extend to larger angles It should, of course, be thinner with increasing values of α It also appears that the ANP-53 shield was drastically overshielded in the rear This was recognized at the time it was designed but was supposed to compensate somewhat for the presence of ducts in the rear hemisphere of the reactor shield

The distribution of the dose inside the crew shield as a function of the angle around the crew compartment midpoint (Fig 38) shows a larger contribution from the rear of the crew shield as would be expected since the crew compartment was taken to be a cylinder with walls of uniform thickness The variations observed in this case are not nearly so large as for the source angle

Figure 39 shows the direct dose as a function of the gamma-ray energy emerging from the reactor shield The dependence of the dose

upon the energy is determined by the large angle at which the major contribution to the direct dose occurs as shown in Fig 40 This figure presents the direct dose as a function of source angle α and again shows the extreme importance of the radiation escaping around the edges of the shadow shield

[redacted]

DWG 19470A

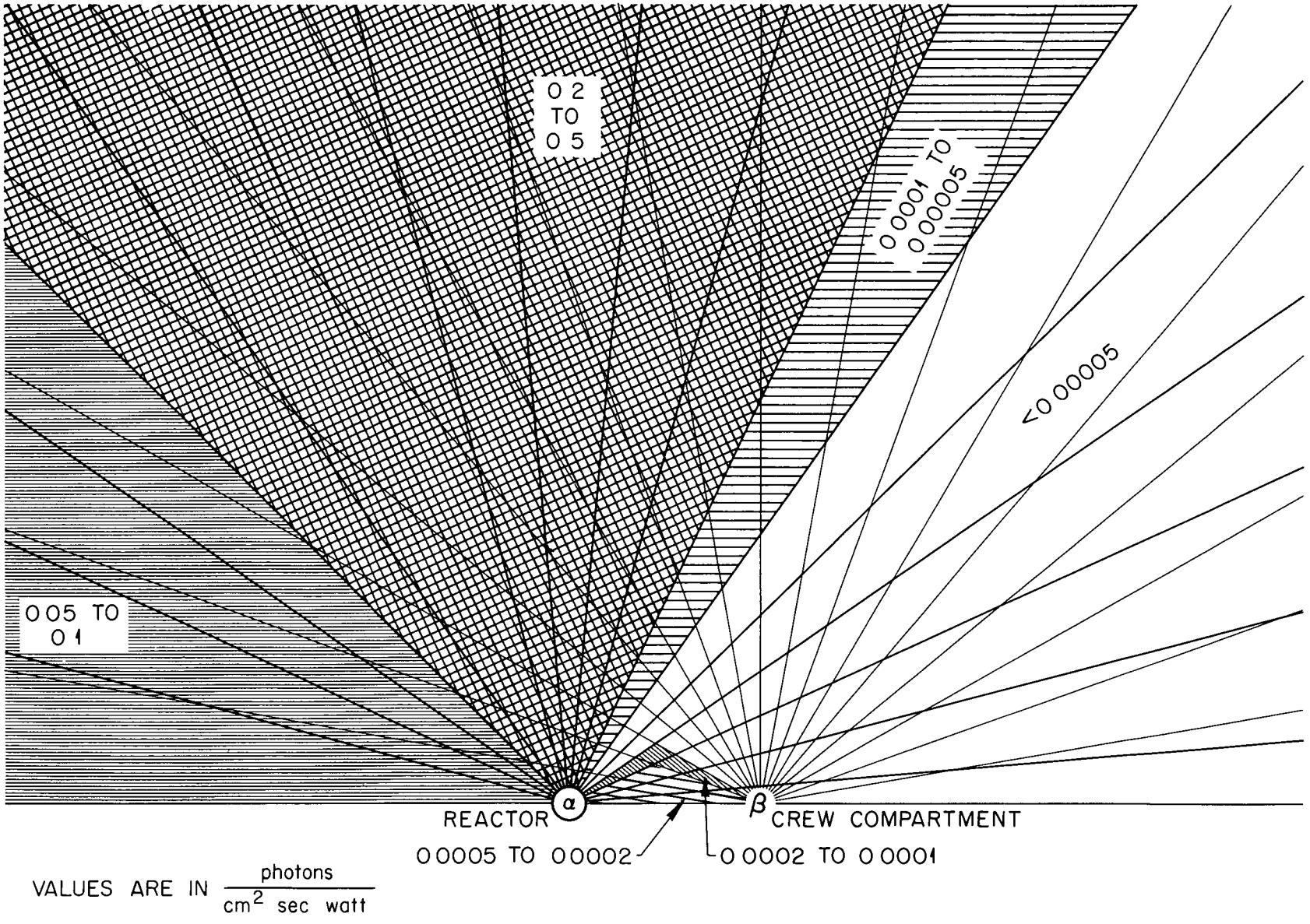

Fig 33 Gamma-Ray Flux at Crew Shield Due to Air Scattering

[redacted]

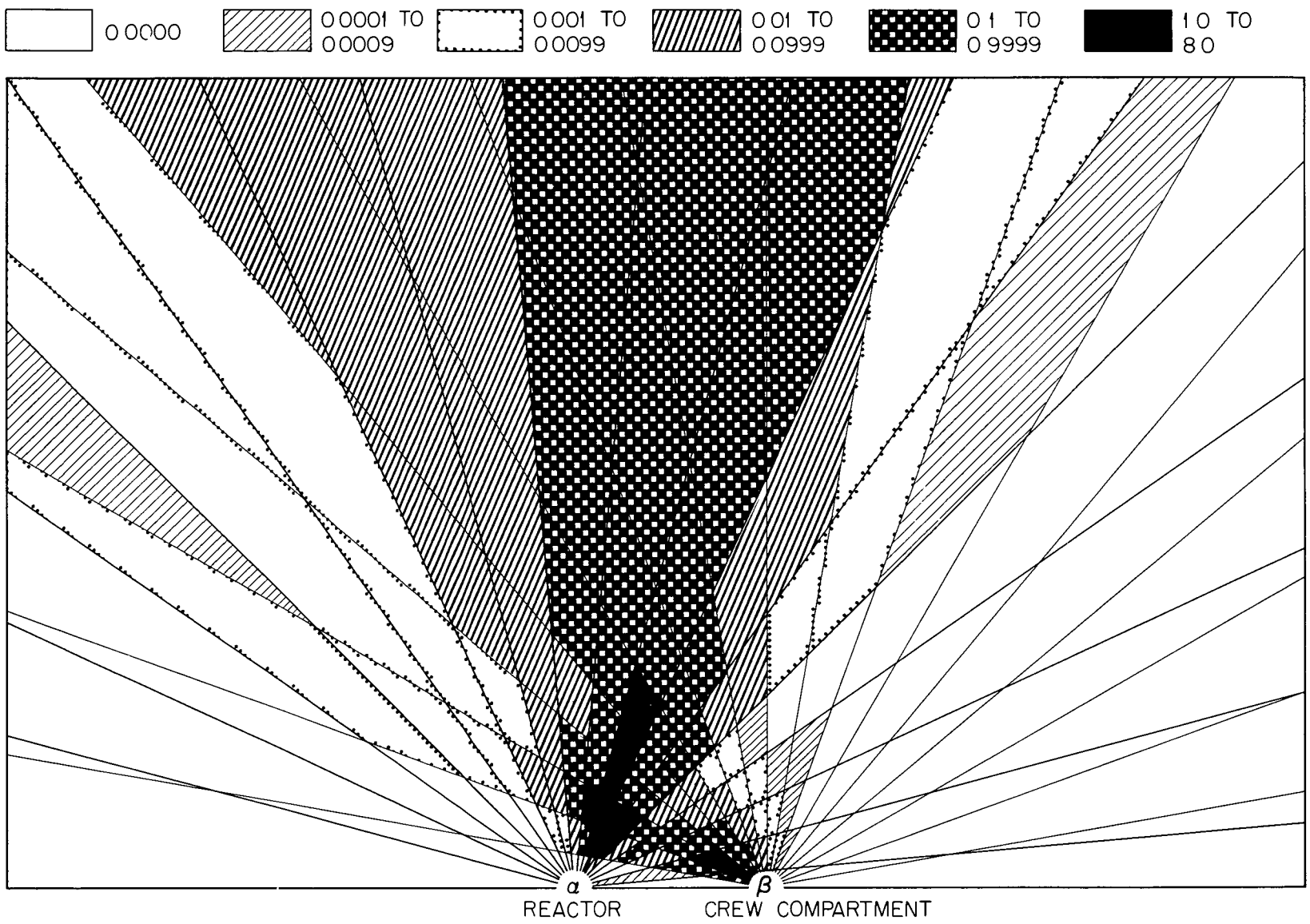

VALUES ARE IN $\frac{r}{hr\ watt}$ (MULTIPLY ALL VALUES BY 10^{-11})

Fig 34 Gamma-Ray Dose Inside Crew Shield Due to Air Scattering

[redacted]

ORNL-LR-DWG 864

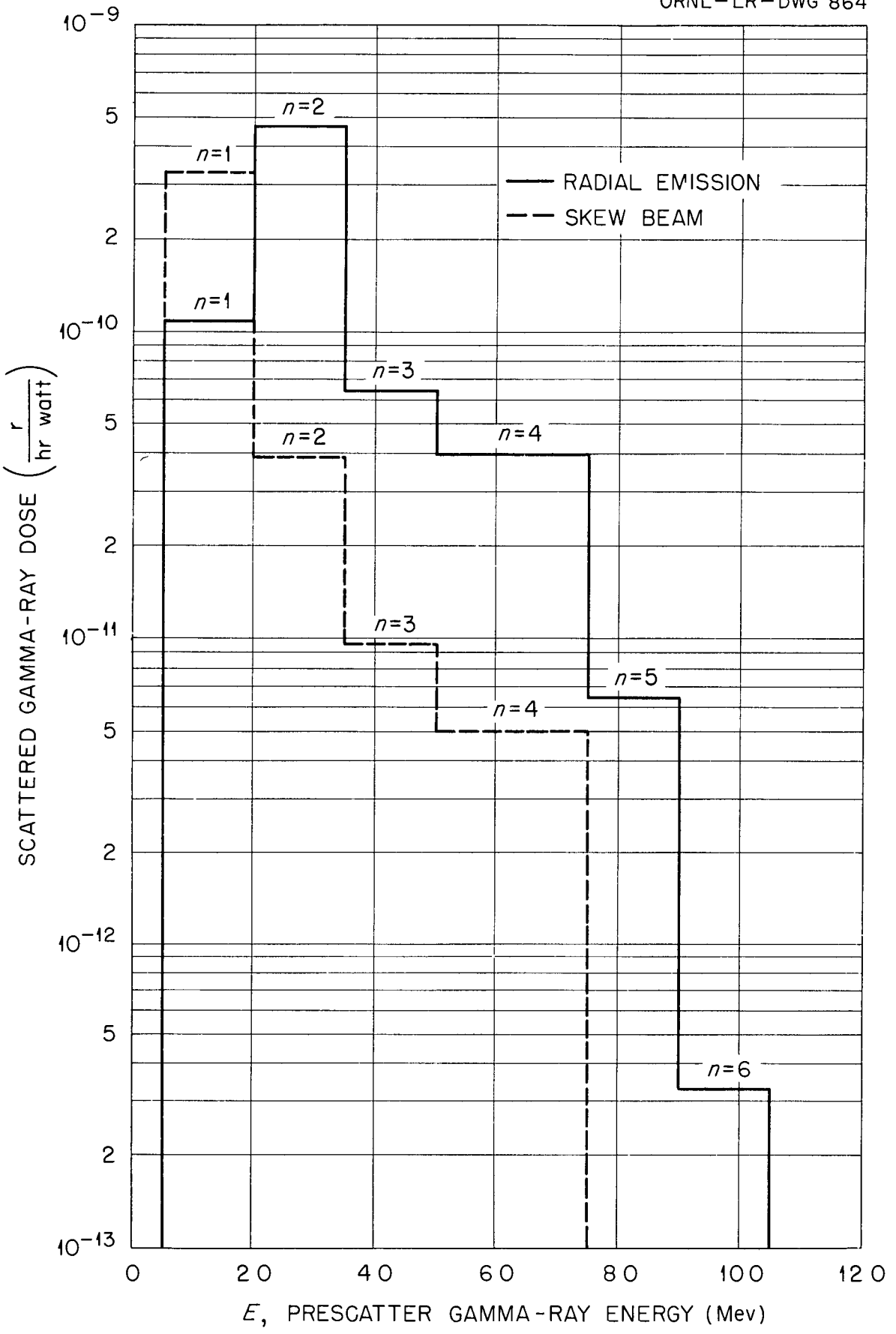

Fig 35 Scattered Gamma-Ray Dose as a Function of Prescatter Energy

[redacted]

ORNL-LR-DWG 865

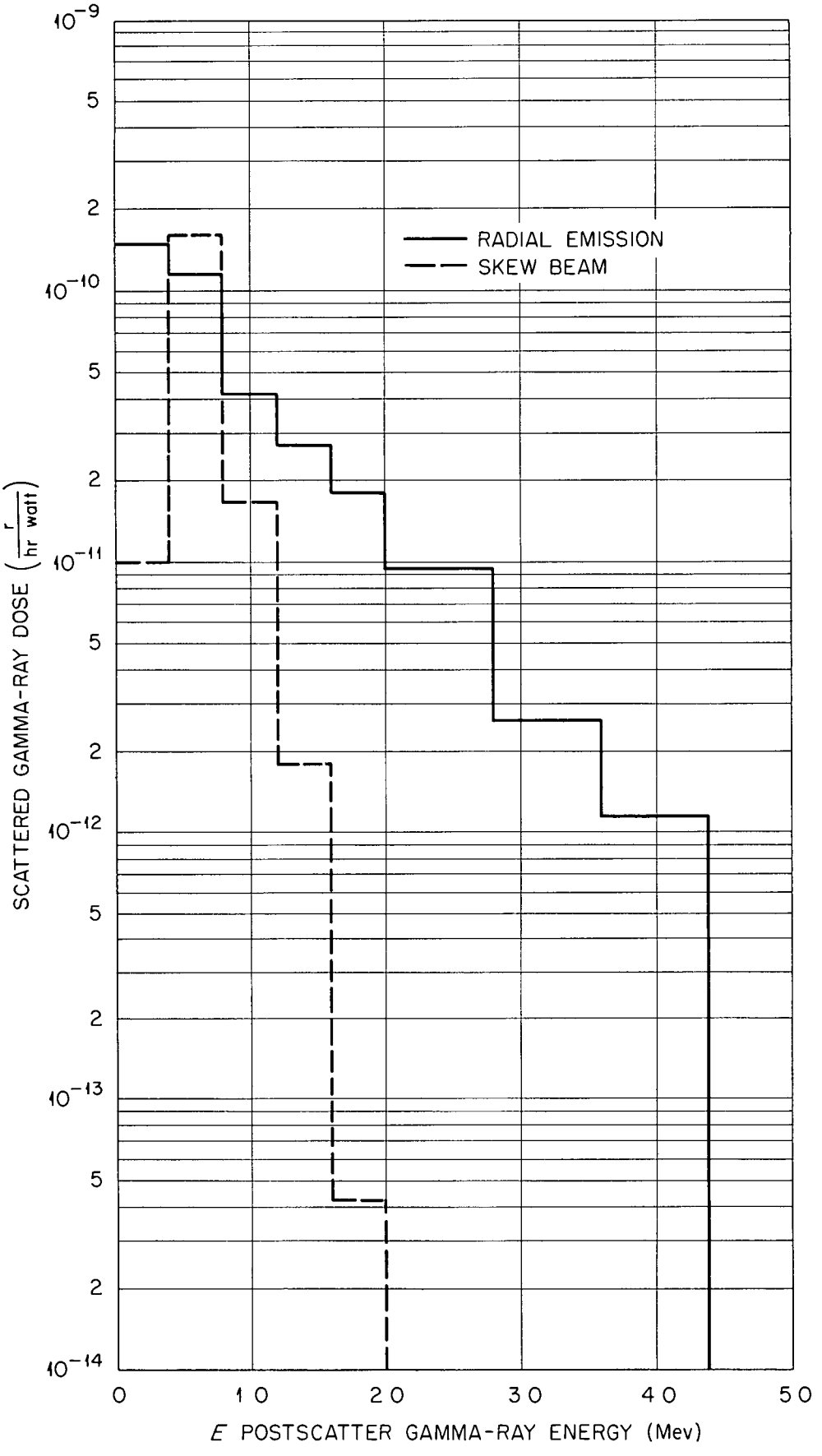

Fig 36 Scattered Gamma-Ray Dose as a Function of Postscatter Energy

[redacted]

ORNL-LR DWG 866

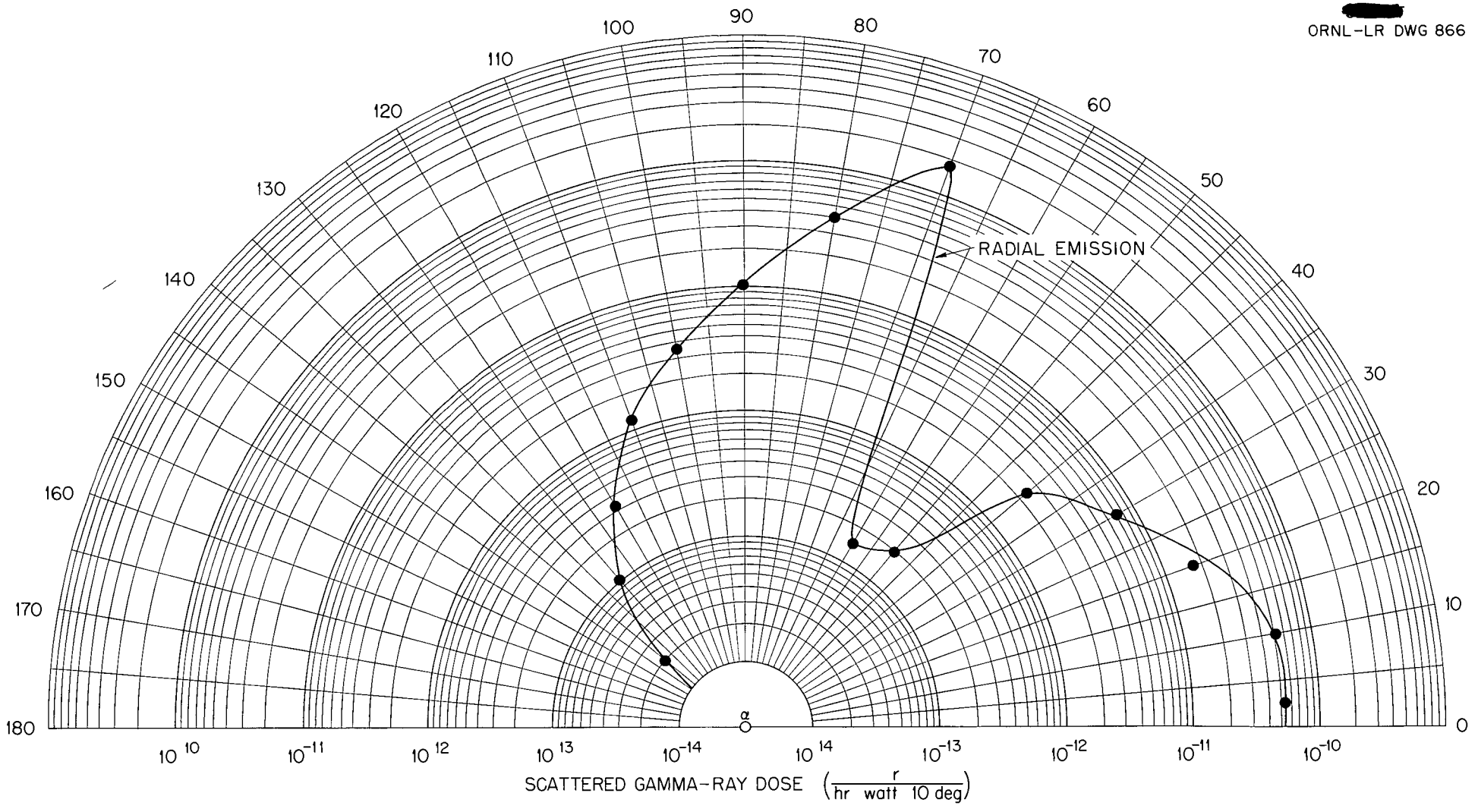

Fig 37 Scattered Gamma-Ray Dose as a Function of Source Angle

[redacted]

[redacted]

ORNL-LR-DWG 867

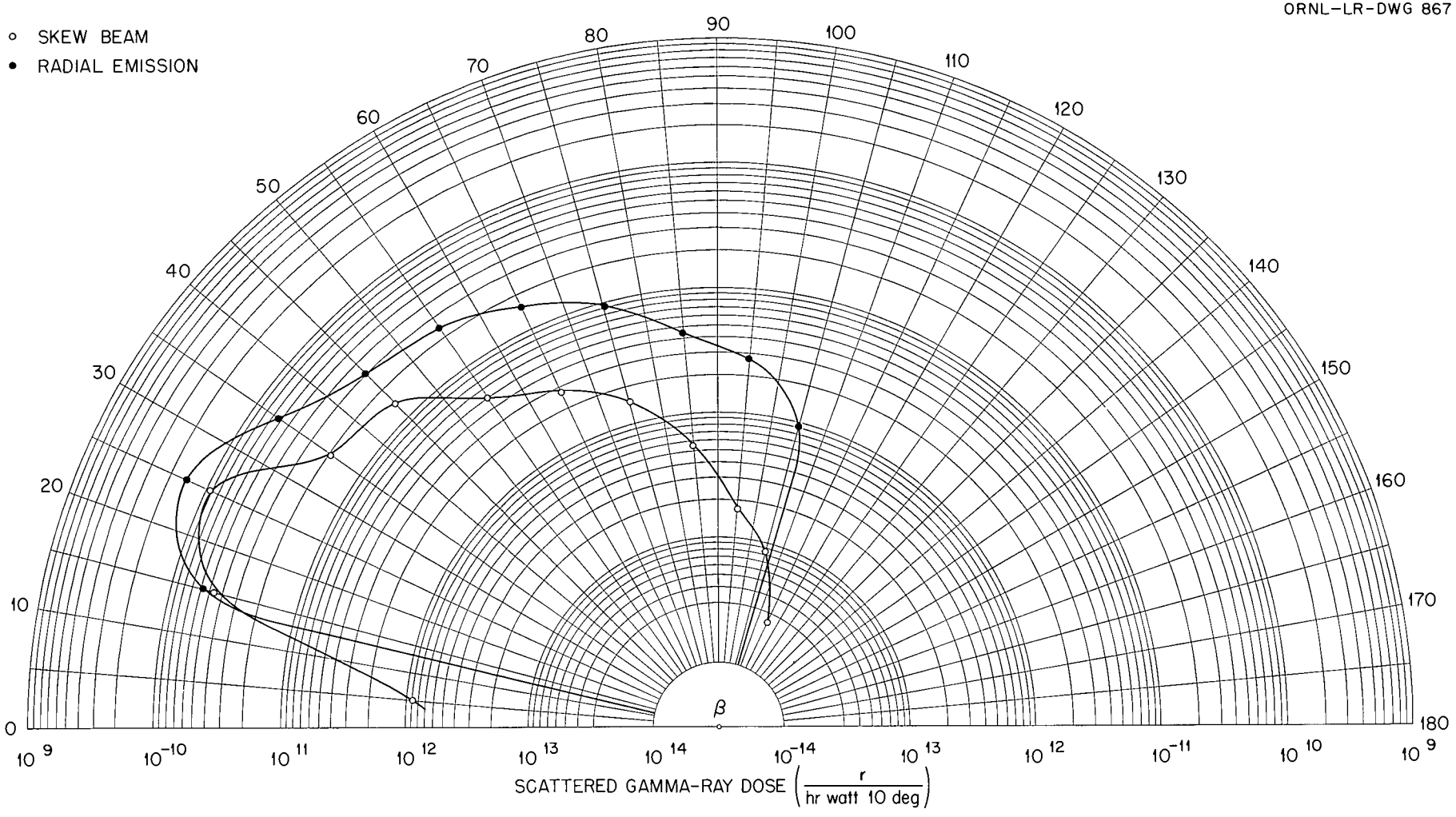

[redacted]

Fig 38 Scattered Gamma-Ray Dose as a Function of Receiver Angle

[redacted]

ORNL LR DWG 1681

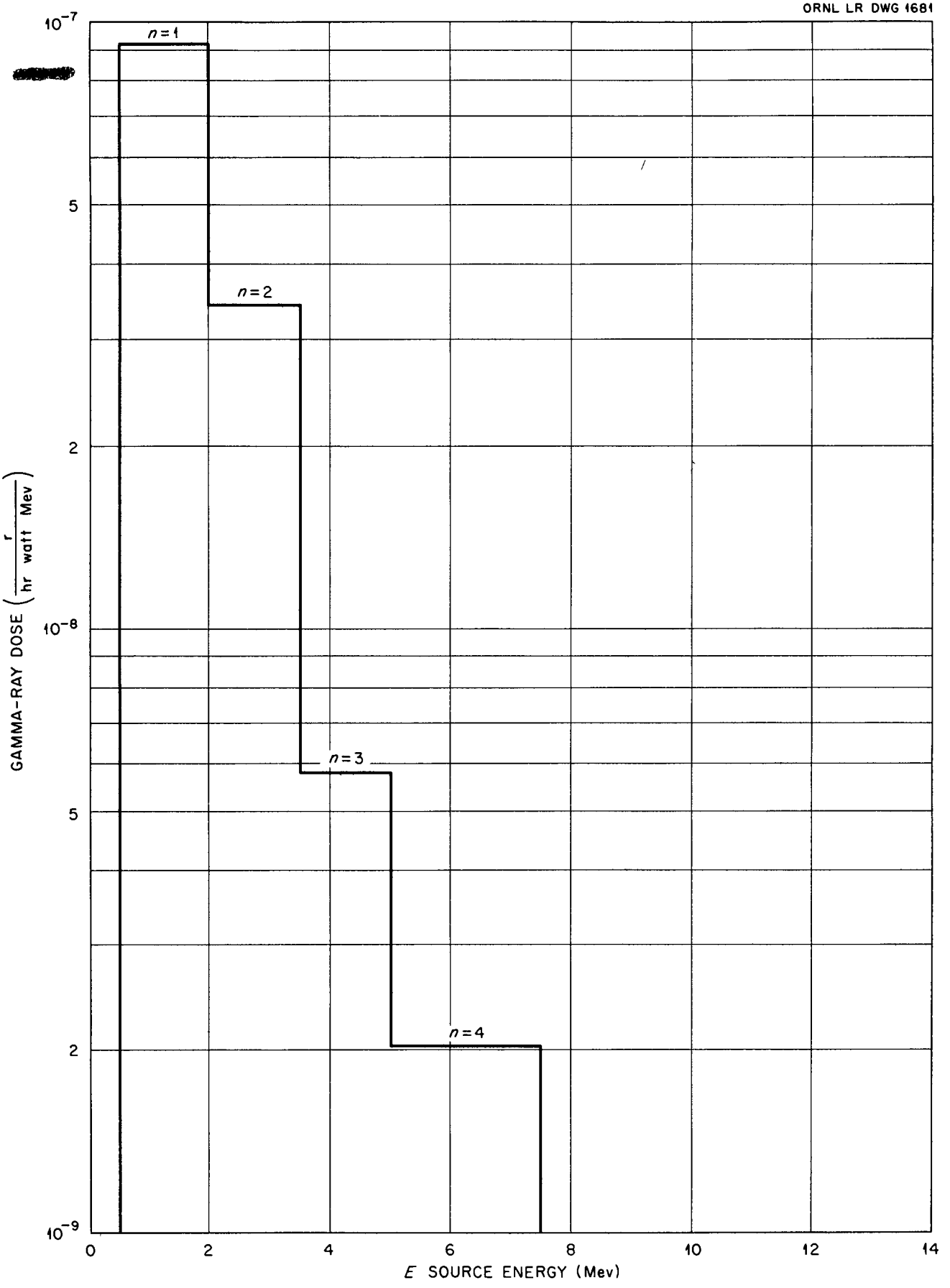

Fig 39 Direct Gamma-Ray Dose as a Function of Source Energy

[redacted]

ORNL-LR-DWG 1680

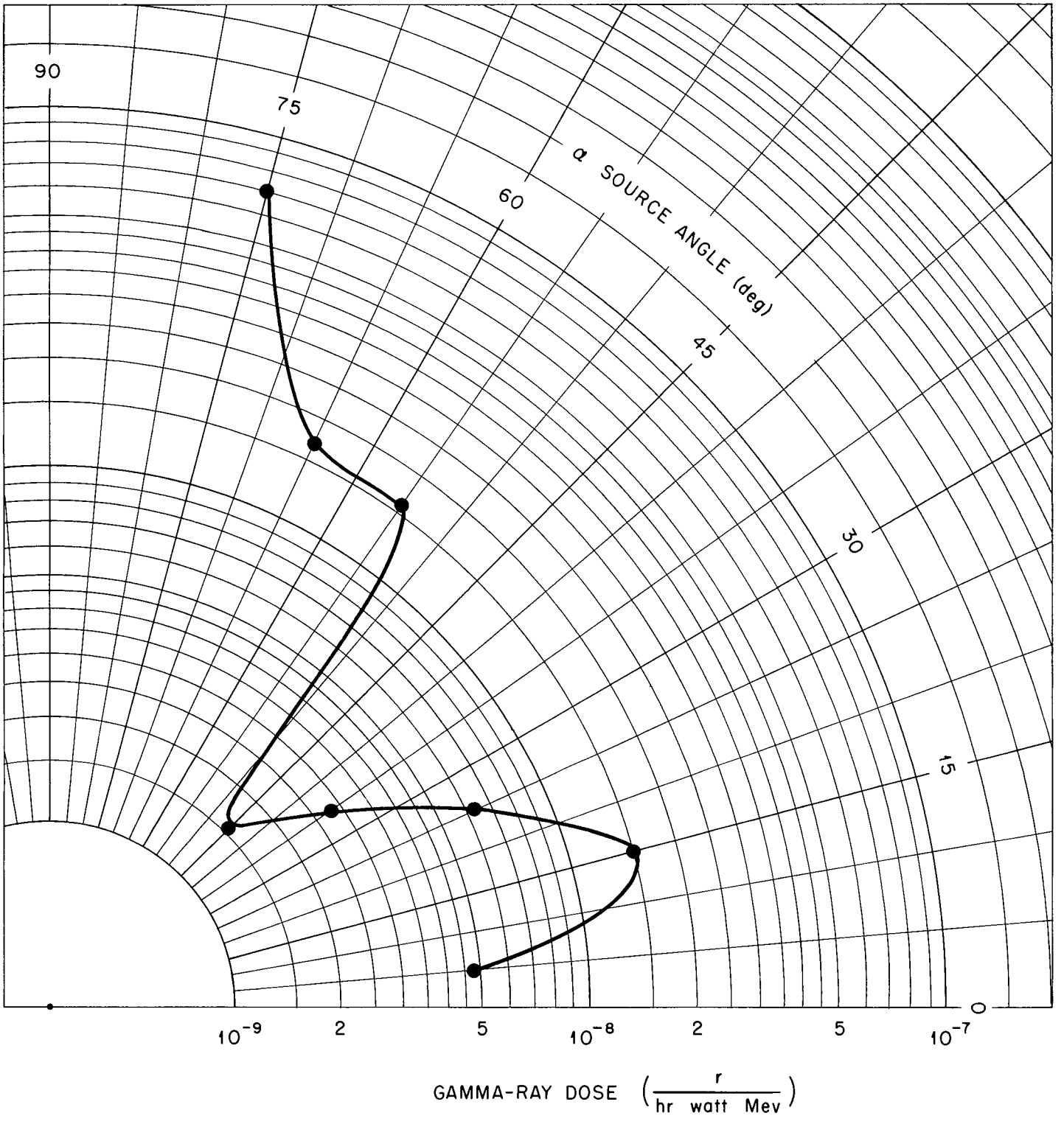

Fig 40 Direct Gamma-Ray Dose as a Function of Source Angle

Appendix A

DETERMINATION OF EXPRESSIONS FOR THE SCATTERING ANGLE AND THE POSTSCATTERING LENGTH

Expressions for Ψ and R^{-2} were determined as follows

If all lengths are treated as vectors (see Fig 30),

$$\overline{r^*} + \bar{y} + \bar{x} + \bar{R} + \bar{s} = 0 \tag{22}$$

and

$$\left.\begin{aligned} \overline{r^*} &= r^* \sin\alpha\, \bar{i} + r^* \cos\alpha\, \bar{j} \\ \bar{y} &= y \sin\alpha\, \bar{i} + y \cos\alpha\, \bar{j} \\ \bar{x} &= x \cos\phi \left[- \cos\alpha\, \bar{i} + \sin\alpha\, \bar{j} \right] + x \sin\phi\, \bar{k} \\ \bar{s} &= -s\, \bar{j} \end{aligned}\right\} \tag{23}$$

Further,

$$\left.\begin{aligned} y &= r \cos\theta \\ x &= r \sin\theta \end{aligned}\right\} \tag{24}$$

Substituting Eqs (23) and (24) into Eq (22) and taking scalar products of the result with $\bar{i}$, $\bar{j}$, and $\bar{k}$, respectively, results in a set of three simultaneous scalar equations in $R_{\bar{i}}$, $R_{\bar{j}}$, and $R_{\bar{k}}$

$$\left.\begin{aligned} r^* \sin\alpha + r \cos\theta \sin\alpha - r \sin\theta \cos\phi \cos\alpha + R_{\bar{i}} &= 0 \\ r^* \cos\alpha + r \cos\theta \cos\alpha + r \sin\theta \cos\phi \sin\alpha + R_{\bar{j}} - s &= 0 \\ r \sin\theta \sin\phi + R_k &= 0 \end{aligned}\right\} \tag{25}$$

Solving for $R_{\bar{i}}$, $R_{\bar{j}}$ and $R_{\bar{k}}$ and substituting into $R^2 = R_{\bar{i}}^2 + R_{\bar{j}}^2 + R_{\bar{k}}^2$ gives the expression for R^2

$$R^2 = \left[r(\cos\theta \sin\alpha - \sin\theta \cos\phi \cos\alpha) + r^* \sin\alpha\right]^2$$
$$+ \left[r(\cos\theta \cos\alpha + \sin\theta \cos\phi \sin\alpha) + (r^* \cos\alpha - s)\right]^2$$
$$+ r^2 \sin^2\theta \sin^2\phi$$

or

$$R^2 = r^2 + 2rr^* \cos\theta - 2rs(\cos\theta \cos\alpha + \sin\theta \cos\phi \sin\alpha) - 2r^*s \cos\alpha + r^{*2} + s^2 \quad (26)$$

Ψ is found by taking the scalar product of Eq (22) with $\bar{r}$, substituting $\bar{r} = \bar{x} + \bar{y}$, and rearranging,

$$\cos\Psi = \frac{1}{R}\left[s(\cos\alpha \cos\theta + \sin\alpha \cos\phi \sin\theta) - r - r^* \cos\theta\right] \quad (27)$$

Appendix B

TEST OF RADIAL EMISSION ASSUMPTION

The first calculation made was for the purpose of checking the validity of the radial emission assumption Essentially, for distributed emission, Eq (7) was summed over i and j under the following conditions

$$2\pi r_k^{*2} \sin\bar{\alpha}_k \, \delta\alpha_k = 1 \text{ cm}^2 \text{ of shield surface,}$$

$$\bar{\alpha}_k = 90^\circ,$$

$$\delta r_m = 1 \text{ cm,}$$

$$\bar{r}_m = 10 \text{ ft,}$$

$$\delta E_n = 1\ 2 \text{ Mev,}$$

$$\bar{E}_n = 1\ 4 \text{ Mev,}$$

$$s = 1716 \text{ cm}$$

Values of R_{kijm}^{-2} and K_{kijmn} were computed as in Eqs (8) Values of Γ_{kijn} were obtained as described below Then

$$\Gamma_n(\theta,\rho t) = \int_{E_{n-1}}^{E_n} \frac{\Gamma(E)}{\delta E_n} dE$$

Γ_n was evaluated graphically from the preceding expression and plotted vs ρt This resulted in n families of curves in which each individual curve represented one value of θ When all available experimental data was plotted thus, each family (n) had a three-point curve, a two-point curve, and three to six single points Further, plotted on semilog coordinates

each of the three-point curves is roughly linear An arbitrary extrapolation was then employed The two- and three-point curves of each family were extrapolated linearly to intersection These intersections were then connected with the single points to complete the family It should be noted that the rather long extrapolation was used only to fix the slope of the single-point curves, in all cases, the data used in computation was fairly near an experimental point A typical plot is shown in Fig 41

The function Γ is symmetrical about y (Fig 28) and ρt is readily scaled from Fig 11 of the 1950 Shielding Board report [1] The relation $\rho t = \sum_\mu \rho_\mu t_\mu$ where μ represents the materials water, gasoline, beryllium oxide, iron, lead, insulation, and sodium The Γ_{kijn} was determined from Fig 41, according to the expression

$$\Gamma_{kijn} = \frac{1}{2}\left[\Gamma_{kjn}(\theta_{i-1}) + \Gamma_{kjn}(\theta_i)\right]$$

The hemispherical scattering shell (Fig 29) was divided into 33ij cells for computation such that throughout each cell $\Psi(\theta,\phi) = \Psi_{ij} \pm 5^\circ$

For the case of radial emission, Eqs (13) and (14) were used under the same conditions as above Here

$$\Gamma^*_{kn} = \sum_{ij} \Gamma_{kni} \sin\bar{\theta}_i \ \delta\theta_i \ \delta\phi_j$$

The limits of integration throughout these computations were $0 < \theta < 90^\circ$ and $0 < \phi < 180^\circ$ The results of the calculations were Φ (radial) = 21 0 sec^{-1} and Φ (distributed) = 24 7 sec^{-1} The radial emission assumption is thus seen to give answers low by about 18%

---

1 "Report of the Shielding Board for the Aircraft Nuclear Propulsion Program," ANP-53 (Oct 16, 1950)

[redacted]

DWG 19858

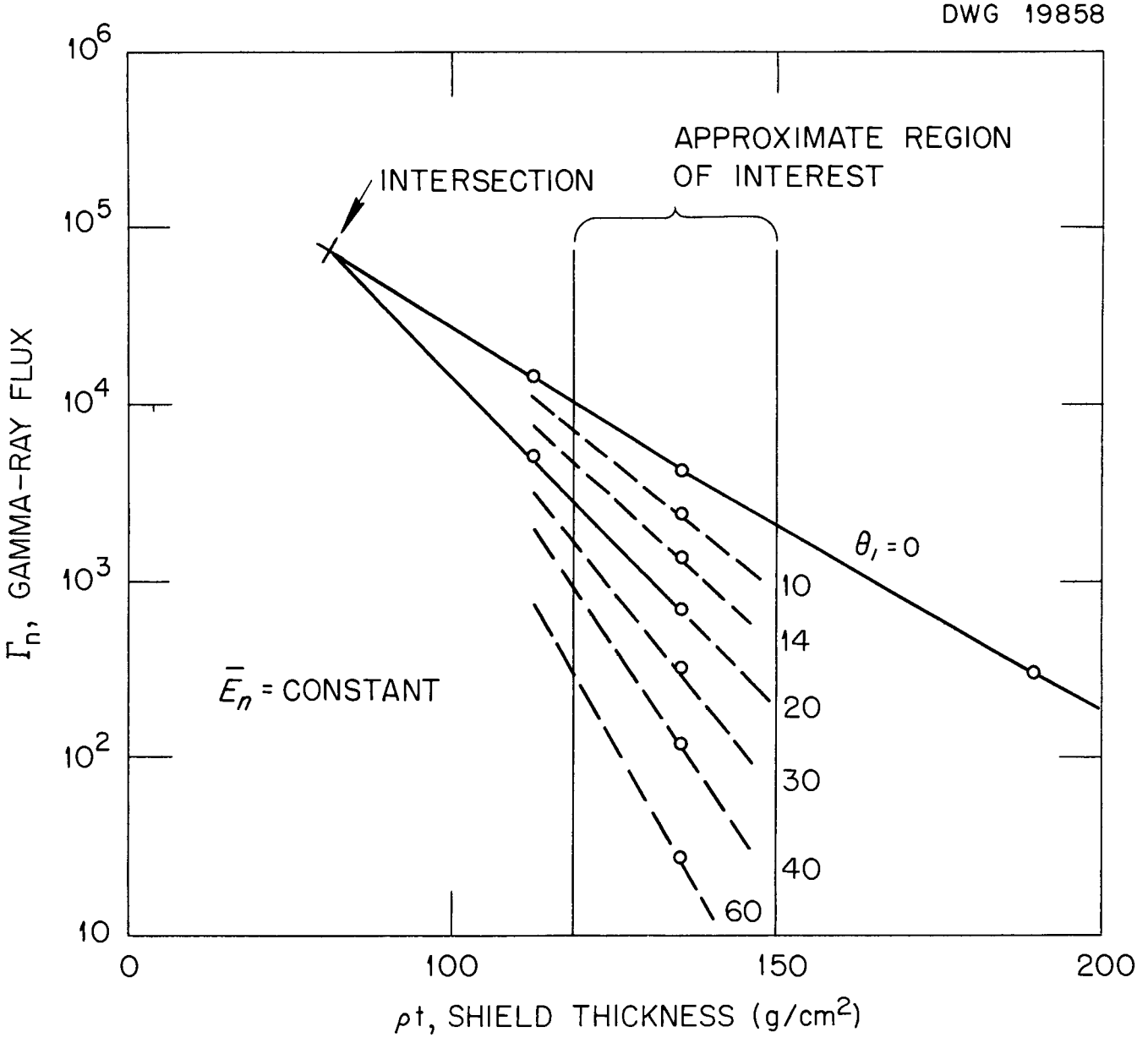

Fig 41 Typical Variation of Emerging Gamma-Ray Flux with Shield Thickness

Appendix C

TRANSFORMATION OF VARIABLE

To avoid computational difficulty due to tabulating β_q, it was desirable to take β as a variable of integration in place of r This was impossible in the general case because R and ψ could not be determined as explicit functions of β, α, θ, and ϕ For radial emission the transformation was made as follows

Remembering that $R^2 = R_{\bar{i}}^2 + R_{\bar{j}}^2 + R_{\bar{k}}^2$ and $R_{\bar{j}} = R \cos\beta$,

$$R^2 \sin^2\beta = R_{\bar{i}}^2 + R_{\bar{k}}^2 \tag{28}$$

Substituting Eq (25) into Eq (28) to eliminate R, $R_{\bar{i}}$ and $R_{\bar{k}}$, and setting $\theta = 0$,

$$r = \frac{s}{(\cos\alpha + \sin\alpha \cot\beta) - r^*(\alpha)} \tag{29}$$

and

$$\frac{\partial r}{\partial \beta} \equiv F(\alpha,\beta) = \frac{s \sin\alpha}{\sin^2(\alpha + \beta)} \tag{30}$$

Applying Eqs. (29) and (30), Eqs (13) and (14) become, respectively,

$$\Phi_q/P = 2\pi N_e r_k^{*2} \sin\bar{\alpha}_k \, \delta\alpha_k \, R_{kp}^{-2} \, F_{kp} \, \delta\beta_p \Gamma^*_{kn} K_{kmn} \, \delta E_n \tag{31}$$

$$
\left.
\begin{aligned}
R^2 &= s^2 \left[(\cos\bar{\alpha}_k + \sin\bar{\alpha}_k \cot\bar{\beta}_p)^{-2} - 2(1 + \tan\bar{\alpha}_k \cot\bar{\beta}_p)^{-1} + 1 \right] \\
K_{knp} &= 3\ 971 \times 10^{-26} \left\{ \frac{1}{\left[1 + 1\ 96E_n(1 - \cos\Psi_{kp})\right]^2} \left[1 \right.\right. \\
&\qquad \left.\left. + \cos^2\Psi_{kp} + \frac{(1\ 96\bar{E}_n)^2(1 - \cos\Psi_{kp})^2}{1 + 1\ 96\bar{E}_n(1 - \cos\Psi_{kp})} \right] \right\} \\
\Psi_{kp} &= \bar{\alpha}_k + \bar{\beta}_p
\end{aligned}
\right\} \quad (32)
$$

(In this case, sub q = sub knp and E_q' is found as before)

Appendix D

GEOMETRY OF SKEW EMISSION CALCULATION

The purpose of this appendix is to show how the gamma-ray data was utilized in the skew emission case It describes the rather complicated geometry which is necessitated by the physical constraint that the spectrometer collimator remain horizontal for all measurements

The symbols α, r^*, θ, ϕ and [RS] have their usual significance Further

α_s = half-angle of cone subtended by shadow shield = 70°,

R_s = radius of shadow shield,

s_1 = distance from [RS] to plane of shadow shield edge = 28 8 cm,

s_2 = distance from plane of shadow shield edge to plane of collimator locus,

ρ_1 = distance from collimator to shadow shield edge,

ρ_2 = radius of collimator locus,

ρ_3 = distance from [RS] to shadow shield edge = 84 1 cm,

h = height of collimator plane above horizontal median plane (plane 1),

x_s = intersection of collimator plane with plane of shadow shield edge (plane 4),

Plane 2 = plane determined by ρ_1 and [RS],

Plane 3 = plane determined by collimator nose and shield axis

Then ϕ is the angle between planes 2 and 3

An expression for θ and ϕ as functions of ϕ^* can now be derived by elementary analytic geometry Cartesian coordiantes are set up as shown in Fig 42 Then the general equation for planes 2 and 3 is

$$A_g x + B_g y + C_g z + D_g = 0 \tag{33}$$

or

$$\begin{vmatrix} x & y & z & 1 \\ x_{g1} & y_{g1} & z_{g1} & 1 \\ x_{g2} & y_{g2} & z_{g2} & 1 \\ x_{g3} & y_{g3} & z_{g3} & 1 \end{vmatrix} = 0$$

where g takes values 2 or 3 representing planes 2 and 3, and subscripts 1, 2, and 3 refer to arbitrary points on the planes g

Expanding the determinant in minors of the first row and selecting points g1 = [RS], 22 = intersection ρ_1 and ρ_3, 32 = any point on the shield axis, and g3 = collimator nose, the following values of the arbitrary constants are found

$$\left.\begin{aligned} A_2 &= -s_2 h & A_3 &= (s_1 + s_2)h \\ B_2 &= h\rho_2 \cos\phi^* - hx_s & B_3 &= 0 \\ C_2 &= x_s(s_1 + s_2) - s_1\rho_2 \cos\phi^* & C_3 &= -(s_1 + s_2)\rho_2 \cos\phi^* \\ D_2 &= 0 & D_3 &= 0 \end{aligned}\right\} \tag{34}$$

[redacted]

DWG 19859

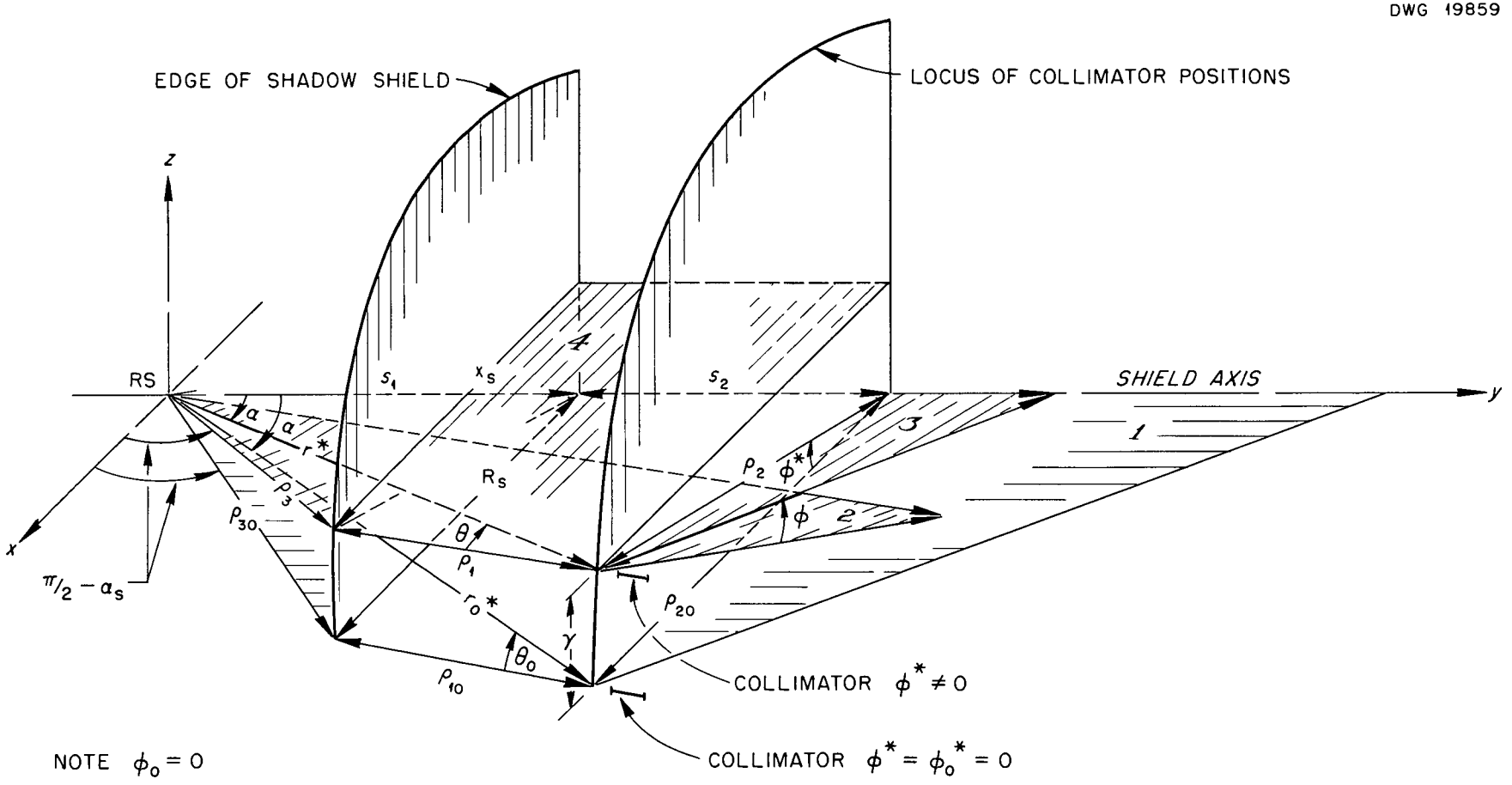

Fig 42 Geometry for Skew Emission Calculation

Further

$$\left.\begin{aligned} x_s &= \sqrt{R_s^2 - \rho_2^2 \sin^2\phi^*} = \sqrt{\rho_3^2 \sin^2\alpha_s - r^{*2} \sin^2\alpha \sin^2\phi^*} \\ h &= \rho_2 \sin\phi^* \\ s_1 + s_2 &= r^* \cos\alpha \\ \rho_2 &= r^* \sin\alpha \end{aligned}\right\} \tag{35}$$

But from geometry

$$\cos\phi = \frac{A_2A_3 + B_2B_3 + C_2C_3}{\left(\pm\sqrt{A_2^2 + B_2^2 + C_2^2}\right) \times \left(\pm\sqrt{A_3^2 + B_3^2 + C_3^2}\right)} \tag{36}$$

where the signs of the radicals are the same as those of C_g Substituting Eqs (34) and (35) into Eq (36) and simplifying,

$$\cos\phi = \frac{\cos\phi^* \cot\alpha\, x_s + \sin^2\phi^* \cos\alpha\, r^* - s_1}{\sqrt{\sin^2\phi^* \left[(s_1 - r^* \cos\alpha)^2 + (\cos\phi^* \sin\alpha\, r^* - x_3)^2 + (x_s \cot\alpha - \cos\phi^* s_1)^2\right]}} \tag{37}$$

To find θ as a function of ϕ^*,

$$\rho_3^2 = r^{*2} + \rho_1^2 - 2r^* \rho_1 \cos\theta \tag{38}$$

But

$$\rho_1^2 = (\rho_2 \cos\phi^* - x_s)^2 + s_2^2 \tag{39}$$

Substituting Eqs (35) and (39) into Eq (38) and rearranging,

$$\cos\theta = \frac{r^{*2} - \rho_3^2 + (r^* \sin\alpha \cos\phi^* - x_s)^2 + (r^* \cos\alpha - r \cos\alpha_s)^2}{2r^* \left[(r^* \sin\alpha \cos\phi^* - x_s)^2 + (r^* \cos\alpha - \rho_3 \cos\alpha_s)^2\right]^{1/2}} \tag{40}$$

From Eqs (37) and (40) values of ϕ and θ were computed for all values of ϕ^* at which data was taken

Using these computations, plus the spectral data already described, angular distributions similar to those shown in Fig 43 were plotted

It should be kept in mind in using Fig 43 that $\Gamma(\theta,\phi) = \Gamma(-\theta,\pi - \phi)$ Since the small circles represent experimental points, the curve for $\phi = 0$ is seen to be fairly well known For $\phi \neq 0$ six points are available, each for a different value of ϕ At each point the collimator was directed toward the edge of the shadow shield, therefore, it was assumed that each bears about the same relation to the peak of the curve Furthermore all curves must coincide at $\theta = 0$ and it is assumed that they all vanish at $\theta = 90^\circ$ With these assumptions, curves for $\phi \neq 0$ were drawn to the same general shape as that for $\phi = 0$

The curves discussed thus far represent the total radiation escaping at $\alpha = 60^\circ$ For computational purposes it proved desirable to subdivide this radiation into two components (1) "radial beam," or radiation penetrating the shadow shield, and (2) "skew beam" or radiation scattered around the shadow shield This distinction is vividly illustrated in Fig 45 for $\alpha = 50^\circ$ The radial beam was assumed to have the same angular distribution as it had near the center of the shadow shield

This shape was then normalized to fit the "total beam" to the left of the origin in Fig 43 In most cases the fit was quite good The radial beam was then reflected into the first quadrant, since manifestly it must be independent of ϕ, and treated as described in the preceding discussion

The skew beam could be determined by subtracting the radial from the total beam on plots of the type of Fig 43 Furthermore, the skew angular distribution peaks are even sharper than the radial Hence it seemed appropriate to sum $\Gamma_{kn}(\theta,\phi)$ over θ and ϕ to obtain Γ^*_{kn}, together with average values of θ and ϕ (designated θ^*_{kn} and ϕ^*_{kn}) For the summation Fig 43 was cross plotted as shown in Fig 44 Curves for θ were plotted at 5° intervals, the summation for Γ^*_{kn} was done by Simpson's rule for volumes Values of θ^*_{kn} and ϕ^*_{kn} were computed, weighting by $\Gamma(\phi,\theta)$

For the case $\alpha = 50^\circ$ no data were available for $\phi \neq 0$ Since $\Gamma(\phi,\theta)$ here was small compared to $\alpha = 60^\circ$, the approximation shown below was considered justifiable Angular distributions were plotted as shown in Fig 45 The total, radial, and skew beams, defined as for Fig 43, stand out very clearly Further, it can be seen that the skew beam for $\alpha = 60^\circ$, $\phi = 0$ has very nearly the same shape as that for $\alpha = 50^\circ$ It was therefore assumed that $\Gamma^*_n(\alpha = 50) = \Gamma^*_n(\alpha = 60)$ times the $\frac{3}{2}$ power of the ratio of areas under the skew beam curves The $\frac{3}{2}$ power is employed because a volume ratio is desired, whereas only the cross-sectional area ratio is available The radial beam was, of course, treated as before

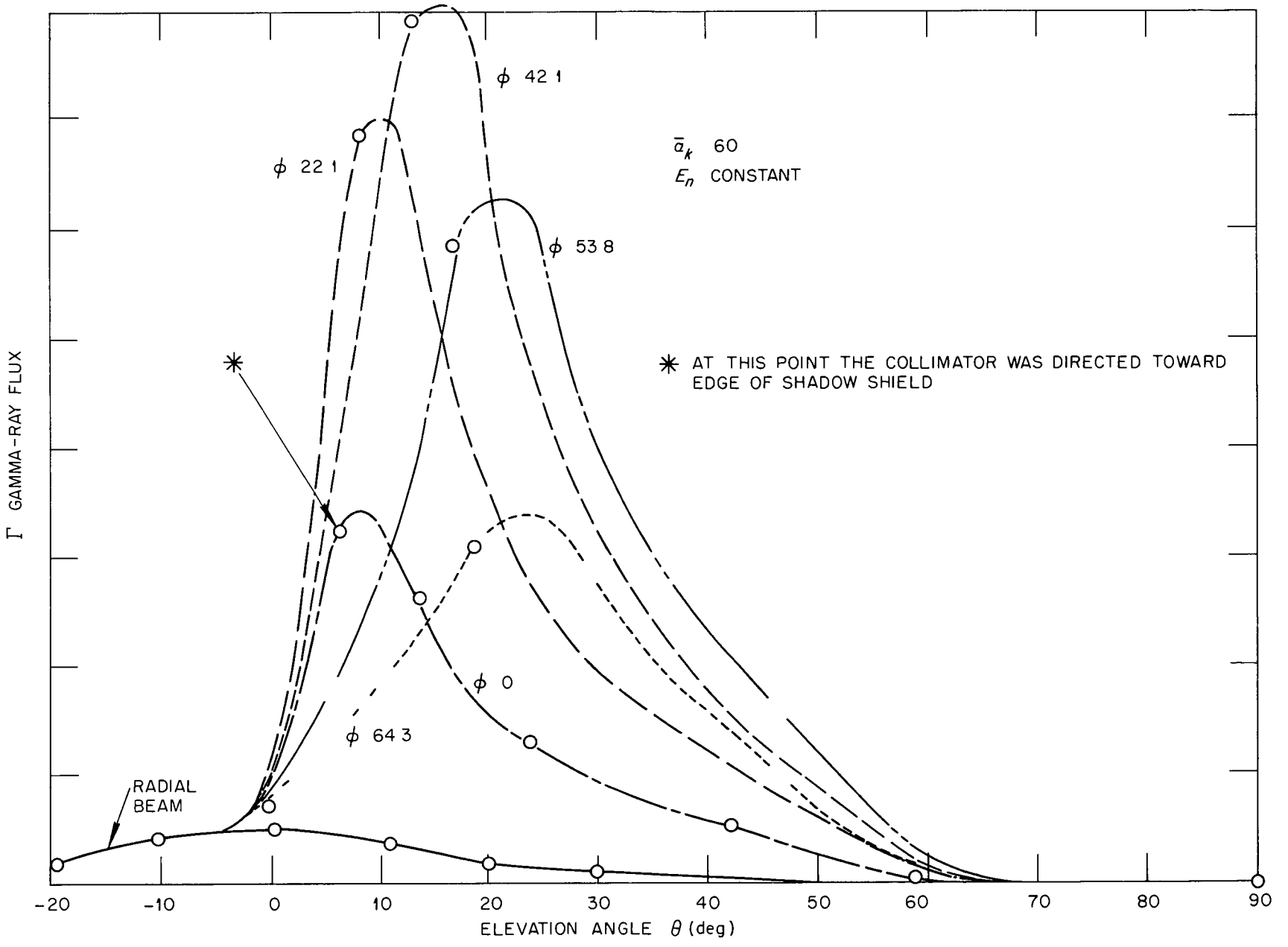

Fig 43 Typical Angular Distribution of Skew Emission Radiation (a 60)

[redacted]

DWG 19861

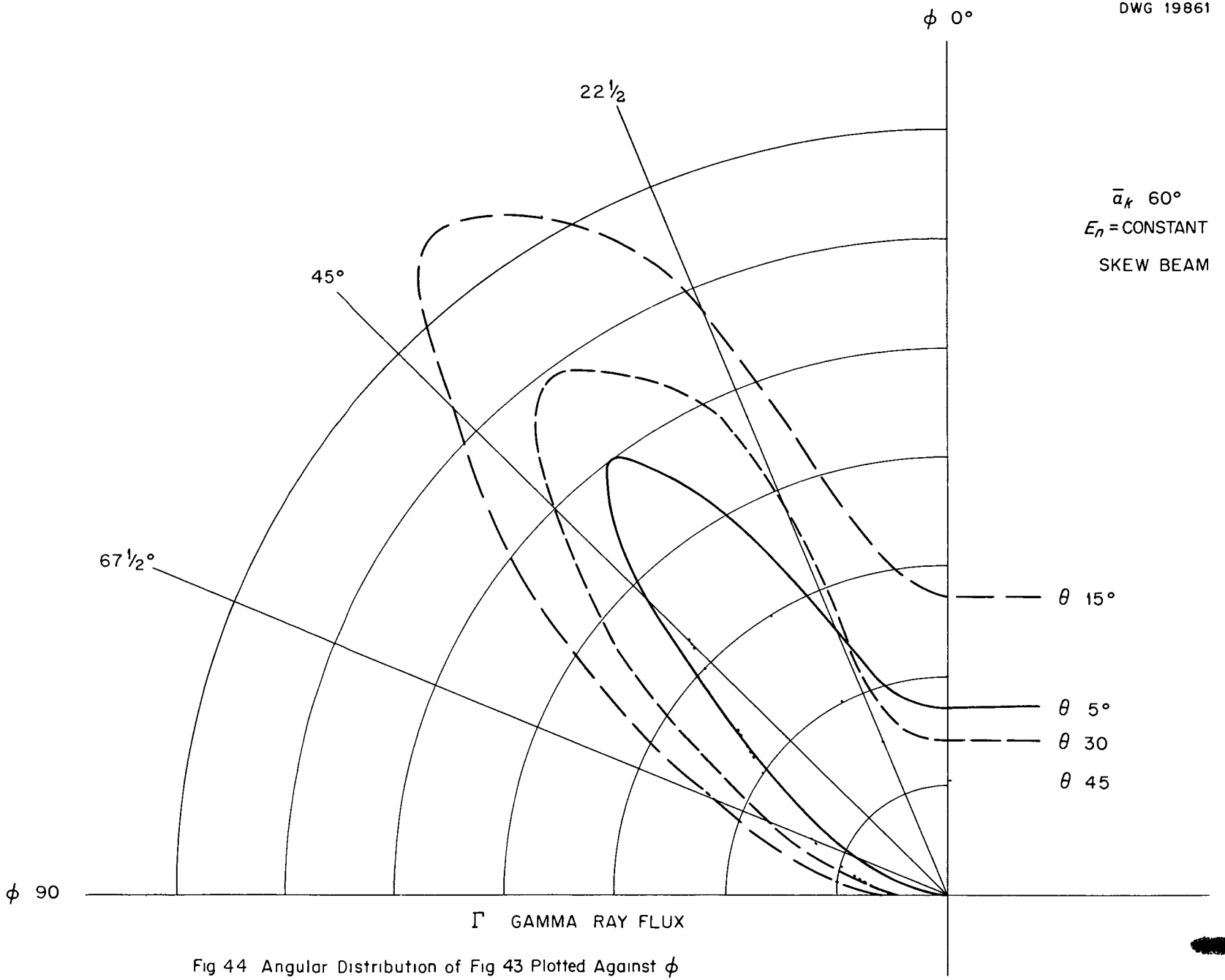

Fig 44 Angular Distribution of Fig 43 Plotted Against ϕ

[redacted]

[redacted]

DWG 19862

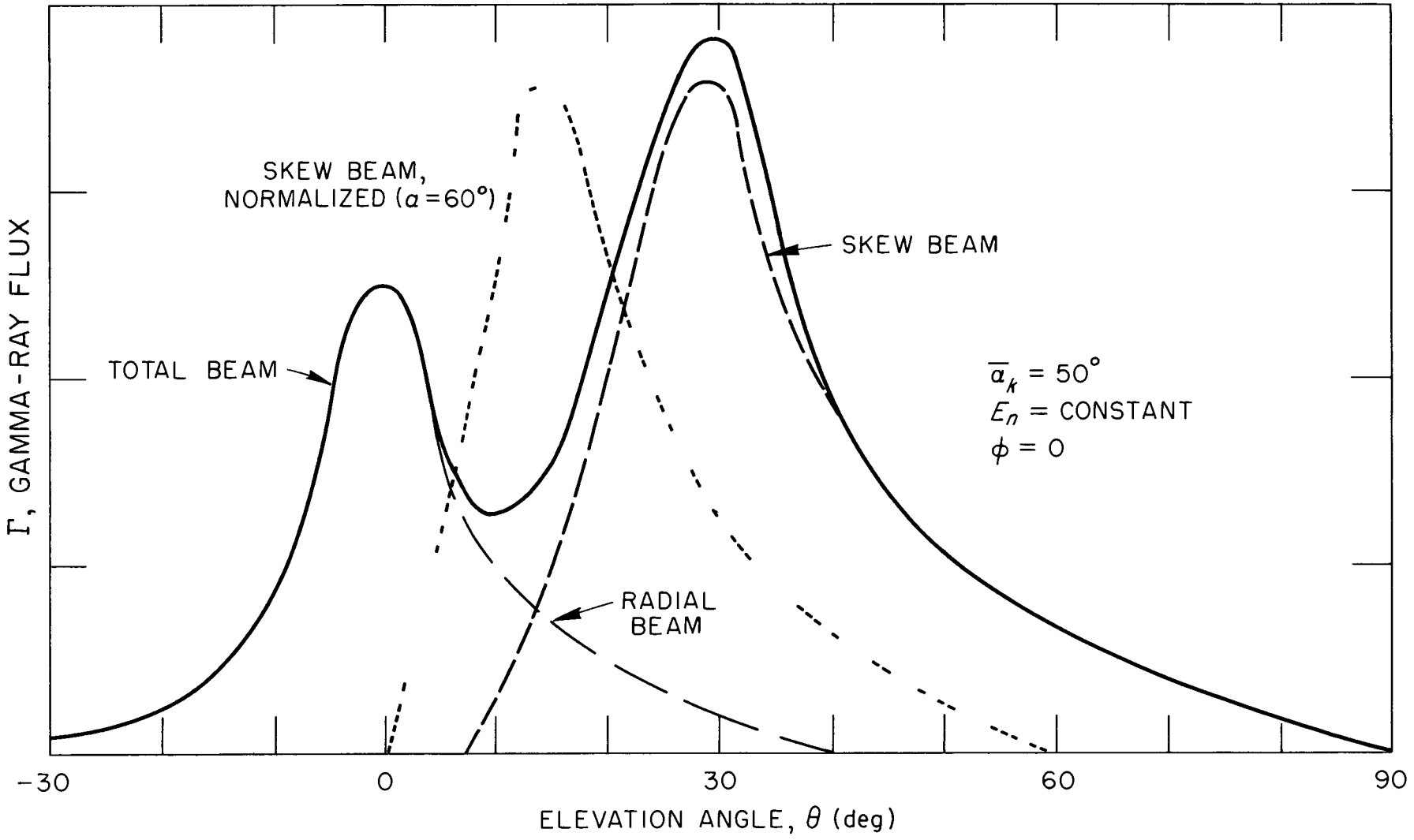

Fig 45 Typical Angular Distribution of Skew Emission Radiation (α = 50°)

[redacted]

It then remained only to find θ^*_{kn} and ϕ^*_{kn} for $\alpha = 50^\circ$ It was assumed that these angles are determined by a point, P, in the plane of the shadow shield P acts as a point source of scattered photons It was further assumed that P also acts as source for the skew beam at $\alpha = 60^\circ$, and its coordinates are thus determined by θ^*_{kn} and ϕ^*_{kn} The geometry is illustrated in Fig 46 The coordinates of P, i e , x_o, y_o and z_o were found as follows

The general equations of planes O and B were found as in Eq (33) and the $\cos\phi^*$ was found by Eq (36) Rearranging,

$$z_o^2 = \frac{\left[(s_{2o} + s_1)x_o - \rho_{6o}s_1\right]^2 \tan^2\phi_o^*}{(s_{2o} + s_1)^2 + \rho_{6o}^2} \tag{41}$$

Applying the cosine law to the triangle in plane O and making appropriate substitutions,

$$z_o^2 = \frac{(r_o^{*2} + s_{2o}^2 - s_1^2 + \rho_{6o}^2 - 2\rho_{6o}x_o)^2}{4r_o^{*2}\cos^2\theta_o^*} - s_{2o}^2 - (x_o - \rho_{6o})^2 \tag{42}$$

Finally, since P lies in plane A,

$$y_o = s_1 \tag{43}$$

[redacted]
DWG 19863

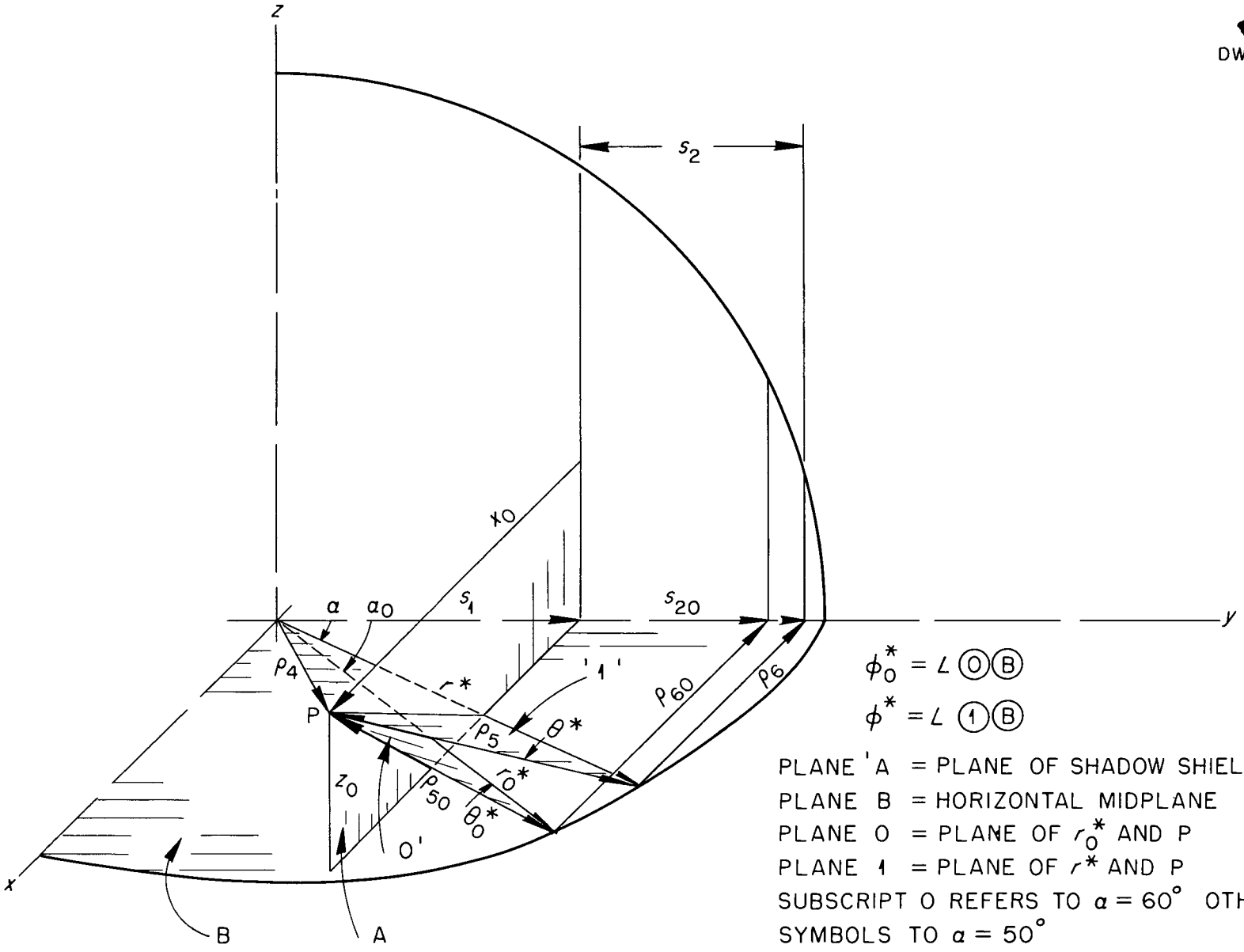

$\phi_0^* = \angle$ (O)(B)

$\phi^* = \angle$ (1)(B)

PLANE 'A = PLANE OF SHADOW SHIELD EDGE
PLANE B = HORIZONTAL MIDPLANE
PLANE O = PLANE OF r_0^* AND P
PLANE 1 = PLANE OF r^* AND P
SUBSCRIPT O REFERS TO $\alpha = 60°$ OTHER SYMBOLS TO $\alpha = 50°$

Fig 46 Geometry for Average Values of θ and ϕ for Skew Emission

Equations (41), (42), and (43) then give x_o, y_o and z_o, remembering that

$$\left.\begin{aligned} \rho_{6o} &= r_o^* \sin\alpha_o \\ s_{2o} + s_1 &= r_o^* \cos\alpha_o \end{aligned}\right\} \tag{44}$$

A similar procedure gives the following equations for ϕ^*_{nk} and ϕ^*_{nk} ($\alpha = 50^o$)

$$\left.\begin{aligned} \cos\theta^*_{nk} &= \frac{r^{*2} + s_2^2 - s_1^2 + \rho_6^2 - 2\rho_6 - x_{on}}{2r^* \sqrt{s_2^2 + (x_{on} - \rho_6)^2 + z_{on}^2}} \\ \tan\phi^*_{nk} &= \frac{z_{on}}{(s_2 + s_1)x_{on} - \rho_6 s_1} \sqrt{(s_2 + s_1)^2 + \rho_6^2} \end{aligned}\right\} \tag{45}$$

where, as before,

$$\left.\begin{aligned} \rho_6 &= r^* \sin\alpha \\ s_2 + s_1 &= r^* \cos\alpha \end{aligned}\right\} \tag{46}$$

The values of Γ^*_{nk}, θ^*_{nk} and ϕ^*_{nk}, obtained as outlined above, were used to compute the radiation scattered from the skew beam to the receiver

Appendix E

PARTITIONS USED IN CALCULATIONS

Table E-1 Radial Beam Partitions

Index	θ_i (deg)	α_k (deg)	β_p (deg)	E_n (Mev)	r^*_k (cm)	$(\rho t)_k$ (g/cm^2)	Γ^*_{kn} $\left(\frac{\text{photons}}{\text{cm}^2 \text{ sec Mev watt}}\right)$ n = 1	n = 2	n = 3	n = 4	n = 5	n = 6
0	0	0	0	0 8								
1	10	5	10	2 0	172	316	2 23	1 634	610	217		
2	14	15	20	3 5	173	316	2 23	1 634	610	217		
3	20	25	30	5 0	178	316	2 23	1 634	610	217		
4	25	35	40	7 5	183	316	2 23	1 634	610	217		
5	30	45	50	9 0	186	316	2 23	1 634	610	217		
6	40	55	60	10 5	182	316	1 26	482	107	0326		
7	60	65	70		173	316	4 82	1 50	158	0347		
8	90	75	80		165	136	19,350	6,490	2,410	948	420	28 4
9		85	90		160	134	22,300	7,220	2,630	1,020	450	30 5
10		95	100		159	134	22,300	7,220	2,630	1,020	450	30 5
11		105	110		160	134	22,300	7,220	2,630	1,020	450	30 5
12		115	120		161	134	22,300	7,220	2,630	1,020	450	30 5
13		125	130		163	132	25,500	8,000	2,860	1,110	483	32 5
14		135	140		169	127	35,140	10,600	3,570	1,390	581	38 6
15		145	150		173	156	5,440	2,490	1,053	433	219	16 0
16		155	160		171	162	3,770	1,880	827	349	175	13 5
17		165	170		163	159	4,500	2,160	930	390	197	14 8
18		180	180		155	157	5,010	2,360	1,000	419	209	15 7

Table E-2 Skew Beam Partitions

(Those partitions not shown are the same as in Table E-1)

Index m	Index n	Index k	r_m (ft)	θ^*_{kn} (deg)	ϕ^*_{kn} (deg)	Γ^*_{kn} $\left(\frac{\text{photons}}{\text{cm}^2 \text{ sec Mev watt}}\right)$
0	1	6	0	41 3	37 2	7 08
1		7	5	31 5	39 2	84 1
2	2	6	10	29 8	23 1	2 41
3		7	15	22 3	36 2	37 9
	3	6		26 7	21 9	1 15
17		7	85	19 2	35 3	12 0
18	4	6	90	25 2	21 2	0 48
19		7	95	17 6	34 7	3 99
20			100			
21			150			
22			200			
37			950			
38			1000			
39			1500			
40			2000			

Table E-3 Direct Beam Partitions

Index k	Γ^*_{kn} $\left(\frac{\text{photons}}{\text{cm}^2 \text{ sec Mev watt steradian}}\right)$			
	n = 1	n = 2	n = 3	n = 4
1	25 6	32 7	12 0	3 80
2	16 20	13 0	4 0	1 20
3	6 20	2 30	0 56	0 20
4	2 9	0 60	0 10	0
5	1 95	0 20	0	0
6	21 2	3 20	0 10	0
7	40 0	6 00	0	0
8	580	50	0	0
9	120	5 0	0	0

Appendix F

POSTSCATTER ENERGY, FLUX, AND DOSE FOR INDIVIDUAL CELLS

Radial Emission

The postscatter energy and flux values of photons emitted radially from the reactor shield and the resultant dose values within the crew compartment are given in Table F-1 for the individual cells The symbols used in the table are defined as follows

k = index for source angle α (given in Table E-1, p 97),

p = index for receiver angle β (given in Table E-1, p 97),

E' = postscatter energy (Mev),

I/P = flux outside crew shield $\left(\frac{\text{photons}}{\text{cm}^3\ \text{sec}}\right)$,

D = dose inside crew shield $\left(\frac{\text{r}}{\text{hr watt}}\right)$

Table F-1. Radial Emission

k	p	E'	$I/P \times 10^6$	$D \times 10^{11}$
1	1	1 37	129	0
		2 63	113	0
		3 97	40 3	0
		5 66	22 5	0
		7 25	0	0
		8 29	0	0
1	2	1 24	103	0 181
		2 20	78 2	0 281
		3 07	24 4	0 154
		3 99	11 9	0 114
		4 72	0	0
		5 14	0	0
1	3	1 07	73 8	0 531
		1 71	48 6	0 828
		2 19	13 8	0 334
		2 62	6 3	0 190
		2 92	0	0
		3 07	0	0
1	4	0 893	50 8	0 379
		1 30	30 9	0 665
		1 56	8 54	0 269
		1 77	3 81	0 143
		1 90	0	0
		1 96	0	0
1	5	0 741	36 7	0 187
		1 00	21 2	0 313
		1 15	5 82	0 126
		1 26	2 58	0 0706
		1 32	0	0
		1 35	0	0
1	6	0 617	26 4	0 0881
		0 787	15 7	0 145
		0 875	4 29	0 0602
		0 937	1 89	0 0325
		0 973	0	0
		0 989	0	0

k	p	E'	I/P x 10^6	D x 10^{11}
1	7	0 520	20 7	0 0423
		0 635	12 3	0 0691
		0 692	3 36	0 0264
		0 730	1 47	0 0141
		0 751	0	0
		0 761	0	0
1	8	0 444	17 2	0 0173
		0 526	10 2	0 0262
		0 565	2 75	0 0100
		0 590	1 20	0 0056
		0 603	0	0
		0 610	0	0
1	9	0 386	15 0	0 0065
		0 447	8 75	0 0101
		0 474	2 34	0 0038
		0 491	1 01	0 0020
		0 501	0	0
		0 505	0	0
1	10	0 341	13 6	0 0020
		0 388	7 74	0 0034
		0 408	2 04	0 0013
		0 421	0 871	0 0007
		0 428	0	0
		0 431	0	0
1	11	0 306	12 6	0 0005
		0 343	7 02	0 0009
		0 359	1 83	0 0004
		0 369	0 773	0 0002
		0 374	0	0
		0 377	0	0
1	12	0 279	12 0	0 0001
		0 310	6 48	0 0002
		0 322	1 67	0 0001
		0 331	0 701	0
		0 335	0	0
		0 337	0	0
1	13	0 259	11 5	0
		0 284	6 09	0
		0 295	1 55	0
		0 302	0 647	0
		0 305	0	0
		0 307	0	0

k	p	E'	I/P x 10^6	D x 10^{11}
1	14	0 243	11 2	0
		0 265	5 80	0
		0 275	1 47	0
		0 280	0 607	0
		0 284	0	0
		0 285	0	0
1	15	0 231	11 0	0
		0 251	5 59	0
		0 260	1 40	0
		0 265	0 579	0
		0 268	0	0
		0 269	0	0
1	16	0 223	10 9	0
		0 242	5 45	0
		0 250	1 36	0
		0 254	0 559	0
		0 257	0	0
		0 258	0	0
1	17	0 218	10 8	0
		0 236	5 37	0
		0 243	1 33	0
		0 248	0 547	0
		0 250	0	0
		0 251	0	0
1	18	0 216	10 7	0
		0 233	5 33	0
		0 240	1 32	0
		0 245	0 542	0
		0 248	0	0
		0 249	0	0
2	1	1 28	223	0
		2 32	176	0 0001
		3 31	57 0	0 0001
		4 41	28 5	0 0001
		5 32	0	0
		5 86	0	0
2	2	1 11	163	0 173
		1 83	111	0 276
		2 39	32 1	0 145
		2 91	14 7	0 105
		3 28	0	0
		3 48	0	0

k	p	E'	I/P x 10^6	D x 10^{11}
2	3	0 936	113	0 566
		1 39	69 6	0 873
		1 70	19 3	0 330
		1 94	8 63	0 193
		2 10	0	0
		2 18	0	0
2	4	0 776	78 6	0 401
		1 07	46 8	0 605
		1 24	12 8	0 237
		1 36	5 71	0 125
		1 44	0	0
		1 47	0	0
2	5	0 645	57 3	0 156
		0 834	34 0	0 267
		0 934	9 31	0 110
		1 00	4 12	0 060
		1 04	0	0
		1 06	0	0
2	6	0 542	44 3	0 0858
		0 669	26 3	0 144
		0 731	7 19	0 0564
		0 774	3 16	0 0303
		0 798	0	0
		0 809	0	0
2	7	0 461	36 4	0 0405
		0 551	21 5	0 0632
		0 592	5 83	0 0237
		0 620	2 54	0 0125
		0 635	0	0
		0 642	0	0
2	8	0 399	31 4	0 0156
		0 464	18 3	0 0247
		0 494	4 91	0 0095
		0 513	2 12	0 0050
		0 523	0	0
		0 528	0	0
2	9	0 351	28 1	0 0057
		0 401	16 1	0 0092
		0 423	4 26	0 0035
		0 436	1 82	0 0018
		0 444	0	0
		0 447	0	0

k	p	E'	I/P x 10^6	D x 10^{11}
2	10	0 314	26 0	0 0017
		0 353	14 5	0 0030
		0 370	3 80	0 0012
		0 381	1 61	0 0006
		0 386	0	0
		0 389	0	0
2	11	0 285	24 5	0 0005
		0 317	13 4	0 0009
		0 331	3 45	0 0003
		0 339	1 45	0 0002
		0 344	0	0
		0 346	0	0
2	12	0 263	23 5	0 0001
		0 290	12 5	0 0002
		0 301	3 19	0 0001
		0 308	1 33	0
		0 312	0	0
		0 314	0	0
2	13	0 246	22 8	0
		0 270	11 9	0
		0 279	3 00	0
		0 285	1 25	0
		0 288	0	0
		0 290	0	0
2	14	0 234	22 4	0
		0 254	11 4	0
		0 263	2 87	0
		0 268	1 18	0
		0 271	0	0
		0 272	0	0
2	15	0 225	22 0	0
		0 244	11 1	0
		0 252	2 77	0
		0 257	1 14	0
		0 259	0	0
		0 260	0	0
2	16	0 219	21 8	0
		0 237	10 9	0
		0 245	2 71	0
		0 249	1 11	0
		0 252	0	0
		0 253	0	0
2	17	0 216	21 7	0
		0 234	10 8	0
		0 241	2 68	0
		0 245	1 10	0
		0 248	0	0
		0 249	0	0

k	p	E'	I/P x 10^6	D x 10^{11}
3	1	1 11	173	0
		1 83	117	0
		2 39	34 0	0
		2 91	15 6	0
		3 28	0	0
		3 48	0	0
3	2	0 936	119	0 0077
		1 39	73 6	0 0151
		1 70	20 4	0 0054
		1 94	9 13	0 0029
		2 10	0	0
		2 18	0	0
3	3	0 776	83 3	0 285
		1 07	49 5	0 355
		1 24	13 6	0 134
		1 36	6 04	0 063
		1 44	0	0
		1 47	0	0
3	4	0 645	60 7	0 118
		0 834	35 9	0 204
		0 934	9 86	0 084
		1 00	4 36	0 050
		1 04	0	0
		1 06	0	0
3	5	0 542	46 9	0 0526
		0 669	27 9	0 0890
		0 731	7 62	0 0380
		0 774	3 34	0 0209
		0 798	0	0
		0 809	0	0
3	6	0 461	38 5	0 0285
		0 551	22 8	0 0480
		0 592	6 18	0 0189
		0 620	2 69	0 0105
		0 635	0	0
		0 642	0	0
3	7	0 399	33 2	0 0134
		0 464	19 4	0 0220
		0 494	5 20	0 0086
		0 513	2 24	0 0045
		0 523	0	0
		0 528	0	0

k	p	E'	I/P x 10^6	D x 10^{11}
3	8	0 351	29 8	0 0053
		0 401	17 0	0 0090
		0 423	4 51	0 0034
		0 436	1 93	0 0018
		0 444	0	0
		0 447	0	0
3	9	0 314	27 5	0 0018
		0 353	15 4	0 0032
		0 370	4 02	0 0012
		0 381	1 70	0 0007
		0 386	0	0
		0 389	0	0
3	10	0 285	26 0	0 0006
		0 317	14 1	0 0010
		0 331	3 65	0 0004
		0 339	1 54	0 0002
		0 344	0	0
		0 346	0	0
3	11	0 263	24 9	0 0002
		0 290	13 2	0 0003
		0 301	3 38	0 0001
		0 308	1 41	0
		0 312	0	0
		0 314	0	0
3	12	0 246	24 2	0
		0 270	12 6	0
		0 279	3 18	0
		0 285	1 32	0
		0 288	0	0
		0 290	0	0
3	13	0 234	23.7	0
		0 254	12 1	0
		0 263	3 04	0
		0 268	1 25	0
		0 271	0	0
		0 272	0	0
3	14	0 225	23 3	0
		0 244	11 7	0
		0 252	2 93	0
		0 257	1 21	0
		0 259	0	0
		0 260	0	0

k	p	E'	I/P x 10^6	D x 10^{11}
3	15	0 219	23 1	0
		0 237	11 5	0
		0 245	2 87	0
		0 249	1 18	0
		0 252	0	0
		0 253	0	0
3	16	0 216	23 0	0
		0 234	11 4	0
		0 241	2 83	0
		0 245	1 16	0
		0 248	0	0
		0 249	0	0
4	1	0 936	126	0
		1 39	77 8	0
		1 70	21 6	0
		1 94	9 66	0
		2 10	0	0
		2 18	0	0
4	2	0 776	88 0	0 0396
		1 07	52 3	0 0659
		1 24	14 4	0 0211
		1 36	6 39	0 0092
		1 44	0	0
		1 47	0	0
4	3	0 645	64 1	0 0964
		0 834	38 0	0 1419
		0 934	10 4	0 0517
		1 00	4 60	0 0273
		1 04	0	0
		1 06	0	0
4	4	0 542	49 6	0 0337
		0 669	29 5	0 0680
		0 731	8 05	0 0281
		0 774	3 53	0 0154
		0 798	0	0
		0 809	0	0
4	5	0 461	40 7	0 0162
		0 551	24 1	0 0307
		0 592	6 53	0 0119
		0 620	2 84	0 0066
		0 635	0	0
		0 642	0	0

k	p	E'	I/P x 10^6	D x 10^{11}
4	6	0 399	35 1	0 0093
		0 464	20 5	0 0164
		0 494	5 50	0 0066
		0 513	2 37	0 0035
		0 523	0	0
		0 528	0	0
4	7	0 351	31 5	0 0044
		0 401	18 0	0 0077
		0 423	4 77	0 0030
		0 436	2 04	0 0015
		0 444	0	0
		0 447	0	0
4	8	0 314	29 1	0 0017
		0 353	16 2	0 0030
		0 370	4 25	0 0012
		0 381	1 80	0 0006
		0 386	0	0
		0 389	0	0
4	9	0 285	27 5	0 0006
		0 317	14 9	0 0011
		0 331	3 86	0 0004
		0 339	1 62	0 0002
		0 344	0	0
		0 346	0	0
4	10	0 263	26 3	0 0002
		0 290	14 0	0 0004
		0 301	3 57	0 0001
		0 308	1 49	0
		0 312	0	0
		0 314	0	0
4	11	0 246	25 6	0
		0 270	13 3	0 0001
		0 279	3 36	0
		0 285	1 39	0
		0 288	0	0
		0 290	0	0
4	12	0 234	25 0	0
		0 254	12 8	0
		0 263	3 21	0
		0 268	1 32	0
		0 271	0	0
		0 272	0	0

k	p	E'	I/P x 10^6	D x 10^{11}
4	13	0 225	24 7	0
		0 244	12 4	0
		0 252	3 10	0
		0 257	1 27	0
		0 259	0	0
		0 260	0	0
4	14	0 219	24 4	0
		0 237	12 2	0
		0 245	3 03	0
		0 249	1 24	0
		0 252	0	0
		0 253	0	0
4	15	0 216	24 3	0
		0 234	12 1	0
		0 241	3 00	0
		0 245	1 23	0
		0 248	0	0
		0 249	0	0
5	1	0 776	90 9	0
		1 07	54 0	0
		1 24	15 0	0
		1 36	6 60	0
		1 44	0	0
		1 47	0	0
5	2	0 645	66 2	0 0117
		0 834	39 2	0 0209
		0 934	10 9	0 0084
		1 00	4 76	0 0047
		1 04	0	0
		1 06	0	0
5	3	0 542	51 2	0 0311
		0 669	30 4	0 0507
		0 731	8 41	0 0197
		0 774	3 65	0 0109
		0 798	0	0
		0 809	0	0
5	4	0 461	42 0	0 0099
		0 551	24 9	0 0200
		0 592	6 82	0 0086
		0 620	2 93	0 0047
		0 635	0	0
		0 642	0	0

k	p	E'	I/P x 10^6	D x 10^6
5	5	0 399	36 2	0 0043
		0 464	21 2	0 0086
		0 494	5 74	0 0036
		0 513	2 45	0 0019
		0 523	0	0
		0 528	0	0
5	6	0 351	32 5	0 0028
		0 401	18 6	0 0052
		0 423	4 99	0 0024
		0 436	2 11	0 0013
		0 444	0	0
		0 447	0	0
5	7	0 314	30 0	0 0013
		0 353	16 8	0 0025
		0 370	4 44	0 0010
		0 381	1 86	0 0005
		0 386	0	0
		0 389	0	0
5	8	0 285	28 4	0 0005
		0 317	15 4	0 0010
		0 331	4 03	0 0004
		0 339	1 68	0 0002
		0 344	0	0
		0 346	0	0
5	9	0 263	27 2	0 0002
		0 290	14 4	0 0004
		0 301	3 73	0 0002
		0 308	1 54	0
		0 312	0	0
		0 314	0	0
5	10	0 246	26 4	0
		0 270	13 7	0
		0 279	3 51	0
		0 285	1 44	0
		0 288	0	0
		0 290	0	0
5	11	0 234	25 8	0
		0 254	13 2	0
		0 263	3 35	0
		0 268	1 37	0
		0 271	0	0
		0 272	0	0

k	p	E'	I/P x 10^6	D x 10^{11}
5	12	0 225	25 5	0
		0 244	12 8	0
		0 252	3 24	0
		0 257	1 32	0
		0 259	0	0
		0 260	0	0
5	13	0 219	25 2	0
		0 237	12 6	0
		0 245	3 16	0
		0 249	1 28	0
		0 252	0	0
		0 253	0	0
5	14	0 216	25 1	0
		0 234	12 5	0
		0 241	3 13	0
		0 245	1 27	0
		0 248	0	0
		0 249	0	0
6	1	0 645	35 8	0
		0 834	11 1	0
		0 934	1 81	0
		1 00	0 684	0
		1 04	0	0
		1 06	0	0
6	2	0 542	27 7	0 0022
		0 669	8 60	0 0017
		0 731	1 40	0 0004
		0 774	0 525	0 0002
		0 798	0	0
		0 809	0	0
6	3	0 461	22 7	0 0043
		0 551	7 03	0 0043
		0 592	1 13	0 0010
		0 620	0 422	0
		0 635	0	0
		0 642	0	0
6	4	0 399	19 6	0 0012
		0 464	5 98	0 0015
		0 494	0 954	0 0004
		0 513	0 352	0 0002
		0 523	0	0
		0 528	0	0

k	p	E'	I/P x 10^6	D x 10^{11}
6	5	0 351	17 6	0 0006
		0 401	5 26	0 0007
		0 423	0 828	0 0002
		0 436	0 303	0 0001
		0 444	0	0
		0 447	0	0
6	6	0 314	16 3	0 0004
		0 353	4 74	0 0004
		0 370	0 737	0 0001
		0 381	0 267	0
		0 386	0	0
		0 389	0	0
6	7	0 285	15 3	0 0002
		0 317	4 36	0 0002
		0 331	0 669	0
		0 339	0 241	0
		0 344	0	0
		0 346	0	0
6	8	0 263	14 7	0
		0 290	4 08	0
		0 301	0 620	0
		0 308	0 222	0
		0 312	0	0
		0 314	0	0
6	9	0 246	14 3	0
		0 270	3 87	0
		0 279	0 583	0
		0 285	0 207	0
		0 288	0	0
		0 290	0	0
6	10	0 234	14 0	0
		0 255	3 73	0
		0 263	0 556	0
		0 268	0 196	0
		0 271	0	0
		0 272	0	0
6	11	0 225	13 8	0
		0 244	3 62	0
		0 252	0 537	0
		0 257	0 189	0
		0 259	0	0
		0 260	0	0

k	p	E'	I/P x 10^6	D x 10^{11}
6	12	0 219	13 6	0
		0 237	3 55	0
		0 245	0 526	0
		0 249	0 185	0
		0 252	0	0
		0 253	0	0
6	13	0 216	13 6	0
		0 234	3 52	0
		0 241	0 520	0
		0 245	0 182	0
		0 248	0	0
		0 249	0	0
7	1	0 542	95 8	0
		0 669	24 2	0
		0 731	1 86	0
		0 774	0 505	0
		0 798	0	0
		0 809	0	0
7	2	0 461	78 6	0 0016
		0 551	19 8	0 0018
		0 592	1 51	0 0002
		0 620	0 406	0 0001
		0 635	0	0
		0 642	0	0
7	3	0 399	67 8	0 0033
		0 464	16 8	0 0033
		0 494	1 27	0 0004
		0 513	0 339	0 0001
		0 523	0	0
		0 528	0	0
7	4	0 351	60 8	0 0010
		0 401	14 8	0 0010
		0 423	1 10	0 0001
		0 436	0 291	0
		0 444	0	0
		0 447	0	0
7	5	0 314	56 2	0 0004
		0 353	13 3	0 0005
		0 370	0 983	0 0001
		0 381	0 257	0
		0 386	0	0
		0 389	0	0

k	p	E'	I/P x 10^6	D x 10^{11}
7	6	0 285	53 0	0 0004
		0 317	12 3	0 0003
		0 331	0 894	0
		0 339	0 232	0
		0 344	0	0
		0 346	0	0
7	7	0 263	50 9	0
		0 290	11 5	0
		0 301	0 827	0
		0 308	0 213	0
		0 312	0	0
		0 314	0	0
7	8	0 246	49 3	0
		0 270	10 9	0
		0 279	0 778	0
		0 285	0 199	0
		0 288	0	0
		0 290	0	0
7	9	0 234	48 3	0
		0 254	10 5	0
		0 263	0 742	0
		0 268	0 189	0
		0 271	0	0
		0 272	0	0
7	10	0 225	47 6	0
		0 244	10 2	0
		0 252	0 717	0
		0 257	0 182	0
		0 259	0	0
		0 260	0	0
7	11	0 219	47 2	0
		0 237	10 0	0
		0 245	0 701	0
		0 249	0 178	0
		0 252	0	0
		0 253	0	0
7	12	0 216	47 0	0
		0 234	9 90	0
		0 241	0 693	0
		0 245	0 175	0
		0 248	0	0
		0 249	0	0

k	p	E'	I/P x 10^6	D x 10^{11}
8	1	0 461	287000	0
		0 551	77800	0
		0 592	20900	0
		0 620	10100	0
		0 635	2120	0
		0 642	104	0
8	2	0 399	247000	0 863
		0 464	66200	1 37
		0 494	17600	0 713
		0 513	8420	0 486
		0 523	1760	0 122
		0 528	86 5	0 0064
8	3	0 351	222000	2 56
		0 401	58200	3 03
		0 423	15300	1 34
		0 436	7240	0 824
		0 440	1510	0 206
		0 447	73 8	0 0109
8	4	0 314	205000	0 700
		0 353	52400	0 871
		0 370	13600	0 394
		0 381	6390	0 252
		0 386	1320	0 061
		0 389	64 7	0 0032
8	5	0 285	194000	0 362
		0 317	48200	0 438
		0 331	12400	0 195
		0 339	5770	0 124
		0 344	1190	0 0299
		0 346	58 0	0 0016
8	6	0 263	186000	0 365
		0 290	45100	0 387
		0 301	11500	0 165
		0 308	5300	0 102
		0 312	1090	0 0246
		0 314	53 0	0 0013
8	7	0 246	180000	0 253
		0 270	42900	0 256
		0 279	10800	0 107
		0 285	4950	0 0656
		0 288	1010	0 0156
		0 290	49 3	0 0008

k	p	E'	$I/P \times 10^6$	$D \times 10^{11}$
8	8	0 234	176000	0 127
		0 254	41200	0 147
		0 263	10300	0 0614
		0 268	4700	0 0378
		0 271	960	0 0090
		0 272	46 6	0 0005
8	9	0 225	174000	0 0846
		0 244	40000	0 0866
		0 252	9940	0 0362
		0 257	4530	0 0223
		0 259	922	0 0053
		0 260	44 7	0 0002
8	10	0 219	172000	0 0501
		0 237	39300	0 0522
		0 245	9720	0 0222
		0 249	4410	0 0134
		0 252	898	0 0032
		0 253	43 6	0 0002
8	11	0 216	171000	0 0302
		0 234	39000	0 0316
		0 241	9610	0 0140
		0 245	4360	0 0087
		0 248	886	0 0021
		0 249	43 0	0 0001
9	1	0 399	268000	0
		0 464	69300	0
		0 494	18100	0
		0 513	8520	0
		0 523	1770	0
		0 528	87 3	0
9	2	0 351	240000	0 115
		0 401	60900	0 222
		0 423	15700	0 114
		0 436	7330	0 0749
		0 444	1520	0 0198
		0 447	74 5	0 0011
9	3	0 314	222000	0 529
		0 353	54900	0 676
		0 370	14000	0 303
		0 381	6470	0 194
		0 386	1330	0 0472
		0 389	65 3	0 0024

k	p	E'	I/P x 10^6	D x 10^{11}
9	4	0 285	210000	0 147
		0 317	50500	0 198
		0 331	12700	0 0900
		0 339	5840	0 0583
		0 344	1200	0 0142
		0 346	58 5	0 0008
9	5	0 263	201000	0 0901
		0 290	47200	0 115
		0 301	11800	0 0511
		0 308	5360	0 0327
		0 312	1100	0 0080
		0 314	53 5	0 0004
9	6	0 246	195000	0 120
		0 270	44900	0 129
		0 279	11100	0 0550
		0 285	5010	0 0340
		0 288	1020	0 0081
		0 290	49 8	0 0004
9	7	0 234	191000	0 0867
		0 254	43100	0 104
		0 263	10600	0 0435
		0 268	4760	0 0267
		0 271	967	0 0063
		0 272	47 1	0 0004
9	8	0 225	188000	0 0736
		0 244	41900	0 0742
		0 252	10200	0 0307
		0 257	4580	0 0188
		0 259	928	0 0044
		0 260	45 2	0 0003
9	9	0 219	187000	0 0543
		0 237	41100	0 0546
		0 245	9980	0 0228
		0 249	4470	0 0136
		0 252	905	0 0032
		0 253	44 0	0 0002
9	10	0 216	186000	0 0412
		0 234	40800	0 0408
		0 241	9870	0 0176
		0 245	4410	0 0106
		0 248	893	0 0025
		0 249	43 4	0 0001

k	p	E'	I/P x 10^6	D x 10^{11}
10	1	0 351	237000	0
		0 401	60100	0
		0 423	15500	0
		0 436	7240	0
		0 444	1500	0
		0 447	73 6	0
10	2	0 314	219000	0 0127
		0 353	54200	0 0283
		0 370	13800	0 0155
		0 381	6390	0 0110
		0 386	1320	0 0028
		0 389	64 5	0 0001
10	3	0 285	207000	0 0954
		0 317	49900	0 136
		0 331	12600	0 0633
		0 339	5760	0 0414
		0 344	1180	0 0102
		0 346	57 8	0 0006
10	4	0 263	199000	0 0296
		0 290	46700	0 0431
		0 301	11600	0 0203
		0 308	5300	0 0134
		0 312	1080	0 0033
		0 314	52 8	0 0002
10	5	0 246	193000	0 0232
		0 270	44300	0 0312
		0 279	10900	0 0142
		0 285	4950	0 0091
		0 288	1010	0 0022
		0 290	49 2	0 0001
10	6	0 234	189000	0 0341
		0 254	42600	0 0467
		0 263	10400	0 0203
		0 268	4700	0 0127
		0 271	955	0 0030
		0 272	46 5	0 0002
10	7	0 225	186000	0 0454
		0 244	41400	0 0486
		0 252	10100	0 0205
		0 257	4520	0 0126
		0 259	917	0 0030
		0 260	44 6	0 0001

k	p	E'	I/P x 10^6	D x 10^{11}
10	8	0 219	184000	0 0426
		0 237	40600	0 0442
		0 245	9860	0 0184
		0 249	4410	0 0112
		0 252	893	0 0027
		0 253	43 4	0 0001
10	9	0 216	183000	0 0406
		0 234	40300	0 0403
		0 241	9750	0 0174
		0 245	4360	0 0105
		0 248	882	0 0025
		0 249	42 9	0 0001
11	1	0 314	222000	0
		0 353	54900	0
		0 370	14000	0
		0 381	6470	0
		0 386	1330	0
		0 389	65 3	0
11	2	0 285	210000	0 0014
		0 317	50500	0 0036
		0 331	12700	0 0020
		0 339	5830	0 0015
		0 344	1200	0 0004
		0 346	58 5	0
11	3	0 263	201000	0 0191
		0 290	47200	0 0292
		0 301	11800	0 0141
		0 308	5360	0 0094
		0 312	1100	0 0023
		0 314	53 5	0 0001
11	4	0 246	195000	0 0067
		0 269	44900	0 0107
		0 279	11100	0 0052
		0 285	5010	0 0034
		0 288	1020	0 0008
		0 290	49 8	0
11	5	0 234	191000	0 0058
		0 254	43100	0 0100
		0 263	10600	0 0047
		0 268	4760	0 0031
		0 271	969	0 0009
		0 272	47 1	0

k	p	E'	$I/P \times 10^6$	$D \times 10^{11}$
11	6	0 225	188000	0 0174
		0 244	41900	0 0210
		0 252	10200	0 0092
		0 257	4580	0 0058
		0 259	929	0 0014
		0 260	45 2	0
11	7	0 219	187000	0 0262
		0 237	41100	0 0288
		0 245	9980	0 0124
		0 249	4470	0 0076
		0 252	905	0 0018
		0 253	44 0	0 0001
11	8	0 216	186000	0 0327
		0 234	40800	0 0331
		0 241	9870	0 0144
		0 245	4410	0 0018
		0 248	893	0 0021
		0 249	43 4	0 0001
12	1	0 285	212000	0
		0 317	51100	0
		0 331	12900	0
		0 339	5910	0
		0 344	1210	0
		0 346	59 3	0
12	2	0 263	204000	0 0002
		0 290	47800	0 0004
		0 301	11900	0 0003
		0 308	5430	0 0002
		0 312	1110	0
		0 314	54 2	0
12	3	0 246	198000	0 0041
		0 270	45400	0 0069
		0 279	11200	0 0034
		0 285	5080	0 0023
		0 288	1030	0 0005
		0 290	50 4	0
12	4	0 234	194000	0 0015
		0 254	43700	0 0032
		0 263	10700	0 0016
		0 268	4820	0 0011
		0 271	979	0 0003
		0 272	47 7	0

k	p	E'	I/P x 10^6	D x 10^{11}
12	5	0 225	191000	0 0027
		0 244	42400	0 0040
		0 252	10300	0 0019
		0 257	4640	0 0013
		0 259	940	0 0003
		0 260	45 7	0
12	6	0 219	189000	0 0097
		0 237	41700	0 0120
		0 245	10100	0 0053
		0 249	4520	0 0034
		0 252	916	0 0008
		0 253	44 5	0
12	7	0 216	188000	0 0191
		0 234	41300	0 0207
		0 241	10000	0 0092
		0 245	4470	0 0057
		0 248	904	0 0014
		0 249	44 0	0
13	1	0 263	239000	0
		0 290	54300	0
		0 301	13300	0
		0 308	6060	0
		0 312	1220	0
		0 314	59 2	0
13	2	0 246	232000	0
		0 270	51600	0
		0 279	12500	0
		0 285	5660	0
		0 288	1140	0
		0 290	55 1	0
13	3	0 234	227000	0 0009
		0 254	49600	0 0022
		0 263	11900	0 0011
		0 268	5370	0 0007
		0 271	1080	0 0002
		0 272	52 1	0
13	4	0 225	224000	0 0007
		0 244	48200	0 0013
		0 252	11500	0 0007
		0 257	5170	0 0004
		0 259	1030	0 0001
		0 260	50 0	0

k	p	E'	I/P x 10^6	D x 10^{11}
13	5	0 219	221000	0 0016
		0 237	47300	0 0024
		0 245	11300	0 0011
		0 249	5050	0 0008
		0 252	1010	0 0002
		0 253	48 6	0
13	6	0 216	221000	0 0008
		0 234	46900	0 0098
		0 241	11100	0 0044
		0 245	4980	0 0028
		0 248	995	0 0007
		0 249	48 0	0
14	1	0 246	343000	0
		0 270	73300	0
		0 279	16800	0
		0 285	7640	0
		0 288	1470	0
		0 290	70 3	0
14	2	0 234	336000	0
		0 254	70400	0
		0 263	16000	0
		0 268	7260	0
		0 271	1390	0
		0 272	66 5	0
14	3	0 225	331000	0 0006
		0 244	68500	0 0011
		0 252	15500	0 0005
		0 257	6980	0 0004
		0 259	1340	0
		0 260	63 8	0
14	4	0 219	328000	0 0005
		0 237	67200	0 0009
		0 245	15100	0 0004
		0 249	6810	0 0003
		0 252	1300	0
		0 253	62 1	0
14	5	0 216	327000	0 0016
		0 234	66600	0 0024
		0 241	14900	0 0011
		0 245	6730	0 0007
		0 248	1290	0
		0 249	61 3	0

k	p	E'	I/P x 10^6	D x 10^{11}
15	1	0 234	54500	0
		0 254	17400	0
		0 263	4950	0
		0 268	2360	0
		0 271	550	0
		0 272	28 9	0
15	2	0 225	53700	0
		0 244	16900	0
		0 252	4780	0
		0 257	2270	0
		0 259	528	0
		0 260	27 7	0
15	3	0 219	53200	0
		0 237	16600	0 0001
		0 245	4670	0 0008
		0 249	2220	0 0006
		0 252	515	0 0002
		0 253	27 0	0
15	4	0 216	53000	0
		0 234	16400	0 0002
		0 241	4620	0 0001
		0 245	2190	0
		0 248	508	0
		0 249	26 6	0
16	1	0 225	36400	0
		0 244	12500	0
		0 252	3670	0
		0 257	1790	0
		0 259	413	0
		0 260	22 8	0
16	2	0 219	36000	0
		0 237	12200	0
		0 245	3580	0
		0 249	1750	0
		0 252	402	0
		0 253	22 2	0
16	3	0 216	35900	0
		0 234	12100	0
		0 241	3550	0
		0 245	1720	0
		0 248	397	0
		0 249	21 9	0

k	p	E'	I/P x 10^6	D x 10^{11}
17	1	0 219	39100	0
		0 237	12800	0
		0 245	3660	0
		0 249	1770	0
		0 252	411	0
		0 253	22 1	0
17	2	0 216	38900	0
		0 234	12700	0
		0 241	3620	0
		0 245	1750	0
		0 248	406	0
		0 249	21 9	0
18	1	0 216	58800	0
		0 233	18700	0
		0 241	5300	0
		0 245	2550	0
		0 248	583	0
		0 249	31 4	0

Skew Emission

The postscatter energy and flux values of photons from the reactor shield that are skew emitted and the resultant dose values within the crew compartment are given in Table F-2 for the individual cells. The symbols used in the table are defined as follows:

k = index for source angle α (given in Table E-1, p 97),

m = index on prescattering path r (given in Table E-2, p 98),

E' = postscatter energy (Mev),

β = receiver angle (deg),

ϕ/P = flux outside crew shield $\left(\frac{\text{photons}}{\text{cm}^3\ \text{sec}}\right)$,

D = dose inside crew shield $\left(\frac{\text{r}}{\text{hr watt}}\right)$

Table F-2 Skew Emission

k	m	E'	β	$\phi/P \times 10^6$	$D \times 10^{11}$
1	1	0 989	5 98	21 5	0 0009
		1 57	6 28	66 8	0 0003
		1 82	6 39	21 6	0 0001
		2 03	6 45	10 8	0
1	2	0 932	8 71	226	0 0281
		1 44	9 33	68 9	0 0086
		1 63	9 67	21 9	0 0027
		1 78	9 83	10 9	0 0014
1	3	0 867	12 3	234	0 194
		1 30	13 0	70 4	0 0582
		1 43	13 6	22 1	0 0183
		1 54	13 9	10 9	0 0090
1	4	0 794	16 8	238	0 636
		1 15	17 6	71 0	0 189
		1 24	18 4	22 1	0 0589
		1 31	18 7	10 9	0 0290
1	5	0 714	22 4	238	1 11
		0 996	23 1	70 7	0 331
		1 05	24 1	21 8	0 102
		1 09	24 5	10 7	0 0501
1	6	0 631	29 1	232	1 11
		0 846	29 7	69 3	0 332
		0 876	30 9	21 2	0 102
		0 901	31 4	10 3	0 0495
1	7	0 548	37 0	222	0 563
		0 706	37 8	66 7	0 169
		0 723	38 9	20 2	0 0513
		0 738	39 4	9 76	0 0247
1	8	0 472	46 3	208	0 337
		0 584	47 2	62 6	0 101
		0 595	48 1	18 7	0 0304
		0 606	48 5	8 95	0 0145
1	9	0 406	56 5	191	0 175
		0 484	57 7	56 8	0 0521
		0 495	58 2	16 8	0 0154
		0 504	58 4	7 9	0 0073
1	10	0 353	67 2	170	0 0722
		0 409	68 8	49 6	0 0210
		0 421	68 6	14 5	0 0061
		0 429	68 5	6 79	0 0029

k	m	E'	β	$\phi/P \times 10^6$	$D \times 10^{11}$
1	11	0 314	77 5	147	0 0286
		0 356	79 6	41 7	0 0081
		0 368	78 7	12 1	0 0023
		0 376	78 3	5 6	0 0011
1	12	0 287	87 0	124	0 0094
		0 320	89 5	33 9	0 0026
		0 332	87 9	9 84	0 0007
		0 340	87 2	4 58	0 0003
1	13	0 268	95 2	102	0 0033
		0 295	98 0	27 2	0 0009
		0 307	96 0	7 92	0 0002
		0 315	95 0	3 69	0 0001
1	14	0 255	102 2	83 5	0 0012
		0 279	105 2	21 7	0 0003
		0 291	102 1	6 36	0 0001
		0 298	101 6	2 97	0
1	15	0 246	108 0	68 3	0 0004
		0 268	111 2	17 4	0 0001
		0 279	108 5	5 13	0
		0 285	107 2	2 40	0
1	16	0 239	112 8	56 1	0 0002
		0 260	115 9	14 0	0 0001
		0 271	113 3	4 18	0
		0 277	111 9	1 96	0
1	17	0 234	116 8	46 4	0 0001
		0 255	120 1	11 5	0
		0 265	117 2	3 43	0
		0 271	115 8	1 61	0
1	18	0 231	120 1	38 8	0
		0 251	123 5	9 51	0
		0 260	120 6	2 86	0
		0 266	119 1	1 35	0
1	19	0 228	122 9	32 8	0
		0 247	126 3	7 96	0
		0 256	123 4	2 41	0
		0 262	121 9	1 14	0
1	20	0 226	125 3	27 9	0
		0 245	128 7	6 74	0
		0 254	125 8	2 05	0
		0 260	124 4	0 97	0

k	m	E'	β	$\phi/P \times 10^6$	$D \times 10^{11}$
1	21	0 221	134	135	0
		0 239	137 2	31 8	0
		0 247	134 5	9 83	0
		0 252	133 1	4 69	0
1	22	0 218	140 8	54 0	0
		0 236	144 0	12 6	0
		0 243	141 5	3 93	0
		0 248	140 2	1 89	0
1	23	0 217	143 9	28 6	0
		0 234	147 1	6 64	0
		0 242	144 5	2 09	0
		0 246	143 5	1 00	0
1	24	0 216	145 7	17 6	0
		0 234	148 8	4 09	0
		0 241	146 6	1 29	0
		0 246	145 4	0 62	0
2	1	0 776	6 97	1540	0 0349
		0 932	7 24	466	0 0106
		1 000	7 32	102	0 0023
		1 05	7 36	61 0	0 0001
2	2	0 717	11 0	1530	0 529
		0 837	11 7	459	0 159
		0 886	11 9	100	0 0346
		0 921	12 0	59 6	0 0021
2	3	0 657	15 7	1510	1 97
		0 746	16 7	449	0 586
		0 781	17 0	97 3	0 127
		0 806	17 2	57 6	0 0751
2	4	0 596	21 1	1470	3 59
		0 661	22 3	435	1 06
		0 687	22 7	93 5	0 228
		0 704	22 9	55 0	0 134
2	5	0 537	27 2	1420	1 08
		0 585	28 5	416	0 319
		0 604	28 9	88 7	0 0680
		0 617	29 1	51 8	0 0397
2	6	0 481	33 9	1350	0 698
		0 518	35 2	393	0 203
		0 533	35 5	82 9	0 0428
		0 543	35 6	48 1	0 0248

k	m	E'	β	$\phi/P \times 10^6$	$D \times 10^{11}$
2	7	0 430	41 2	1280	0 392
		0 461	42 2	365	0 112
		0 474	42 3	76 3	0 0234
		0 483	42 4	43 9	0 0135
2	8	0 387	48 9	1190	0 265
		0 415	49 3	334	0 0745
		0 426	49 2	69 0	0 0154
		0 434	49 2	39 4	0 0088
2	9	0 351	56 7	1090	0 188
		0 377	56 3	300	0 0519
		0 388	56 0	61 5	0 0106
		0 395	55 9	34 9	0 0060
2	10	0 322	64 3	981	0 109
		0 348	63 1	266	0 0295
		0 358	62 5	54 1	0 0060
		0 365	62 2	30 6	0 0034
2	11	0 299	71 5	871	0 0592
		0 325	69 4	233	0 0158
		0 335	68 6	47 2	0 0032
		0 341	68 1	26 6	0 0018
2	12	0 282	78 0	762	0 0348
		0 307	75 2	203	0 0092
		0 317	74 1	40 9	0 0019
		0 323	73 6	23 0	0 0010
2	13	0 268	83 9	662	0 0204
		0 293	80 5	175	0 0054
		0 303	79 1	35 4	0 0011
		0 309	78 4	19 9	0 0006
2	14	0 258	89 2	571	0 0100
		0 282	85 1	152	0 0026
		0 292	83 6	30 6	0 0005
		0 298	82 8	17 2	0 0003
2	15	0 250	93 7	493	0 0060
		0 274	89 3	131	0 0016
		0 283	87 6	26 5	0 0003
		0 289	86 7	14 9	0 0002
2	16	0 244	97 7	426	0 0038
		0 267	92 9	114	0 0010
		0 277	91 1	23 0	0 0002
		0 283	90 1	12 9	0 0001

k	m	E'	β	$\phi/P \times 10^6$	$D \times 10^{11}$
2	17	0 240	101 2	369	0 0024
		0 262	96 1	99 3	0 0006
		0 271	94 2	20 1	0 0001
		0 277	93 2	11 3	0 0001
2	18	0 236	104 3	321	0 0016
		0 258	99 0	87 0	0 0004
		0 267	97 0	17 6	0 0001
		0 273	95 9	9 91	0
2	19	0 233	107 0	281	0 0012
		0 255	101 5	76 5	0 0003
		0 263	99 5	15 5	0 0001
		0 269	98 4	8 74	0
2	20	0 231	109 3	247	0 0008
		0 252	103 7	67 7	0 0002
		0 261	101 6	13 7	0
		0 266	100 6	7 74	0
2	21	0 223	118 3	1330	0 0015
		0 243	112 5	374	0 0004
		0 251	110 3	76 7	0 0001
		0 256	109 2	43 3	0
2	22	0 219	126 3	581	0 0002
		0 238	120 7	168	0 0001
		0 245	118 5	34 8	0
		0 250	117 3	19 7	0
2	23	0 217	130 3	320	0 0001
		0 236	124 8	93 8	0
		0 243	122 6	19 5	0
		0 248	121 4	11 1	0
2	24	0 217	132 6	201	0
		0 235	127 2	59 5	0
		0 242	125 1	12 4	0
		0 247	123 9	7 08	0

Direct Beam

The dose values within the crew compartment due to direct beam radiation from the reactor shield are given in Table F-3 The symbols used in the table are defined as follows

k = index for source angle (given in Table E-3, p 99),

n = index for energy (given in Table E-3, p 99),

D = dose inside crew shield $\left(\frac{r}{hr\ watt}\right)$

[redacted]

Table F-3 Direct Beam

k	n	$D(\frac{r}{hr\ watt})$
1	1	0 81
	2	2 48
	3	1 00
	4	0 49
2	1	3 93
	2	7 52
	3	2 55
	4	1 17
3	1	2 81
	2	2 50
	3	0 67
	4	0 36
4	1	1 74
	2	0 85
	3	0 18
	4	0
5	1	1 22
	2	0 30
	3	0
	4	0
6	1	10 94
	2	3 97
	3	0 14
	4	0
7	1	12 9
	2	4 7
	3	0
	4	0
8	1	57 5
	2	12 0
	3	0
	4	0

[redacted]